Using Piezoelectricity to Develop Syntheses to Access Polymeric Materials via Force

Sarah Zeitler

A dissertation submitted in partial fulfillment of the requirements for the degree of

Doctor of Philosophy

University of Washington

2024

Reading Committee:

Matthew Golder, Chair

Alshakim Nelson

Gojko Lalic

Program Authorized to Offer Degree:

Chemistry

University of Washington

Abstract

Using Piezoelectricity to Develop Syntheses to Access Polymeric Materials via Force

Sarah Zeitler

Chair of the Supervisory Committee:
Matthew Golder
Department of Chemistry

Mechanochemistry provides a promising way to make polymer and materials synthesis more sustainable and applicable to diverse systems, allowing for the use of many force sources and the incorporation of various monomers. Particularly, mechanoredox catalysis, utilizing piezoelectricity to do redox catalysis, presents an avenue to develop reactions that mimic traditional redox mechanisms but occur when force is applied. In polymer chemistry, mechanoredox catalysis has been rapidly developed in the last five years, utilizing different force sources and being applied to many polymerizations and materials syntheses. Detailed within this thesis are our reports of $BaTiO_3$-mediated mechanoredox polymerizations utilizing primarily aryl iodonium salts, readily accessible and functionalizable radical initiators; the required force can be generated within ultrasound baths, ball mills, and vortexers. Mechanoredox polymerizations can require very little solvent, allowing for less waste and incorporation of immiscible monomers. Both free and reversible deactivation radical polymerizations are

demonstrated, and while much of the work presented focuses on industrially-relevant polyacrylates and polymethacrylates, it is established that more challenging monomers can be incorporated into polymer systems. Block copolymers can be made with traditionally compatible and incompatible monomer systems, some with unique self-assembly properties useful for the development of electronic devices. Additionally, composite materials with acrylates and $BaTiO_3$ nanoparticles are made via free radical mechanoredox polymerization, both with and without the incorporation of crosslinkers. The methods developed throughout these thesis projects also show less energy consumption than traditional stimulus, increasing the sustainability profile of mechanoredox catalysis.

Acknowledgements

While this work has my name on it, none of it would be possible without the continual support and encouragement from my community: my mentors, committee, and colleagues, my family and friends. I am so grateful for all I have been privileged to learn and all the wonderful memories I have collected. I do not have the words or space to truly express my gratitude.

First, I want to thank my high school science teacher, Mr. Newton, for exposing me to the wonders of science. I was given the confidence to become a scientist because of your inspiration.

My Whitworth professors had an immense impact on my journey to pursue a scientific career. Dr. Russell, thank you for taking me under your wing and training me to be an effective researcher. Your support as a chemist gave me the courage to pursue my PhD, and your support as a person gave me the desire to follow in your footsteps and train undergraduate students as a professor. Dr. Breno, thank you for convincing a very resistant pupil that chemistry is amazing. I walked into organic chemistry thinking it would be the end of the chemistry journey, and here I am today having completed eight additional years of chemistry education.

Sam, Andrea, Debbie, and all the others who have given me chances to learn how to be an effective collegiate educator, thank you for investing in me and my passion. I feel blessed to have had many opportunities to learn new educational skills throughout my graduate career.

Matt, thank you for convincing me that the University of Washington was the correct place for me to pursue my graduate studies. Since then, I have been grateful for your consistent mentorship and encouragement to pursue the things that are important to me, even if they have been less conventional. You have given me and allowed me to take the opportunities to develop the skills I need as a scientist and educator. Thank you for taking a chance on me.

To the Golder group, both former and current members, thank you for being the best colleagues and friends one could ask for. I have learned so much from all of you, and the memories I hold dearest from graduate school are the ones I have made with all of you. You are all brilliant researchers who are going to have profound impacts on your communities. Meredith, thank you for not only being my colleague and cohort-mate, but one of my very best friends. I cannot express how grateful I am to have gone on this journey with you.

To my external community, friends and family, thank you for grounding me, reminding me of the important things outside of my academic bubble, and being patiently supportive while I muddled my way through this season. To my Sojourn friends, thank you for the weekly space to enjoy one another's company and reflect on the big things in life. To our youth group kiddos, thank you for keeping me young and excited about life. To my in-laws, thank you for being so supportive of Michael and I as we have navigated life changes and weird schedules. I am so blessed to have

gained such a wonderful family when we got married. To Sam, you have passionately taken me under your wing as an extra little sister. Thank you for the time you take, whether coerced or by choice, to listen to practice talks, to share wisdom, and to encourage me. To my parents, your selfless, unconditional, and complete support of every decision I have made is incomprehensible. I cannot understand nor express that extreme gratitude I have to always know you have my back in every and any situation. Hannah, I have always stood in awe of how you generously and unselfishly share your time, your thoughts, your encouragement, and your friendship with me. You have put up with your annoying little sister for a long time, and I do not have words to truly appreciate you. Most people do not get to have their role model as their sister and best friend; I feel very lucky to get to.

Michael, the best part of being in graduate school is that I was here to meet you, the love of my life, my constant supporter, and my very best friend. Your patience with me and your never-ending willingness to sustain me in every high and low, both in life and in my academic pursuits is astounding. Thank you for being willing to step outside your comfort zone to support me pursuing my dreams. You are the most amazing, compassionate, level-headed, generous, strong, selfless person I have ever had the privilege of knowing, and I could not have asked for a better husband, life partner, adventure partner, and animal dad.

Jesus is my source of joy, strength, love, and life each and every day.

2 Corinthians 12:9

Table of Contents

Table of Figures

Table of Schemes

Table of Tables

Chapter 1: Introduction

1.1 Polymer Mechanochemistry

As polymer chemistry developed throughout the early twentieth century, the utility of synthetic polymers rapidly became apparent. However, methods for making such synthetic polymers were lacking, and polymer chemists sought to develop simple methods to access property-targeted polymeric materials. One such method that has grown exponentially in popularity is free radical polymerization (FRP) which is commonly used due to its versatility (i.e. monomer tolerance) and simplicity (i.e. minimal additives required).[1] Utilizing this straightforward method which employs radical initiators and unsaturated monomers, polymers with numerous desirable properties and structures can be made for commercial purposes, from hard plastics to hydrophobic packaging to paints and coating products. While many high molecular weight species can be synthesized, FRP does not allow for molar mass or spatiotemporal control, both of which are critical considerations for advanced applications.[2] Spatiotemporal control is particularly important as it allows for directed regulation of when and where polymer chains are growing which allows for the synthesis of more complex materials; chain growth will only occur where stimulus is applied, and polymeric materials can therefore be programmed to have varying compositions at different locations. For example, Esser-Kahn demonstrated the ability to pattern materials with force via spatiotemporal distribution of engineered stress maps throughout soft materials using an electrodynamic shaker. This spaciotemporal directing can be quantified using mechanical testing and corroborated with computational modeling, thereby demonstrating how stress is applied at different locations throughout the sample matrix and thus produces a material with varying materials properties at unique locations.[3]

The mechanism for FRP is well established – stimuli-promoted (e.g., heat, light) homolytic cleavage of an initiator molecule commences the polymerization process. Chain

growth continues via monomer propagation until termination occurs by H-atom abstraction or chain recombination.[1,4] *In FRP, all active chain ends propagate until such termination occurs*.

To expand the utility of radically formed synthetic polymers beyond what is offered by FRP, reversible deactivation radical polymerization (RDRP) techniques have been developed to allow for the synthesis of well-defined living polymers. The two most common RDRP methods are atom transfer radical polymerization (ATRP) and reversible addition-fragmentation chain transfer polymerization (RAFT).[5–7] Both of these RDRP methods utilize deactivation mechanisms to ensure uniform growth of all propagating polymer chains.

Additionally, both ATRP and RAFT have well-studied mechanisms.[6,8,9] While the radical initiation steps are similar to those of FRP, ATRP and RAFT mechanisms introduce chain end "capping", a deactivated dominant equilibrium state of the propagating polymer chain. In ATRP, this reversible deactivation process occurs through metal mediation, typically Cu(II)/Cu(I) or Fe(II)/Fe(I), to facilitate halide chain capping in the M(I) oxidation state and chain propagation in the M(II) oxidation state (Scheme 1.1A).[10,11] As expanded upon below, the stimulus needs to be applied continuously for ATRP in order to regenerate the activated state of the transition metal catalyst. For example, as the stimulus is applied, Cu(I)X is consistently regenerated by the reduction of $Cu(II)X_2$, permitting subsequent electron transfer to reactivate dormant capped chain ends.[12–15] In RAFT, this reversible deactivation process occurs via a chain transfer agent (CTA) (e.g., dithiocarbonate, trithiocarbonate). Growing chains quickly react with CTAs to establish the RAFT equilibrium; degenerate chain transfer facilitates piecemeal chain propagation of each growing polymer (Scheme 1.1B).[8]

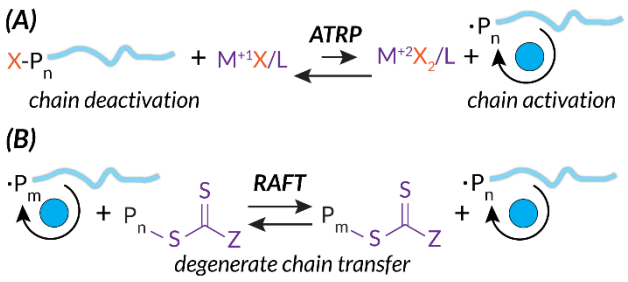

Scheme 1.1 ATRP and RAFT mechanisms share similarities in deactivation via unique chain capping strategies leading to more control of chain length.

Historically, traditional polymerizations in the field are subject to conventional reaction stimuli such as heat or light. Thermal initiations have been used readily both in academia and industry, and while the polymerization of unsaturated monomers can be thermally propagated, undesirable side reactions and degradation readily occur due to frequent thermal instability of polymer and reactant species.[16] Thermal reactions also require a large amount of energy to apply heat uniformly in a reactor and consequently suffer from poor spatiotemporal control.[17]

On the other hand, photoinduced radical polymerizations offer a unique alternative to thermal methods, and due to an expansive library of photochemical methodology, these polymerizations are currently of high interest to the polymer community.[18–20] Photoinitiation offers increased spatiotemporal control (e.g., vat photopolymerizations[21]) compared to other stimuli and often requires less energy[22] than thermal initiation. In recent years, photoredox methodologies pioneered by Hawker, Johnson, Fors, Boyer, Miyake, and Chen build on established energy transfer mechanisms established in small molecule synthesis to gain spatiotemporal control on the macromolecular scale.[23–28] Still, a major limitation of photochemistry is that photon penetration is governed by the refractive index of a material or solution.[29] Therefore, if colored or opaque media is employed, photochemical processes become more challenging.

Complimentary to these ongoing developments in the field to effectively apply stimuli to macromolecular systems, mechanochemistry is recognized as a reemerging area utilized by synthetic chemists. [29] While relevant in the field of polymer chemistry since Staudinger in the

1930's,[30] only recently have mechanically generated radicals become synthetically useful. Homolytic bond scission under mechanical stress generates so-called mechanoradicals that can then be used to initiate radical reactions, translating the mechanical energy into chemical energy.[31–34] Grzybowski exemplifies this phenomenon by demonstrating that mechanoradicals can even be generated within commodity materials (e.g., tires, sneaker soles) upon mechanical flexing, akin to ordinary stress experienced by these commonplace polymers.[31] Due to mechanochemistry's ability to transfer energy in situ or through materials and its ability to access traditionally inaccessible products, it is rapidly being reevaluated as a useful method for polymer synthesis and upcycling processes traditionally performed in solution.[35–44]

1.2 Mechanochemical Tools and Early Reports

One way to utilize force as a stimulus for chemical reactions is to harness the power of piezoelectricity. Piezoelectricity is a phenomenon present in materials with non-centrosymmetric crystal lattice structures and uneven charge distribution (i.e., poling). This specific crystal structure translates mechanical force into a piezopotential, or the inverse can occur within piezoelectric materials in which electric potential can cause a mechanical output (i.e., actuation).[45-46] In effect, piezoelectric materials (e.g., PVDF, $BaTiO_3$, ZnO, etc.)[47,48] are able to translate mechanical force into electric potential to effect redox chemistry by disrupting the crystal structure equilibrium and facilitating single electron transfer from the surface of the materials (Figure 1.1).[29,48–50] At this time, piezoelectric nanoparticles or nanorods are typically utilized due to their high surface area to volume ratio which permits efficient charge transfer. Ongoing efforts suggest that incorporating piezoelectric components directly into engineered reaction vessels might be even more effective at capturing the maximum possible energy.[51]

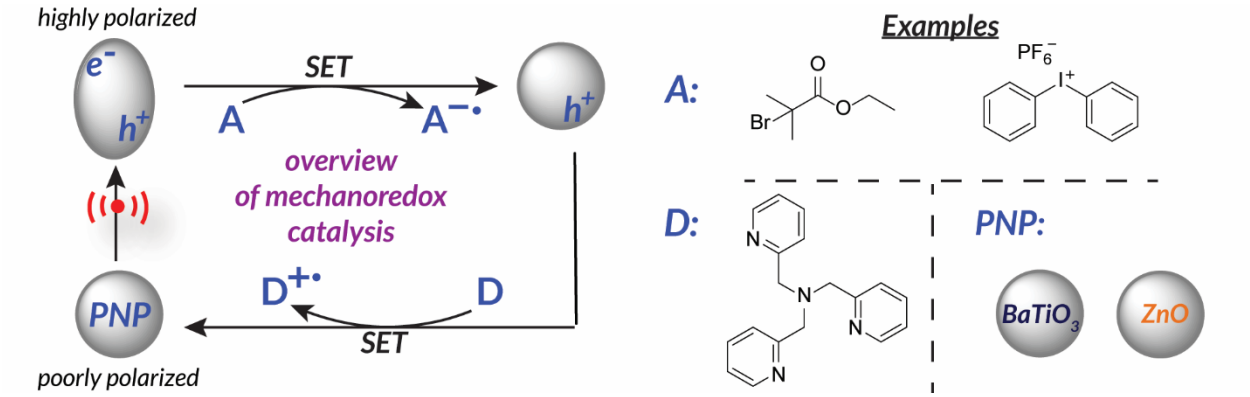

Figure 1.1 Piezoelectricity can be utilized for single electron transfer to reduce an "acceptor" initiator. Nanoparticles become activated upon application of force.

The use of mechanical force to facilitate synthetic redox chemistry, specifically with piezoelectric materials (i.e. mechanoredox catalysis), draws inspiration from utilizing piezoelectric materials like ZnO and $BaTiO_3$ for water splitting. In these works, piezoelectric nanorods are subjected to ultrasonic irradiation for the conversion of water into H_2 and O_2.[52–54]

The requisite force for mechanically induced processes can come from many different sources. Historically, a mortar and pestle or hammer have been used for grinding reactions, and while sometimes still utilized in recent times,[55,56] more replicable sources include ultrasonic horns, ultrasonic baths, and ball mills.[17,57]

Sonication (i.e., ultrasonic irradiation) is a common "force source" for mechanochemistry.[57] Ultrasound waves cause bubbles to form and expand where hot spots develop. Upon collapse, these cavitation bubbles exert a shear force within the reaction mixture to drive mechanochemical reactions.[58] Ultrasonic horns apply ultrasound to a pinpointed region with higher power outputs than ultrasound baths. Ultrasonic baths are more readily available but apply force more broadly and can create hotspots.[59] Both types of ultrasonic generators are readily employed in mechanochemistry.

Ball mills are alternative force sources consisting of a sealable reaction jar containing a specified number and size of ball bearings.[60] The jars are then shaken, rolled, or spun at a particular frequency; ball bearings impact the sides of the reaction jar and transfer this energy

to the reaction components. Ball milling reactions can uniquely occur in the solid state or near solid state due to the lack of dependence on solvent for energy transfer and mixing. Some reactions have been shown to be more efficient with miniscule amounts of solvent (0 – 2 μL/mg) added to aid in mixing and solubility; this phenomenon is termed liquid assisted grinding (LAG) and has been utilized in mechanochemical reactions since the early 2000's.[61–64]

Previously, the intuitive use of force in polymer mechanochemistry was centered around bond scission, or destructive chemistry. Polymer degradation has been reported in an ultrasound bath, and applied stress has been repeatedly shown to activate bulk mechanophores, mechanically active molecules incorporated into polymers, via bond scission or molecular rearrangement. However, there have been some reports of constructive bond-forming mechanochemistry to produce polymers. Limited reports[65,66] utilize high frequency ultrasound (> 400 kHz) to induce homolytic solvent cleavage; the solvent radicals then induce radical polymerization. Other reports have shown that various types of post-polymerization functionalization and non-radical polymerizations can occur in the ball mill setting precedent for efficient constructive radical polymer chemistry to be developed in the ball mill without concern of structural degradation.[35,67]

Using this foundation for mechanoredox chemistry, in 2019 Kubota and Ito published work in which the "mechanically-activated" piezopotential from $BaTiO_3$ was coupled to borylation reactions with aryl diazonium salts.[55] This study demonstrates that force generated by ball bearings impacting the walls of ball milling jars induces the piezoelectric effect in the $BaTiO_3$ nanoparticles. Then, single electron transfer from the $BaTiO_3$ surface reduces the aryl diazonium salt; the resulting aryl radical (following N_2 evolution) couples with bis(pinacolato)diboron for C-B bond formation; heteroarenes can also be utilized for C-C bond formation (Scheme 1.2). While this work was naturally motivated by earlier accounts of

mechanoredox polymerizations (*vide infra*), the unique combination of mechanoredox catalysis under ball milling conditions served as a particularly important inspiration to my chemistry discussed in this thesis when designing approaches to the macromolecular challenges described below.

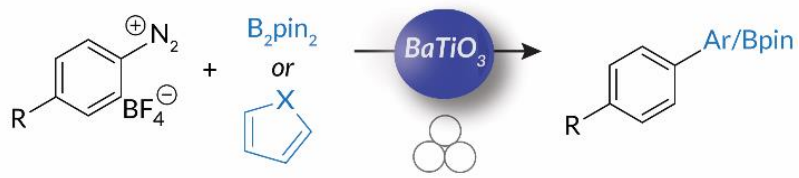

Scheme 1.2 As demonstrated by Kubota and Ito, mechanoredox catalysis can be used to perform arylations and borylations. In these examples, aryl diazonium salts are reduced by piezoelectric nanoparticles in the ball mill.

1.3 Ultrasonicated Polymerizations

In 2017, the Esser-Kahn group published seminal work that utilized mechanoredox catalysis with ultrasonic irradiation to control ATRP. In this study (Figure 1.2), Cu(II) is reduced by the mechanically-perturbed $BaTiO_3$ piezoelectric nanoparticles. The Cu(II) system, $Cu(OTf)_2/Me_6TREN/Bu_4NBr$, was specifically selected due to its reduction potential appropriately matching the generated reduction potential of the $BaTiO_3$ (benchmarked to be at least –1.23 V via its water splitting ability),[52] an important consideration for all mechanoredox polymerizations. An ultrasonic horn (20 kHz) was used to activate the $BaTiO_3$ and subsequently reduce the Cu(II) catalyst. The produced Cu(I) can then activate the ATRP initiator to commence chain growth; continuous sonication is required for sustained monomer propagation. Overall, various polyacrylates were formed, although molar masses did not exceed 3 kDa. While limited in scope, this seminal work was crucial in demonstrating how mechanoredox catalysis can drive initiation and reversible activation/deactivation processes within a radical polymerization system.[68]

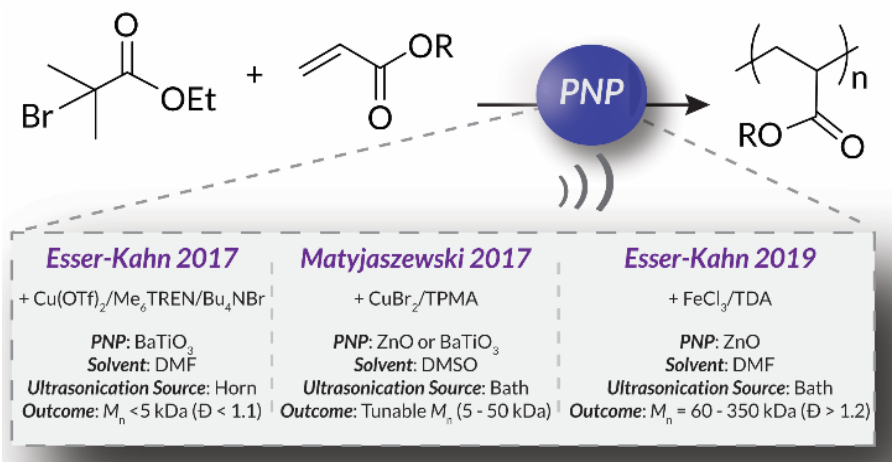

Figure 1.2 Comparison of the seminal Esser-Kahn/Matyjaszewski mechanoredox polymerization conditions highlighting important outcomes and progress. These works lay the foundation for the mechanoredox polymerization field.

Following this initial ATRP report, the Matyjaszewski group optimized reaction conditions to utilize more readily accessible ultrasonic baths (rather than ultrasonic horns), examine the specifics of mechanoredox catalyst nanoparticle (e.g., size, geometry, surface ligands), and expand the target molar mass range (Figure 1.2).[69] The monomer scope was also expanded to encompass myriad acrylate monomers with good temporal control demonstrated in on-off experiments (Figure 1.3). Importantly, Matyjaszewski highlighted how it is possible to decrease catalyst loading and utilize ZnO instead of $BaTiO_3$ as another low toxicity, lead-free piezoelectric material alternative.[70,71]

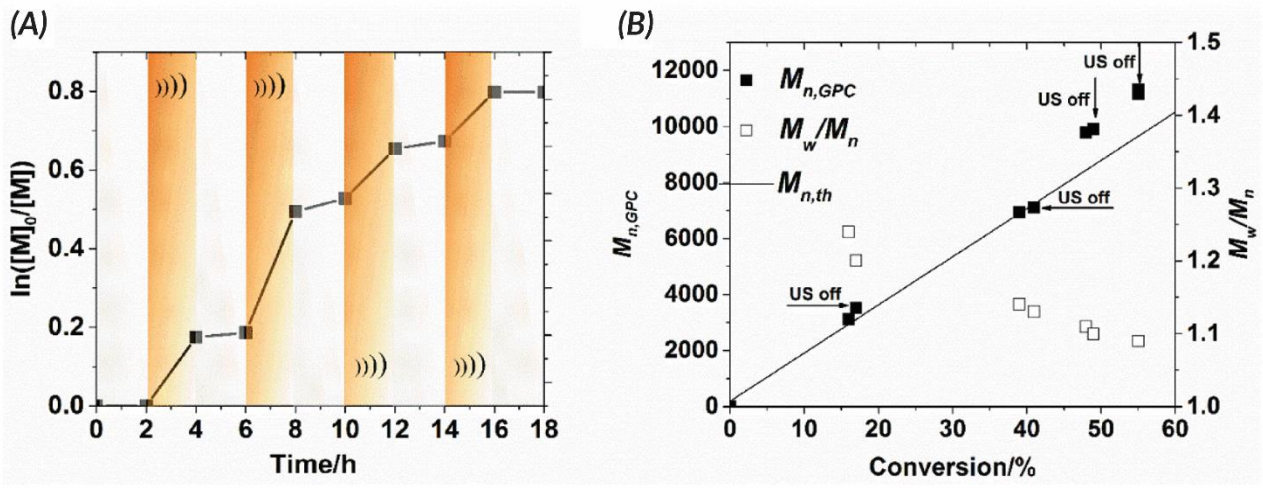

Figure 1.3 Matyjaszewski refined the work of Esser-Kahn to create an optimized mechanoredox-catalyzed ATRP system which is demonstrated in the ability to "turn off" polymerization with the removal of stimuli. (A) Kinetic studies demonstrate lack of significant chain growth when ultrasound is turned off. (B) Molecular weight and dispersities match the expected ATRP values with low dispersities and conisistent growth while sonication is applied. Reaction conditions: $[monomer]_0 : [initiator]_0 : [metal]_0 : [ligand]_0 = 200:1:0.03:0.18$ with 4.5 wt. % $BaTiO_3$ in DMSO. *Reprinted with permission from Ref. 69. Copyright 2017 American Chemical Society.*

In 2019, the Esser-Kahn group further expanded upon their initial ATRP work to demonstrate that mechanoredox FRP could also be conducted to access higher molar mass polymers. Utilizing the improvements outlined by the Matyjasweski reports, a low ZnO loading was used in conjunction with an ultrasound bath and a Fe catalyst to achieve polymerization (Figure 1.2). While Fe-catalyzed ATRP has been reported,[72] the system in this report better approximates FRP mechanistically. High molar masses (50-340 kDa) were achieved with a variety of monomers (Figure 1.4); however, consistent with a free-radical mechanism there was only moderate control of dispersity (Đ = 1.2-1.3) (Table 1.1). The versatility of mechanoredox catalysis was also demonstrated in the synthesis of block copolymers emanating from macroinitiators.[73]

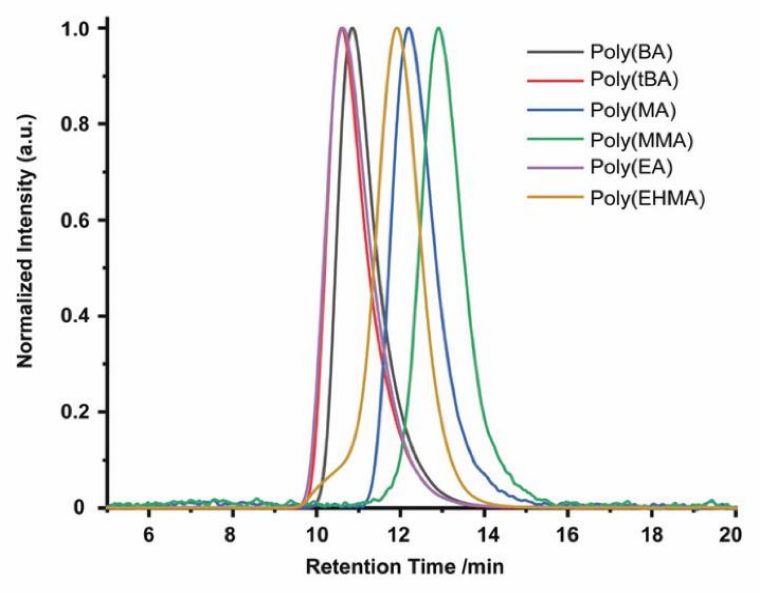

Figure 1.4 GPC-RI traces from Esser-Kahn's mechanoredox FRP methodology. *Adapted with permission from Ref. 73. Copyright 2019 Wiley Journals.*

Table 1.1: Esser-Kahn established mechanoredox FRP can be used to synthesis high molecular weight polymers and dispersities. Reaction conditions: $[monomer]_0 : [initiator]_0 : [metal]_0 : [ligand]_0 = 100:1:1:2$ with 9 wt. % ZnO in DMF. *Adapted with permission from Ref. 62. Copyright 2019 Wiley Journals.*

Entry	Monomer	Conversion[a] (%)	M_n (kDa) [b]	Đ[b]
1	*t*BA	80	341	1.27
2	BA	74	246	1.22
3	EA	55	212	1.27
4	MA	71	62	1.18
5	MMA	52	50	1.30
6	EHMA	60	145	1.22

Most mechanoredox polymerizations require both the piezoelectric nanoparticles and an exogenous initiator, much like photoredox polymerizations that require a sensitizer and an initiator.[74] Alternatively, Stenzel and coworkers were able to demonstrate initiation via water molecules adsorbed on the surface of the $BaTiO_3$ mechanoredox catalyst (*vide infra*).[56] In mechanoredox catalyzed polymerizations, the piezoelectric material is activated by force, allowing for single electron transfer to govern initiation. The mechanism following initiation

is similar to conventional controlled radical chain growth mechanisms. For example, in the ATRP reactions demonstrated by the Esser-Kahn and Matyjaszewski groups, constant force is required to continue polymerization as the chain ends need to be continuously reactivated via a reduced metal species.[68–70] These works demonstrate that temporal control observed with traditional stimuli can also be achieved with mechanical force for reversible-deactivation radical polymerizations.

As previously mentioned, the choice of initiator is important to consider. Although high frequency ultrasound can homolytically cleave solvent to produce radical initiators,[75] the "effective force" generated in the aforementioned mechanoredox processes is generally not great enough to directly reduce solvent or other small molecules in solution. Instead, force must be transduced through the mechanoredox catalyst which subsequently generates an appropriate potential for downstream reactivity. Because the piezoelectric nanoparticles will only produce a measurable electric potential when activated, only certain radical initiators are eligible for use in initiation.

Building upon the initial reports of mechanoredox ATRP,[68–70,73,76,79] Pang recently expanded upon such previous work by studying the influence of ZnO nanoparticle shape and size on polymerization efficiency. Prior to this work, commercially available 20 – 200 nm nanoparticles with traditional morphologies (i.e. cubic, tetragonal, hexagonal) had primarily been utilized for mechanoredox polymerizations; however, it is known that nanoparticle morphology can impact the generated mechanoredox potential.[80,81] Pang found that by substituting commercial ZnO for various sized nanorods (300-530 nm in diameter and 1.9-6.8 μm in length), less ZnO was needed to initiate polymerization with higher conversion and lower power ultrasonication than previously used (Figure 1.5). The nanorods with the highest aspect ratio (L/D = 13) show an increase in piezoelectric activity as they afforded polyacrylates with experimental M_n values closely matching theoretical M_n values in only 4 h;

previous reports require at least 8 h for full monomer consumption. Uniquely when utilizing these nanorods, acrylonitrile monomers can also be polymerized to high molar mass and low dispersity, a shortcoming of prior mechanoredox ATRP processes.[82] Pang also further expanded upon the study of ZnO nanoparticles by also identifying optimized BaTiO3 morphologies in a separate report.[83]

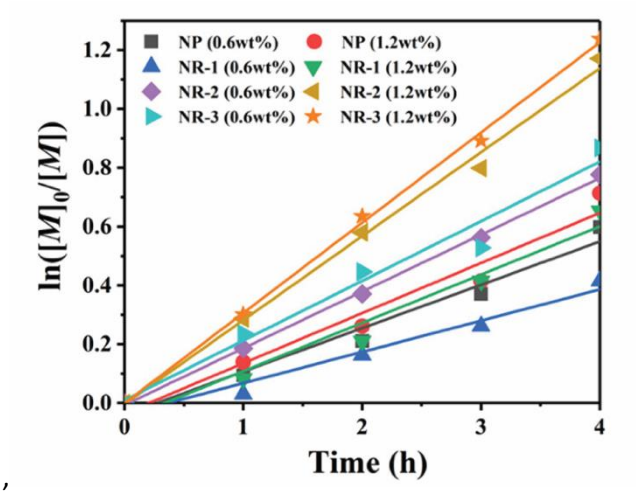

Figure 1.5 Pang compared ZnO nanoparticle sizes and shapes to their polymerization efficiencies. Reaction conditions: $[monomer]_0$: $[initiator]_0$: $[metal]_0$: $[ligand]_0$ = 100:1:0.03:0.18 with ZnO in DMSO. *Adapted with permission from 82. Copyright 2022 American Chemical Society.*

Akin to solution-state mechanoredox ATRP processes, analogous RAFT polymerizations are also possible as recently demonstrated by Zhang. Using a bis(trithiocarbonate) bisulfide chain transfer agent in conjunction with previously described alkyl halide initiators,[68–70,73] high monomer conversion was achieved when sonicating in the presence of ZnO. Controlled molar masses and dispersities were consistent with RAFT polymerizations (Figure 1.6), and the high chain end fidelity was demonstrated by reactivating a macroinitiator synthesized via mechanoredox RAFT to form block copolymers. This report also introduces the use of a tris(2-pyridylmethyl) amine (TPMA) ligand that is hypothesized to fill holes following single electron transfer. TPMA is reported to be on the surface of the ZnO after sonication, as observed by X-ray photoelectron spectroscopy. Finally, the report uniquely shows the ability to cure opaque acrylic resins using force (Figure 1.7). Photochemistry is

typically used to cure such resin formulations, but photons cannot penetrate deeply into opaque materials; mechanoredox catalysis increases the percentage of cured resin (ca. 95%) compared to that of photocuring (ca. 59%) and allows for filler and composite incorporation without decreasing stimulus penetration.[84] This specific application-driven example is complemented by work from Esser-Kahn in which soft organogels were hardened via mechanoredox catalysis-induced disulfide bond formation (Figure 1.8).[85]

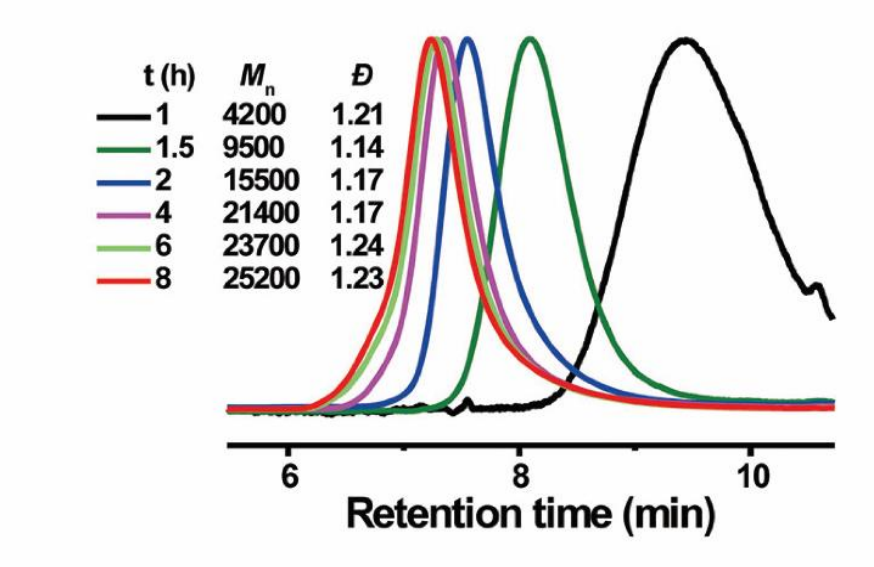

Figure 1.6 GPC-RI traces over time from Zhang's mechanoredox RAFT method demonstrating good control over M_n and dispersities. Reaction conditions: $[monomer]_0$: $[initiator]_0$: $[chain\ transfer\ agent]_0$: $[ligand]_0$ = 75:2:1:0.7 with 4.4 wt.% ZnO in DMSO. *Adapted with permission from Ref. 84. Copyright 2022 American Chemical Society.*

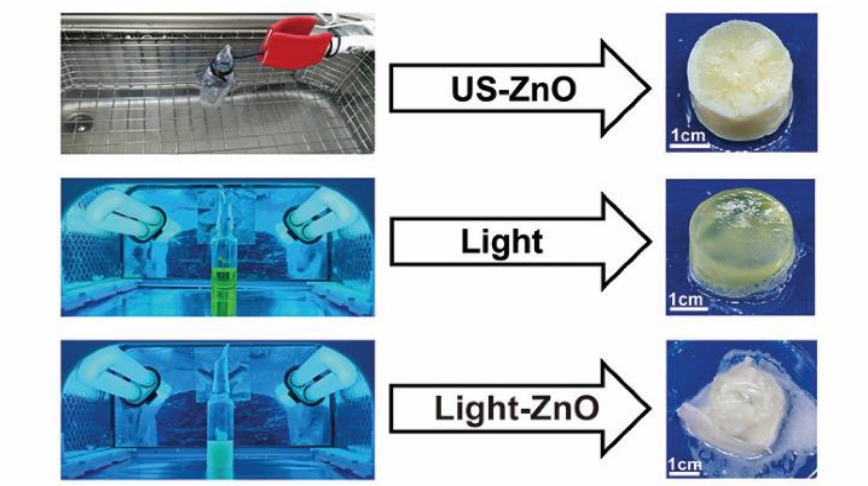

Figure 1.7 After showing that mechanoredox polymerizations can be translated to RAFT, Zhang further expanded the work to force cure ZnO opaque composites. *Adapted with permission from Ref. 84. Copyright 2022 American Chemical Society.*

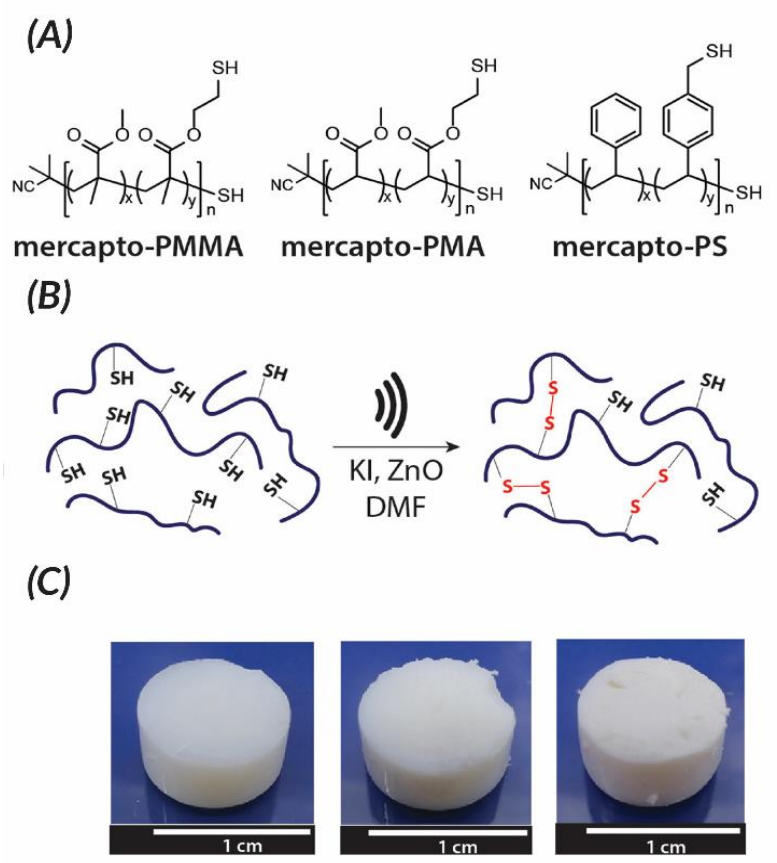

Figure 1.8 Esser-Kahn also demonstrated force can be used to induce crosslinking of organogels by causing the formation of disulfides. (A) Polymers used for force curing. (B) When force is applied in the presence of piezoelectric nanoparticles, disulfide bonds are formed. (C) Crosslinking for the different polymer systems after sonication occurs: PMMA, PMA, and PS (from left to right). *Adapted with permission from Ref. 85 Copyright 2019 American Chemical Society.*

A feature of the initial RAFT polymerizations by Zhang is the moderate initiator efficiencies ranging from ca. 6.1-44.8%. Following the initial report and inspired by the work of Pang examining the effects of the structure of ZnO on piezoelectric activity,[82] Zhang improved the efficiency of the system by synthesizing "tuned" ZnO nanomaterials. ZnO hexagonal rods containing polar facets (i.e., crystal faces) improved piezoelectric catalytic activity and consequently increased initiator efficiency.[86] In addition to improving initiator efficiency, this report also demonstrates that using an optimized trithiocarbonate chain transfer agent leads to better agreement of experimental M_n and theoretical M_n with lower dispersities.

1.4 Ball Milled Polymerizations

In 2023, Stenzel and coworkers further examine the utility of mechanoredox-mediated polymerizations by studying the nature of $BaTiO_3$ nanoparticles in more depth. Looking into water adsorbed to the surface of the nanoparticles, they report the generation of hydroxy radicals when ball milled in the presence of a hydroxyl specific radical trap, terephthalic acid, with an increase in radical production in the presence of oxygen relative to an inert environment. The qualitative production of surface radicals was even possible by striking samples with a hammer! After demonstrating and quantifying radical formation, solid vinyl monomers were added to the reaction vessel and polymerized in high conversion to access high molar mass polymers (>250 kDa) without the need for any additional initiator or exogenous additives, although mechanochemical chain degradation is observed as milling time increases. While surface radical concentration increases in air, the polymerization system does need to be conducted in an inert environment.[56] Interestingly, crosslinking is also possible in the ball mill (Figure 1.9) to form an insoluble $BaTiO_3$-poly(acrylamide) composite that is both swellable and moldable. It is hypothesized that interchain radical transfer causes the branching and physical self-crosslinking that would be required to form the insoluble material. Other solid-state polymerizations have now been developed as well.[100,101]

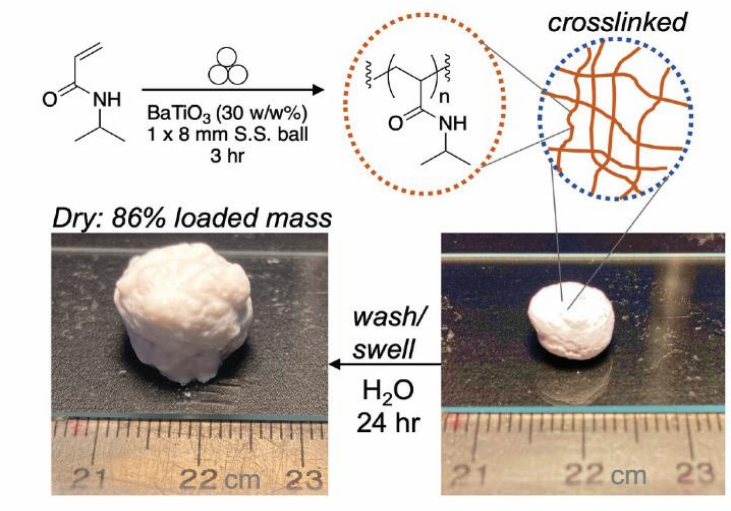

Figure 1.9 Stenzel conducted polymerization of acrylamides in the ball mill which can then form physical crosslinks. *Adapted with permission from Ref. 56. Copyright 2023 Wiley Journals.*

1.5 Future Outlook for Mechanoredox-Mediated Polymerizations

The burgeoning field of mechanoredox polymerizations offers opportunities to optimize systems that provide more penetrable, energy efficient, and environmentally friendly opportunities for the synthesis of commodity and novel polymers alike. From FRP and RDRP reactions to crosslinking mechanisms using diverse mechanical and piezoelectric sources, we as a field have merely scratched the surface of using mechanoredox catalysis for constructive polymer chemistry.[17,56,68–70,73,76,82,84–86,100] Yet, there are still many unanswered challenges that exist, including the quantification of "force" in a given system, recapitulating mechanoredox processes on large scale, exploring the scope of mechanoredox catalysts for specific applications (including the use of organic piezoelectric materials), and pushing the limits on accessing soft materials that are fully *inaccessible* using solution-state processes. Even more, the utility of mechanoredox chemistry will surely reach beyond polymer synthesis and into more applied areas of research such as the synthesis of anisotropic composites and layered materials. Finally, the life cycle and technoeconomic analyses of mechanoredox reactions need to be evaluated; a significant advantage of using mechanical force is the diminished need for toxic solvents and lower energy consumption. Building upon the work of small molecule

chemists and physicists, we can continue to improve our systems and incorporate the concepts of mechanoredox into new methods and applications, developing more sustainable methods to make novel materials that are impossible, or at least challenging, and/or inefficient to make using the current state of the art.

1.6 Dissertation Summary

Here within, I will address the work I have conducted in the Golder lab contributing to this developing field. In Chapter 2, I will begin with discussion of early demonstrations of "onium" salt initiated free radical polymerizations. I will then highlight the advances made to utilize mechanochemistry to synthesize polymers via reversible addition fragmentation chain transfer polymerizations (RAFT) in Chapter 3 and expand upon current work to utilize these chemistries to make unique multiblock polymers.

I developed mechanochemical free radical polymerizations utilizing "onium" salt aryl radical precursors as polymerization initiators first using ultrasound and then with ball milling. Aryl iodonium salts have been the primary initiator used in this work, although extensive examination of aryl diazonium salts and aryl sulfonium salts was conducted in preliminary studies. Different piezoelectric nanoparticles, $BaTiO_3$ and ZnO, are compared in their ability to transfer mechanical force into redox potential. The influence of different solvents used for liquid assisted grinding on reactivity and monomer scope is also discussed in detail. Also, the kinetic profiles and unique reactivity of the polymerizations set up on the benchtop and in inert environments are explored. Finally, the synthesis and mechanical testing of nanoparticle-containing composite materials is introduced, highlighting the utility of such materials.

Building upon the free radical polymerizations, I, along with my colleagues, then began developing a mechanochemical reversible deactivation radical polymerization technique, mechanoredox RAFT. Using the same aryl radical initiators, RAFT was conducted using multiple force sources, ultrasound, ball milling, and vortexing, achieving high monomer

conversion, control over chain length, and an expanded monomer scope. The ability to readily synthesize high χ block copolymers for unique self-assembly is discussed, demonstrating the ability to scale up such syntheses. Finally, as a significant advantage of mechanochemistry is lower energy stimuli sources, the energy consumption of different sources, a ball mill, a vortexer, and a traditional hot plate and stirrer, is presented showing significantly less energy being consumed by the mechanochemical sources than the traditional source.

As an exciting application, mechanoredox RAFT has been used to make multiblock polymers with varying monomer incorporation. First, extended up to pentablock incorporation, traditionally compatible monomers with similar solubilities and mechanical properties act as a proof of concept that this chemistry is highly effective in making distinct multiblock polymers. As mechanochemistry has less reliance on solvent than traditional methods, immiscible and incompatible monomers are also shown to be uniquely polymerized together in multiblock polymers as well. Additionally, the expansiveness of the chemistry is further demonstrated via the ability to synthesize very well defined but short blocks.

The work discussed in this dissertation lays a solid foundation for the expansion of mechanochemical polymer synthesis. Though varying utilities of this chemistry have already been shown, future work will show that it can be used to make materials with exclusive self-assembly and mechanical properties. Additionally, these initial studies have begun to highlight the sustainability of mechanoredox, but there is still extensive work needed to show that these syntheses can be an effective, scalable way to make commodity polymers at the industrial level.

1.7 Publication Acknowledgements

This chapter was adapted from the publication below publication:

- **S. Zeitler**, M. Golder, *Chem. Commun.,* 2024, **60**, 26-35.

1.8 References

1 B. Yamada and P. B. Zetterlund, *Handbook of Radical Polymerization*, John Wiley and Sons Inc., Hoboken, NJ, 2002.

2 D. Colombani, *Prog. Polym. Sci.*, 1997, **22**, 1649–1720.

3 Z. Wang, J. Wang, J. Ayarza, T. Steeves, Z. Hu, S. Manna and A. P. Esser-Kahn, *Nat. Mater.*, 2021, **20**, 869–874.

4 G. Moad, J. Chiefari, R. T. A. Mayadunne, C. L. Moad, A. Postma, E. Rizzardo and S. H. Thang, *Macromol. Symp.*, 2002, **182**, 65–80.

5 J. Chiefari, Y. K. Chong, F. Ercole, J. Krstina, J. Jeffery, T. P. T. Le, R. T. A. Mayadunne, G. F. Meijs, C. L. Moad, G. Moad, E. Rizzardo and S. H. Thang, *Macromolecules*, 1998, **31**, 5559–5562.

6 K. Matyjaszewski and J. Xia, *Chem. Rev.*, 2001, **101**, 2921–2990.

7 H. S. Bisht and A. K. Chatterjee, *J. Macromol. Sci. – Rev. Macromol. Chem. Phys.*, 2001, 41, 139–173.

8 S. Perrier, *Macromolecules*, 2017, **50**, 7433–7447.

9 G. Moad, E. Rizzardo and S. H. Thang, *Aust. J. Chem*, 2009, **62**, 1402–1472.

10 K. Matyjaszewski, *Isr. J. Chem.*, 2012, **52**, 206–220.

11 K. Matyjaszewski, *Macromolecules*, 2012, **45**, 4015–4039.

12 B. P. Fors and C. J. Hawker, *Angew. Chem. Int. Ed.*, 2012, **51**, 8850–8853.

13 P. Chmielarz, A. Sobkowiak, M. Fantin, S. Park, K. Matyjaszewski, A. A. Isse, A. Gennaro and A. J. D. Magenau, *Prog. Polym. Sci.*, 2017, **69**, 47–78.

14 X. Pan, M. Fantin, F. Yuan and K. Matyjaszewski, *Chem. Soc. Rev.*, 2018, **47**, 5457–5490.

15 S. Dadashi-Silab, M. Atilla Tasdelen, A. Mohamed Asiri, S. Bahadar Khan and Y. Yagci, *Macromol. Rapid Commun.*, 2014, **35**, 454–459.

16 J. L. Howard, Q. Cao and D. L. Browne, *Chem. Sci.*, 2018, **9**, 3080–3094.

17 P. Chakma, S. M. Zeitler, F. Baum, J. Yu, W. Shindy, L. D. Pozzo and M. R. Golder, *Angew. Chem. Int. Ed.*, 2023, **62**, e202215733.

18 T. Otsu, *J. Poly. Sci.*, 1956, **221**, 559–561.

19 M. A. Tasdelen, B. Kiskan and Y. Yagci, *Macromol. Rapid Commun.*, 2006, **27**, 1539–1544.

20 M. A. Tasdelen, N. Moszner and Y. Yagci, *Polym. Bull.*, 2009, **63**, 173–183.

21 F. Zhang, L. Zhu, Z. Li, S. Wang, J. Shi, W. Tang, N. Li and J. Yang, *Addit. Manuf.*, 2021, 48.

22 N. Corrigan, J. Yeow, P. Judzewitsch, J. Xu and C. Boyer, *Angew. Chem. Int. Ed,* 2019, **58**, 5170-5189.

23 M. Chen, Y. Gu, A. Singh, M. Zhong, A. M. Jordan, S. Biswas, L. T. J. Korley, A. C. Balazs and J. A. Johnson, *ACS Cent. Sci.*, 2017, **3**, 124–134.

24 J. Xu, K. Jung, A. Atme, S. Shanmugam and C. Boyer, *J. Am. Chem. Soc.*, 2014, **136**, 5508–5519.

25 K. Chen, Y. Zhou, S. Han, Y. Liu and M. Chen, *Angew. Chem. Int. Ed.,* 2022, **61**, e202116135.

26 J. C. Theriot, C.-H. Lim, H. Yang, M. D. Ryan, C. B. Musgrave and G. M. Miyake, *Science*, 2016, **352**, 1082–1086.

27 V. Kottisch, Q. Michaudel and B. P. Fors, *J. Am. Chem. Soc.*, 2017, **139**, 10665–10668.

28 N. J. Treat, H. Sprafke, J. W. Kramer, P. G. Clark, B. E. Barton, J. Read De Alaniz, B. P. Fors and C. J. Hawker, *J. Am. Chem. Soc.*, 2014, **136**, 16096–16101.

29 J. A. Leitch and D. L. Browne, *Chem. Eur. J.*, 2021, **27**, 9721–9726.

30 W. H. Binder, *Polymer*, 2020, **202**, 122639.

31 H. T. Baytekin, B. Baytekin and B. A. Grzybowski, *Angew. Chem. Int. Ed.*, 2012, **51**, 3596–3600.

32 J. Kwiczak-Yiğitbaşı, M. Demir, R. E. Ahan, S. Canlı, U. Ö. Şafak Şeker and B. Baytekin, *ACS Sustain. Chem. Eng.*, 2020, **8**, 18879–18888.

33 Z. J. Wang, J. Jiang, Q. Mu, S. Maeda, T. Nakajima and J. P. Gong, *J. Am. Chem. Soc.*, 2022, **144**, 3154–3161.

34 M. K. Beyer and H. Clausen-Schaumann, *Chem. Rev.*, 2005, **105**, 2921–2948.

35 A. Krusenbaum, S. Grätz, G. T. Tigineh, L. Borchardt and J. G. Kim, *Chem. Soc. Rev.*, 2022, **51**, 2873–2905.

36 H. Y. Cho and C. W. Bielawski, *Angew. Chem. Int. Ed.*, 2020, **59**, 13929–13935.

37 G. S. Lee, H. W. Lee, H. S. Lee, T. Do, J.-L. Do, J. Lim, G. I. Peterson, T. Friščić and J. G. Kim, *Chem. Sci.*, 2022, **68**, 42–61.

38 N. Ohn, J. Shin, S. S. Kim and J. G. Kim, *ChemSusChem*, 2017, **10**, 3529–3533.

39 C. V. Oprea and F. Weiner, *Acta Polym.*, 1987, **38**, 429–432.

40 G. S. Lee, B. R. Moon, H. Jeong, J. Shin and J. G. Kim, *Polym. Chem.*, 2019, **10**, 539–545.

41 M. B. Larsen and A. J. Boydston, *Macromol. Chem. Phys.*, 2016, **217**, 354–364.

42 S. Grätz, M. Oltermann, E. Troschke, S. Paasch, S. Krause, E. Brunner and L. Borchardt, *J. Mater. Chem. A Mater.*, 2018, **6**, 21901–21905.

43 H. Y. Cho and C. W. Bielawski, *Angew. Chem. Int. Ed.*, 2020, **59**, 13929–13935.

44 O. Maurin, P. Verdié, G. Subra, F. Lamaty, J. Martinez and T. X. Métro, *Beilstein J. Org. Chem.*, 2017, **13**, 2087–2093.

45 M. B. Starr and X. Wang, *Sci. Rep.*, 2013, **3**, 2160.

46 A. Aabid, M. A. Raheman, Y. E. Ibrahim, A. Anjum, M. Hrairi, B. Parveez, N. Parveen and J. Mohammed Zayan, *Sensors*, 2021, **21**, 4145.

47 T. D. Usher, K. R. Cousins and S. Ducharme, *Poly. Int.,* 2018, **67**, 790-798.

48 A. Cafarelli, A. Marino, L. Vannozzi, J. Puigmartí-Luis, S. Pané, G. Ciofani and L. Ricotti, *ACS Nano*, 2021, **15**, 11066–11086.

49 H. Xia and Z. Wang, *Science*, 2019, **366**, 1450–1451.

50 Z. Ren, Y. Peng, H. He, C. Ding, J. Wang, Z. Wang and Z. Zhang, *Chin. J. Chem.*, 2023, 41, 111–128.

51 E. M. Marrero, C. J. Caprara, C. N. Gilbert, E. E. Blanco and R. G. Blair, *Faraday Discuss.*, 2022, **241**, 91–103.

52 K. S. Hong, H. Xu, H. Konishi and X. Li, *J. Phys. Chem. Lett.*, 2010, **1**, 997–1002.

53 S. Ikeda, T. Takata, M. Komoda, M. Hara, J. N. Kondo, K. Domen, A. Tanaka, H. Hosono and H. Kawazoe, *Phys. Chem. Chem. Phys.*, 1999, **1**, 4485–4491.

54 J. M. Wu, Y.-G. Sun, W.-E. Chang and J.-T. Lee, *Nano Energy*, 2018, **46**, 372–382.

55 K. Kubota, Y. Pang, A. Miura and H. Ito, *Science*, 2019, **366**, 1500–1504.

56 M. D. Nothling, J. E. Daniels, Y. Vo, I. Johan and M. H. Stenzel, *Angew. Chem. Int. Ed.*, 2023, **62**, e202218955.

57 K. S. Suslick, *Science*, 1990, **247**, 1439–1445.

58 G. Cravotto, E. C. Gaudinoa and P. Cintas, *Chem. Soc. Rev.*, 2013, **42**, 7521–7534.

59 P. A. May and J. S. Moore, *Chem. Soc. Rev.*, 2013, **42**, 7497–7506.

60 T. Friščić, C. Mottillo and H. M. Titi, *Angew. Chem. Int. Ed.*, 2019, **59**, 1018–1029.

61 T. Friščić, L. Fábián, J. C. Burley, W. Jones and W. D. S. Motherwell, *Chem. Commun.*, 2006, 5009–5011.

62 T. Friščić, A. V. Trask, W. Jones and W. D. S. Motherwell, *Angew. Chem. Int. Ed.*, 2006, **45**, 7546–7550.

63 N. Shan, F. Toda and W. Jones, *Chem. Commun.*, 2002, 2372–2373.

64 P. Ying, J. Yu and W. Su, *Adv. Synth. Catal.*, 2021, **363**, 1246–1271.

65 T. G. McKenzie, E. Colombo, Q. Fu, M. Ashokkumar and G. G. Qiao, *Angew. Chem. Int. Ed.*, 2017, **56**, 12302–12306.

66 J. Collins, T. G. McKenzie, M. D. Nothling, M. Ashokkumar and G. G. Qiao, *Polym. Chem.*, 2018, **9**, 2562–2568.

67 G. S. Lee, H. W. Lee, H. S. Lee, T. Do, J. L. Do, J. Lim, G. I. Peterson, T. Friščić and J. G. Kim, *Chem. Sci.*, 2022, **13**, 11451–11698.

68 H. Mohapatra, M. Kleiman and A. P. Esser-Kahn, *Nat. Chem.*, 2017, **9**, 135–139.

69 Z. Wang, X. Pan, J. Yan, S. Dadashi-Silab, G. Xie, J. Zhang, Z. Wang, H. Xia and K. Matyjaszewski, *ACS Macro. Lett.*, 2017, **6**, 546–549.

70 Z. Wang, X. Pan, L. Li, M. Fantin, J. Yan, Z. Wang, Z. Wang, H. Xia and K. Matyjaszewski, *Macromolecules*, 2017, **50**, 7940–7948.

71 P. Zhu, Y. Chen and J. Shi, *Adv. Mat.*, 2020, **32**, e202001976.

72 Z. Xue, D. He and X. Xie, *Polym. Chem.*, 2015, **6**, 1660–1687.

73 Z. Wang, J. Ayarza and A. P. Esser-Kahn, *Angew. Chem. Int. Ed.*, 2019, **58**, 12023–12026.

74 M. Chen, M. Zhong and J. A. Johnson, *Chem. Rev.*, 2016, **116**, 10167–10211.

75 T. G. McKenzie, F. Karimi, M. Ashokkumar and G. G. Qiao, *Chem. – Eur. J.*, 2019, **25**, 5372–5388.

76 S. M. Zeitler, P. Chakma and M. R. Golder, *Chem. Sci.*, 2022, **13**, 4131–4138.

77 E. A. Merritt and B. Olofsson, *Angew. Chem. Int. Ed.,* 2009, **48**, 9052–9070.

78 H. E. Bachofner, F. M. Beringer and L. Meites, *J. Am. Chem. Soc.*, 1958, **80**, 4274–4278.

79 Z. Ren, C. Ding, R. Ding, J. Wang, Z. Li, R. Tan, X. Wang, Z. Wang and Z. Zhang, *ACS Macro. Lett.*, 2023, **12**, 1159–1165.

80 L. Kou and W. Guo, *IEEE*, 2008, 354–359.

81 S. Goel and B. Kumar, *J. Alloys Compd.*, 2020, 816.

82 K. Liu, W. Zhang, L. Zong, Y. He, X. Zhang, M. Liu, G. Shi, X. Qiao and X. Pang, *J. Phys. Chem. Lett.*, 2022, **13**, 4884–4890.

83 S. Xu, W. Zhang, C. Wang, W. Peng, G. Shi, Z. Cui, P. Fu, M. Liu, Y. He, X. Qiao and X. Pang, *Polymer*, 2022, **252**, 124949.

84 C. Ding, Y. Yan, Y. Peng, D. Wu, H. Shen, J. Zhang, Z. Wang and Z. Zhang, *Macromolecules*, 2022, **55**, 4056–4063.

85 J. Ayarza, Z. Wang, J. Wang and A. P. Esser-Kahn, *ACS Macro. Lett.*, 2021, **10**, 799–804.

86 C. Ding, Z. Ren, J. Wang, L. Zhang, Y. Yan, D. Wu, Z. Wang and Z. Zhang, *Chin. J. Chem.*, 2023, **41**, 2691–2696.

87 G. I. Peterson, W. Ko, Y. J. Hwang and T. L. Choi, *Macromolecules*, 2020, **53**, 7795–7802.

88 W. Yao, Y. Li and X. Huang, *Polymer*, 2014, **55**, 6197–6211.

89 Y. Koda, T. Terashima, M. Sawamoto and H. D. Maynard, *Polym. Chem.*, 2015, **6**, 240–247.

90 L. Chen and F. Wu, *J. Appl. Polym. Sci.*, 2012, **125**, 376–381.

91 H. Gong, Y. Gu and M. Chen, *Synlett*, 2018, **29**, 1543–1551.

92 K. Chen, X. Guo and M. Chen, *Angew. Chem. Int. Ed.*, 2023, **62**, e202310636.

93 Y. Inoue, J. Watanabe, M. Takai, S. I. Yusa and K. Ishihara, *J. Polym. Sci. A: Polym. Chem.*, 2005, **43**, 6073–6083.

94 S. Perrier, S. G. Jackson, D. M. Haddleton, B. Améduri and B. Boutevin, *Macromolecules*, 2003, **36**, 9042–9049.

95 H. Gong, Y. Zhao, X. Shen, J. Lin and M. Chen, *Angew. Chem. Int. Ed.*, 2018, **57**, 333–337.

96 J. Xia, T. Johnson, S. G. Gaynor, K. Matyjaszewski and J. DeSimone, *Macromolecules*, 1999, **32**, 4802–4805.

97 E. H. Discekici, A. Anastasaki, R. Kaminker, J. Willenbacher, N. P. Truong, C. Fleischmann, B. Oschmann, D. J. Lunn, J. Read De Alaniz, T. P. Davis, C. M. Bates and C. J. Hawker, *J. Am. Chem. Soc.*, 2017, **139**, 5939–5945.

98 A. Anastasaki, B. Oschmann, J. Willenbacher, A. Melker, M. H. C. Van Son, N. P. Truong, M. W. Schulze, E. H. Discekici, A. J. McGrath, T. P. Davis, C. M. Bates and C. J. Hawker, *Angew. Chem. Int. Ed.*, 2017, **56**, 14483–14487.

99 Z. Ma and P. Lacroix-Desmazes, *J. Polym. Sci. A: Polym. Chem.*, 2004, **42**, 2405–2415.

100 M. Zhou, Y. Zhang, G. Shi, Y. He, Z. Cui, X. Zhang, P. Fu, M. Liu, X. Qiao and X. Pang, *ACS Macro. Lett.*, 2023, **12**, 26–32.

101 F. Effaty, L. Gonnet, S. G. Koenig, K. Nagapudi, X. Ottenwaelder and T. Friščić, *Chem. Commun.*, 2022, **59**, 1010–1013.

Chapter 2: Mechanoredox Free Radical Polymerization

2.1 Introduction

Mechanochemistry[1–5] is an interdisciplinary field spanning small molecule methodology, crystal engineering and polymer science. Chemical processes induced by mechanical force offer advantages over other stimuli. For example, undesirable thermal byproducts can be avoided and limited stimuli penetration (e.g. photochemistry) into solutions can be mitigated.[1,5] For macromolecules, force-responsive polymers with engineered mechanophores[6,7] can change color[8], alter bulk electronic[9] or structural[10–13] properties, and release cargo[14,15] on demand via mechanochemically-driven processes; such systems find utility in sensing[10], additive manufacturing[16,17], and therapeutic delivery[18,19] applications. One common form of mechanochemical input is ultrasound (US) irradiation.[20] Ultrasonic waves in solution generate cavitation bubbles[21] that collapse and produce forces that fuel subsequent chemical processes. US itself is readily accessible and has numerous biological applications[22–24] in diagnostic imaging[25] and targeted drug release[26,27]. A complimentary method to generate force in mechanochemical systems is ball mill grinding, a sustainable and economical technique due to the removal of nearly all solvent.[3] This industrially scalable technology was originally developed for the breakdown of minerals and biopolymers[28] but recently became a widespread method for solid-state synthesis.[3,29] The ubiquity of force-induced macromolecular *deconstruction* largely dominates the field of mechanochemistry, even back to Staudinger's work breaking down polymers mechanochemically.[30] Counterintuitively, analogous systems also exist that *construct* matter[31] via covalent bond formations under mechanical stimulation.

One mechanism to facilitate the use of force in chemical synthesis is mechanoredox catalysis[32] (Figure 2.1); the piezoelectric effect[33–36] converts mechanical energy into a usable electric potential. Many applications mirror bone growth[37] and mechanogenetics[24,38] mechanisms found in biological systems. Other uses of piezoelectric materials and molecules

include water splitting and treatment.[39–42] Wearable devices can also utilize piezoelectricity as a means to couple human motion with energy storage.[43] Only recently have chemists used this concept in modern synthetic polymer chemistry to conduct redox reactions (i.e. mechanoredox catalysis). Several examples now exist that harness US and the piezoelectric effect via piezoactive nanopaticles to drive mechanoredox polymerization processes (Figure 2.1A).[33] Both the Esser-Kahn and Matyjaszewski groups have developed systems where piezoelectric nanoparticles (PNP) facilitate either free radical polymerization (FRP) or atom transfer radical polymerization (ATRP) in the presence of US.[44–47] While both works demonstrate the feasibility of mechanoredox-initiated polymerizations, these methods require transition metal additives (e.g. copper or iron salts)[45,46] and have significant non-mechanoredox background reactions.[44,45] The current state of the art leaves vast opportunities to further refine mechanoredox polymerization methodology and expand its scope of usability. Such fundamental developments are imperative to the development and implementation of next-generation stimuli-responsive soft materials.

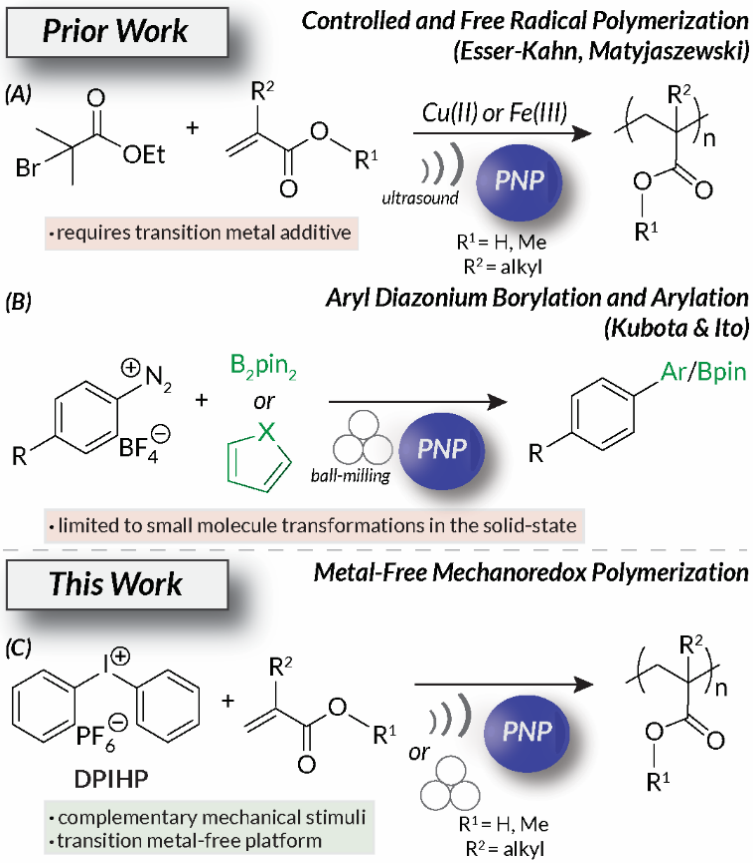

Figure 2.1 Evolution of **(A)** mechanoredox polymerizations and **(B)** small molecule transformations (e.g., borylation, arylation) as an inspiration for **(C)** our metal-free ultrasonic irradiation and ball milling mechanoredox polymerization methodology.

PNPs are also used to drive small molecule mechanoredox transformations. In recent work by Kubota and Ito, ball mill grinding with PNPs (e.g. ZnO, $BaTiO_3$) initiates C-H borylations and arylation reactions (Figure 2.1B).[48] Similar solid-state techniques also affect aryl trifluoromethylation[49] and atom-transfer radical cyclization reactions.[50] Interestingly, mechanoredox radical *polymerizations* have never been initiated under ball milling conditions. In the initial small molecule mechanoredox study by Kubota and Ito, aryl diazonium salts were used as "initiators" to drive the subsequent radical C-H functionalization reactions.[48] These salts, along with other aryl "onium" salts (e.g. diaryl iodoniums and triaryl sulfoniums), have been used in photoredox systems as tuneable aryl radical[51] surrogates with varying reduction potentials[52]; aryl diazoniums are extremely easy to reduce while diaryl iodoiniums and triaryl sulfoniums (E_{red} = –0.3 V to –1.0 V vs. SCE) are significantly less susceptible to reduction. The reactivity of "onium" salts can be further manipulated through substituent effects, leading

to a wide array of reactivity.[53] Many "onium" salts are also either commercially available or readily synthesized, making them accessible, bench-stable building blocks for synthetic manipulations. Furthermore, "onium" salts can be integrated into soft material, presenting opportunities for tuneable polymer grafting and composites.[54,55]

Using these recent works as inspiration, we now report the mechanoredox "onium" salt-initiated FRP of (meth)acrylates under both ultrasonic irradiation and ball milling conditions (Figure 2.1C). This work details the first examples of metal-free mechanoredox polymerizations and compares the consequences of these conditions under complementary reaction conditions (i.e. ultrasonic irradiation and ball mill grinding). Overall, we demonstrate the broad application of mechanical force to access industrially relevant high molecular weight polymeric materials without relying on traditional thermal[56–58] or photochemical[59–62] inputs.

2.2 Ultrasonic Irradiation (US) Mechanoredox Polymerizations

Inspired by the work[48] of Kubota and Ito, we initially questioned whether aryl diazonium salts could be used as mechanoredox initiators for FRP of commercially available acrylates. To investigate, 4-bromobenzenediazonium tetrafluoroborate (BBDT) and 4-methoxybenzenediazonium tetrafluoroborate (MBDT) were used as initiators in the presence of a suitable PNP (e.g. ZnO or $BaTiO_3$) and acrylate monomer. Degassed reaction mixtures were immersed into a temperature-controlled ultrasonic bath (see Figure 2.2 for a typical reaction setup). While high monomer conversion was achieved in a variety of different organic solvents in the presence of both US and PNPs, similar results were obtained in the absence of US (Table 2.1). Despite numerous examples employing BBDT or MBDT as aryl radical precursors in (photo)redox processes[52], we found after extensive studies that aryl diazoniums were too capricious to use in this system. The background reactions in the absence of force affirm that even a low concentration of radicals, presumably from aryl diazonium decomposition in solution, can initiate FRP. These early studies prompted us to investigate

alternative “onium” salts with more negative reduction potentials; we rationalized that such initiators would exhibit superior solution-state stability.

Figure 2.2: Photograph of a typical US-mediated FRP reaction setup. Reaction vials are immersed into the water bath via clamps and a coiled copper tube connected to a recirculating chiller is used for temperature control of the bath.

Table 2.1: Results for US-mechanoredox FRP using aryl diazonium initiators.

Entry	Nanoparticle	Ultrasound?	Monomer	Solvent	Initiator	Conversion (%)[c]
1[a]	ZnO	Yes	*t*BA	DMAc	BBDT	95%
2[a]	ZnO	No	*t*BA	DMAc	BBDT	70%
3[a]	ZnO	Yes	BA	DMF	BBDT	90%
4[a]	ZnO	No	BA	DMF	BBDT	55%
5[a]	ZnO	Yes	*t*BA	DMAc	MBDT	63%
6[a]	ZnO	No	*t*BA	DMAc	MBDT	32%
7[b]	ZnO	Yes	EA	DMAc	MBDT	62%
8[b]	ZnO	No	EA	DMAc	MBDT	27%
9[a]	$BaTiO_3$	No	*t*BA	DMAc	BBDT	90%

Reaction conditions: $[monomer]_0$:$[diazonium\ salt]_0$ = 100:1, PNP loading: 7 wt%. Ultrasonic bath (40 kHz, 70 W, 20 °C). Reaction time: 20 h. [a] [monomer] = 7.3 M, [diazonium salt] = 0.073 M. [b] [monomer] = 9.3 M, [diazonium salt] = 0.093 M. [c] conversion was determined by ^{1}H NMR spectroscopy.

We hypothesized that diaryliodonium salts[63], which are more difficult to reduce (E_{red} = ca. –0.5 V vs. SCE), should be more stable in solution than aryl diazonium salts and thus be more suitable for mechanoredox FRP. To explore this new system, we first studied the polymerization of *tert*-butyl acrylate (*t*BA) in DMF by using diphenyl iodonium hexafluorophosphate (DPIHP) as our initiator (Table 2.2) with either $BaTiO_3$ or ZnO (Table 2.2, entries 1 – 5) as the PNP. With both PNPs, the reaction mixtures became visibly viscous within 8 h of sonication, suggesting high monomer conversion (see Figure 2.3 representative photographs). In the presence of 7 wt% $BaTiO_3$ and ZnO (relative to the combined mass of the monomer, solvent, and DPIHP), ^{1}H NMR analysis of the resulting polymers showed 92% and 68% monomer conversion after 20 h, respectively. In the absence of US or PNP, however, little to no conversion was observed over the same time course. A direct correlation of PNP loading to monomer conversion was observed, indicating the pivotal role of nanoparticles. Maximum monomer conversion was achieved with 7 wt% PNP, therefore this loading was used for all future experiments. Results remained consistent with high monomer conversion on scale-up (10x scale = 5 g tBA monomer) using $BaTiO_3$ (Figure 2.4), highlighting the potential scalability of ultrasonic irradiation mechanoredox polymerizations.

Table 2.2: Importance of nanoparticle identity for mechanoredox tBA FRP.

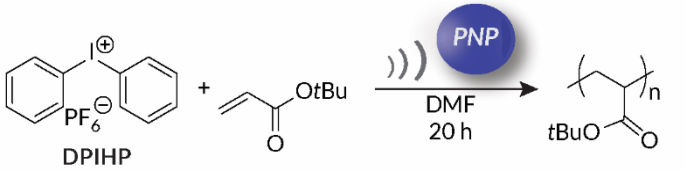

Entry[a]	Nanoparticle	Ultrasound?	Conversion (%) [b]
1	$BaTiO_3$ (1.5 wt%)	Yes	35
2	$BaTiO_3$ (3.5 wt%)	Yes	80
3	$BaTiO_3$ (7 wt%)	Yes	92
4	$BaTiO_3$ (7 wt%)	No	<5
5	ZnO (7 wt%)	Yes	70
6	TiO_2 (7 wt%)	Yes	17
7	None	Yes	14

Reaction conditions: $[monomer]_0:[DPIHP]_0$ = 100:1. [a] [*t*BA] = 7.3 M, [DPIHP] = 0.073 M in DMF; [b] conversion was determined by ^1H NMR spectroscopy. Ultrasonic bath (40 kHz, 70 W, 20 °C); Reaction time: 20 h.

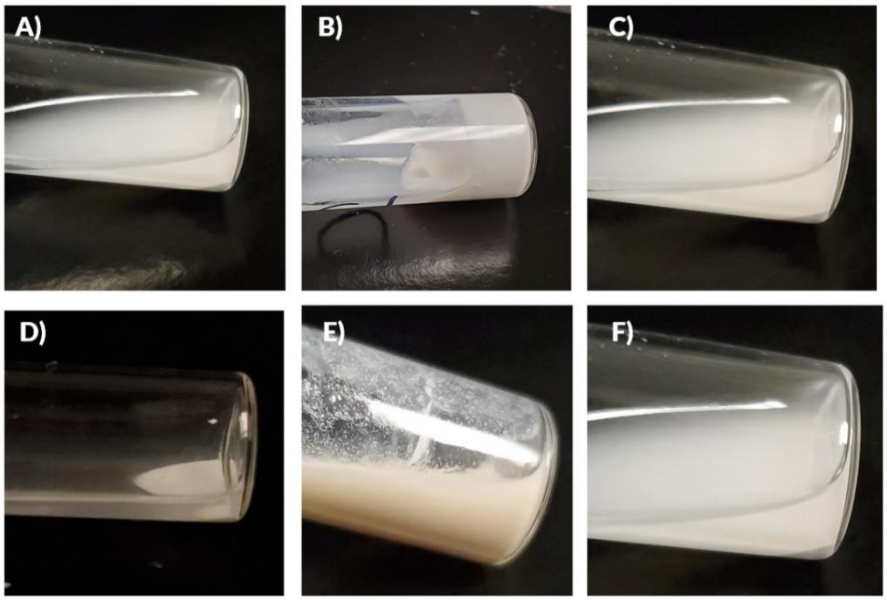

Figure 2.3: Photographs of US-mediated FRP reaction mixtures: A) at time = 0 h, $BaTiO_3$ (before sonication); B) at time = 20 h, $BaTiO_3$ (after sonication); C) at time = 20 h, $BaTiO_3$ (without sonication); D) at time = 0 h, ZnO (before sonication); E) at time = 20 h, ZnO (after sonication); F) at time = 20 h, TiO_2 (after sonication).

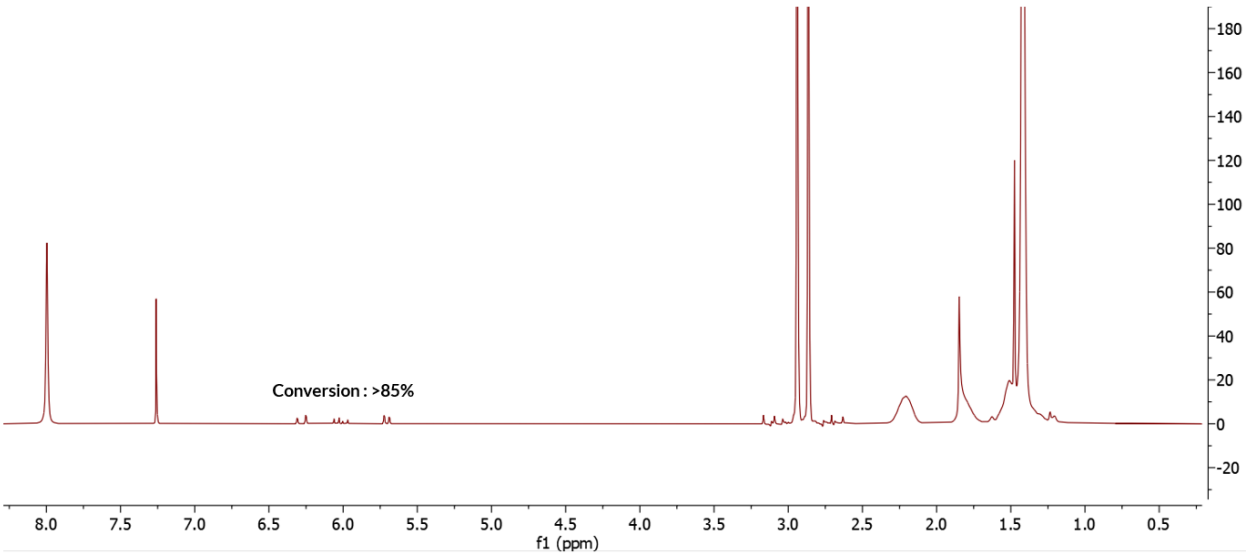

Figure 2.4: Representative crude ^{1}H NMR spectrum of poly(*t*BA) synthesized on 5 g scale in 10 mL round bottom flask using US-mechanoredox FRP. Reaction conditions $[t\text{BA}]_0$:$[\text{DPIHP}]_0$ = 100:1. [*t*BA] = 7.3 M in DMF. Ultrasonic bath (40 kHz, 70 W, 20 °C). Reaction time: 20 h. >85% monomer conversion is measured by ^{1}H NMR spectroscopy; M_n (GPC-MALS): 180 kDa.

Intriguingly, in the absence of either US (Table 2.2, entry 4) or PNP (Table 2.2, entry 7), no visual change to the reaction mixture was observed and little to no conversion was detected by ^{1}H NMR spectroscopy. Similar results (Figure 2.3) were obtained when a neutral non-PNP (TiO_2) was used (Table 2.2, entry 6). Based on these results, we surmised that solvent played a key role in the background processes (Table 2.2, entries 6 & 7) observed. While the exact nature of all initiating species is not fully clear, these collective data demonstrate the importance of iodonium salt for efficient polymerization.

We postulated that the trivial conversion (ca. 15%) measured in the absence of PNPs could be attributed to solvent initiated polymerization (Table 2.2, entry 7 and Figure 2.5). Organic solvent radicals are known to form in response to high frequency US (ca. 500 kHz); subsequent homolytic C-C, C-N, or C-H bond cleavage forms species that can initiate radical polymerization.[64–68] Unfortunately, the role of solvent radicals in background reactions are often overlooked in recent mechanoredox polymerization reports. To examine whether low frequency (40 kHz) US-mediated solvent radical generation can also induce significant

polymerization, control experiments were conducted where *t*BA was sonicated in different organic solvents without PNP and DPIHP. A maximum monomer conversion of 15% was observed over 20 h (Table 2.3), suggesting that although certain solvents can generate radicals in response to low frequency US, the local concentration of active initiator is not sufficient to achieve high monomer conversion.

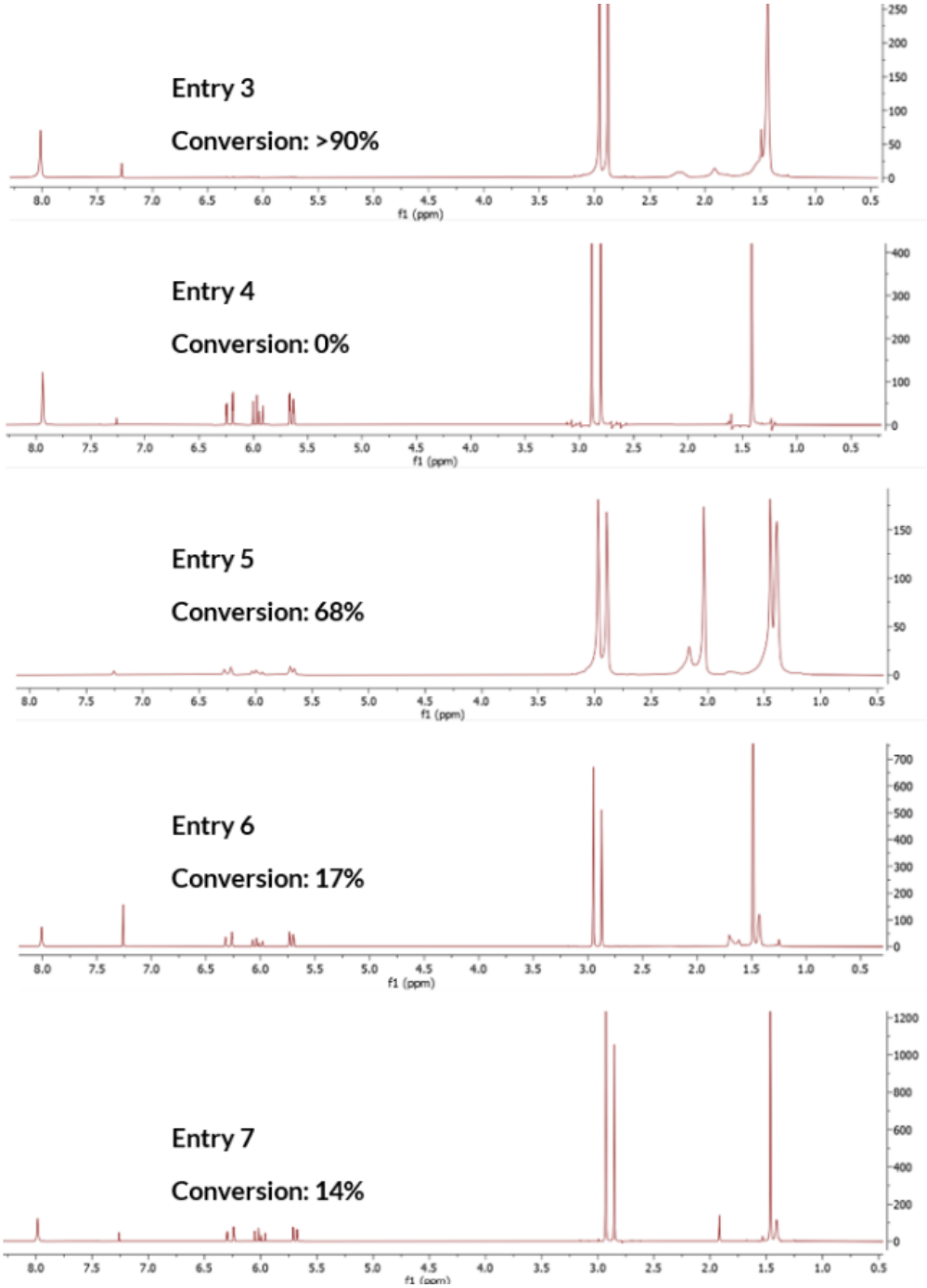

Figure 2.5: Representative crude ^{1}H NMR spectra of reaction mixtures from Table 2.2 in the main text.

Table 2.3: Results for US-promoted ("solvent initiated") FRP in different organic solvents.

Entry[a]	Solvent	Conversion (%) [b]
1	DMAc	13
2	DMF	12
3	DMSO	15
4	Dioxane	14
5	Toluene	0
6	Anisole	0

Reaction conditions: Ultrasonic bath (40 kHz, 70 W, 20 °C). Reaction time: 20 h. [a] [*t*BA] = 7.3 M; [b] Conversion was determined by ^{1}H NMR spectroscopy.

While the importance of PNPs is already established (Table 2.4, entry 1), additional control experiments were necessary to further probe the polymerization mechanism. When the DPIHP initiator was removed from the reaction mixture, less than 15% monomer conversion was observed in 20 h (Table 2.4, entry 2). The trivial monomer conversion can be attributed to US-mediated solvent radical polymerization (*vide supra*) and confirms the significant role the diaryliodonium salt plays in the observed US-mechanoredox FRPs. This result was corroborated with a simple control experiment; *t*BA and $BaTiO_3$ were sonicated in DMF without DPIHP for 8 h and ~10% conversion was observed by ^{1}H NMR spectroscopy. Upon addition of DPIHP to this reaction mixture, >90% monomer conversion was observed after an additional 12 h (20 h total reaction time) (Figure 2.6). Additionally, when polymerizations were run without exclusion of air (Table 2.4, entry 3) or with 1 equiv. of radical inhibitor 4-methoxyphenol (MEHQ) (Table 2.4, entry 4), <5% conversion was observed, supporting the envisaged free-radical polymerization mechanism.

Table 2.4: US-mechanoredox tBA polymerization control experiments.

Entry	Conditions	Conversion (%) [b]
1[a]	Standard reaction	92
2	Without DPIHP	14
3	Under air	<5
4	MEHQ (1:1 eq to DPIHP)	<5

Reaction conditions: $[monomer]_0:[DPIHP]_0 = 100:1$. Ultrasonic bath (40 kHz, 70 W, 20 °C); Reaction time: 20 h. [a] [*t*BA] = 7.3 M, [DPIHP] = 0.073 M in DMF, 7 wt% $BaTiO_3$; [b] conversion was determined by ^1H NMR spectroscopy.

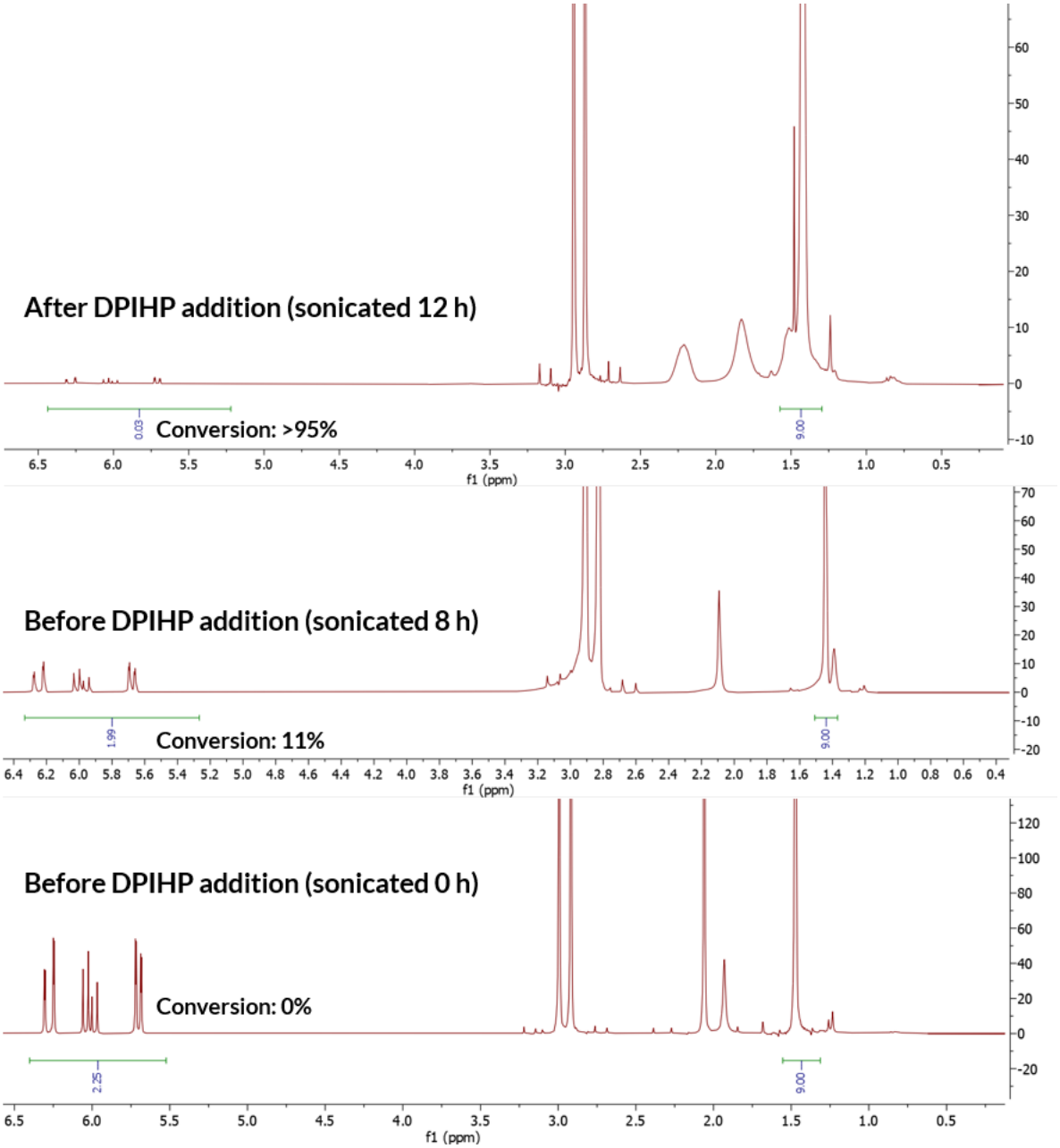

Figure 2.6: Crude ^{1}H NMR spectra of *t*BA US-mechanoredox FRP reaction mixtures **before DPIHP addition** (*t*BA, $BaTiO_3$, DMF; 8 h total reaction time) and **after DPIHP addition** (*t*BA, $BaTiO_3$, DPIHP, DMF; additional 12 h reaction time leads to 20 h total reaction time). Experimental conditions are given in the experimental section.

To further optimize reaction conditions, we then evaluated solvent scope in the mechanoredox polymerization of *t*BA with $BaTiO_3$ and ZnO (Table 2.5). In general, >30% monomer conversion was observed in polar aprotic organic solvents (i.e., DMF, DMAc, DMSO, 1,4-dioxane (Table 2.5, entries 1-8)) but no conversion was observed in non-polar solvents (i.e., toluene, anisole (Table 2.5, entries 9-12)). These differences are likely in part due to poor DPIHP solubility in less polar solvents. In all cases, <5% conversion was observed in the absence of US (Table 2.6). Additionally, when US- mechanoredox FRP was carried out in anhydrous solvent, no significant difference in monomer conversion was observed, confirming minimal radical generation from water.[68–70] Overall, higher monomer conversion was achieved using $BaTiO_3$ than with ZnO. Based upon these cumulative results (Table 2.5, entries 1-8), $BaTiO_3$/DMF and ZnO/DMAc were used for the remainder of the studies reported below.

Table 2.5: Results for US-mechanoredox *t*BA FRP in different solvents.

Entry[a]	Solvent	Nanoparticle	Conversion[b] (%)
1	DMF	$BaTiO_3$	92
2	DMF	ZnO	62
3	DMAc	$BaTiO_3$	82
4	DMAc	ZnO	68
5	DMSO	$BaTiO_3$	62
6	DMSO	ZnO	52
7	Dioxane	$BaTiO_3$	82
8	Dioxane	ZnO	32
9	Toluene	$BaTiO_3$	<5
10	Toluene	ZnO	<5
11	Anisole	$BaTiO_3$	<5
12	Anisole	ZnO	<5

Reaction conditions: $[monomer]_0:[DPIHP]_0 = 100:1$. Ultrasonic bath (40 kHz, 70W, 20 °C). Reaction time: 20 h. [a][*t*BA] = 7.3 M, [DPIHP] = 0.073 M; PNP loading: 7 wt%. [b] Conversion was determined by ^{1}H NMR spectroscopy.

Table 2.6: US-mechanoredox FRP controls: conversion of *t*BA in the absence of US as a function of solvent.

Entry[a]	Solvent	Nanoparticle	Conversion[b] (%)
1	DMF	$BaTiO_3$	<5
2	DMF	ZnO	<5
3	DMAc	$BaTiO_3$	<5
4	DMAc	ZnO	<5
5	DMSO	$BaTiO_3$	<5
6	DMSO	ZnO	<5
7	Dioxane	$BaTiO_3$	<5
8	Dioxane	ZnO	<5
9	Toluene	$BaTiO_3$	<5
10	Toluene	ZnO	<5
11	Anisole	$BaTiO_3$	<5
12	Anisole	ZnO	<5

Reaction conditions: $[monomer]_0:[DPIHP]_0 = 100:1$. Reaction time: 20 h, 23 °C. [a] [*t*BA] = 7.3 M, [DPIHP] = 0.073 M; PNP loading: 7 wt%. [b] Conversion was determined by ^1H NMR spectroscopy.

Next, to study the viability of the optimized conditions with other monomers, the mechanoredox polymerizations of butyl acrylate (BA), ethyl acrylate (EA), methyl acrylate (MA), and methyl methacrylate (MMA) were studied. The resulting monomer conversions (Table 2.7 and Figure 2.8A) reveal consistently higher conversions of $BaTiO_3$ reactions over ZnO reactions (Table 2.7 and Figure 2.8B) and acrylates over methacrylates. The number average molecular weights (M_n), and dispersity ($Đ = M_w/M_n$) data measured by gel permeation chromatography coupled with a multi-angle light scattering detector (GPC-MALS) reveals high molecular weight (>100 kDa) polymer with little control over dispersity as is expected

from a conventional mechanoredox FRP process (Figure 2.7). Again, no polymerization was observed when reactions were carried out in the absence of US (Table 2.8).

Table 2.7: Results for US-mechanoredox (meth)acrylate FRP.

Entry	Monomer	Nanoparticle	Conversion[d] (%)	M_n (kDa) [e]	Đ[e]
1[a]	*t*BA	$BaTiO_3$	92	284	1.7
2[a]	*t*BA	ZnO	68	347	1.6
3[a]	BA	$BaTiO_3$	82	431	1.8
4[a]	BA	ZnO	56	358	1.7
5[b]	EA	$BaTiO_3$	64	491	1.5
6[b]	EA	ZnO	51	533	1.5
7[c]	MA	$BaTiO_3$	78	1230	1.8
8[c]	MA	ZnO	32	357	2.0
9[b]	MMA	$BaTiO_3$	38	105	1.7
10[b]	MMA	ZnO	35	107	1.5

Reaction conditions: $[monomer]_0$:$[DPIHP]_0$ = 100:1. 7 wt% nanoparticle loading was used for all reactions. Ultrasonic bath (40 kHz, 70 W). Reaction time: 20 h. [a] [monomer] = 7.3 M, [DPIHP] = 0.073 M; [b] [monomer] = 9.3 M, [DPIHP] = 0.093 M; [c] [monomer] = 10.9 M, [DPIHP] = 0.109 M. DMF and DMAc were used as solvents for mechanoredox reactions with $BaTiO_3$ and ZnO, respectively. [d] Conversion was determined by ^{1}H NMR spectroscopy. [e] M_n and Đ were determined by GPC-MALS.

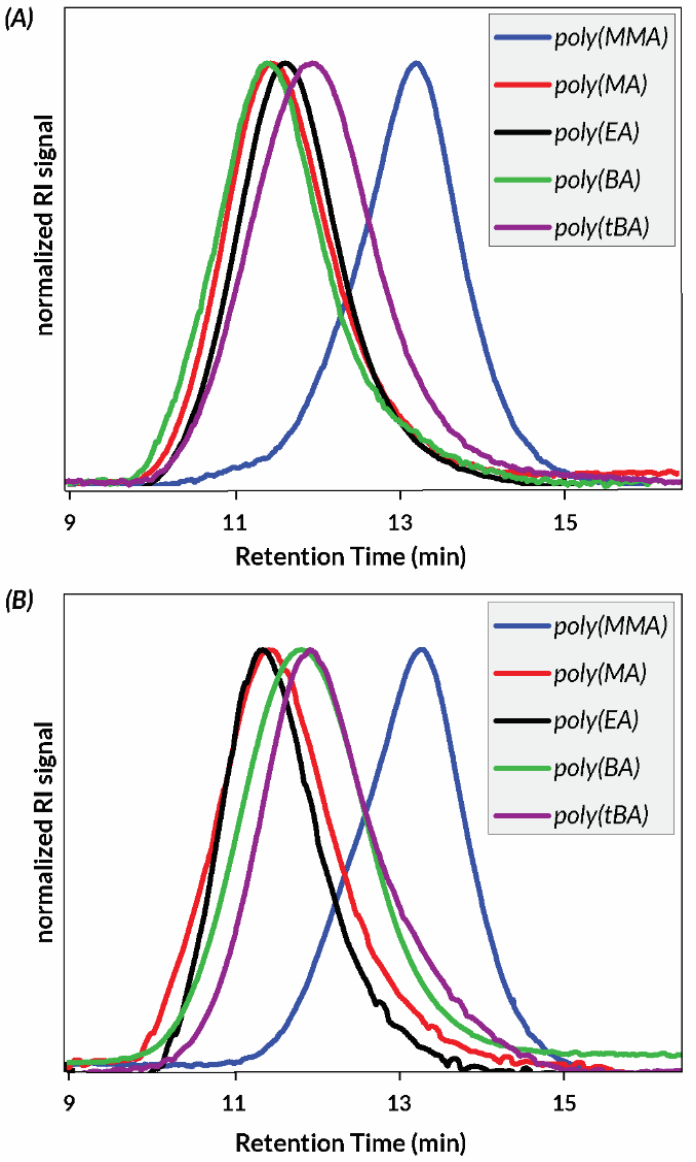

Figure 2.7 GPC-RI traces of US-mechanoredox (meth)acrylate FRP using **(A)** $BaTiO_3$ or **(B)** ZnO as the PNP (see Table 2.7).

Finally, *t*BA mechanoredox polymerization kinetics were studied and the resulting data were analysed by ^{1}H NMR spectroscopy and GPC-MALS., Within the 20 h reaction window, a time dependent progression of polymer formation was observed. Polymerizations were faster with $BaTiO_3$ than with ZnO at all analysed time points. In both cases, high molar mass polymer was observed from GPC-MALS traces, indicating fast propagation rates relative to initiation rates. To study whether any decrease in M_n over time (Figure 2.8) was due to mechanochemical polymer cleavage,[71] US-mediated chain scission experiments were carried out on DMF solutions of freshly synthesized poly(*t*BA) and poly(MMA). After sonication for 24 h, analysis of the resulting materials by GPC-MALS (Figure 2.9) indicated that mechanochemical chain scission is operative at extended reaction times. For example, 170 kDa poly(*t*BA) synthesized through US-mechanoredox FRP was reduced to 21 kDa after prolonged ultrasonication. Hence, we believe that the observed molecular weight evolutions (Figure 2.8) likely are complicated through competing propagation and chain scission pathways.

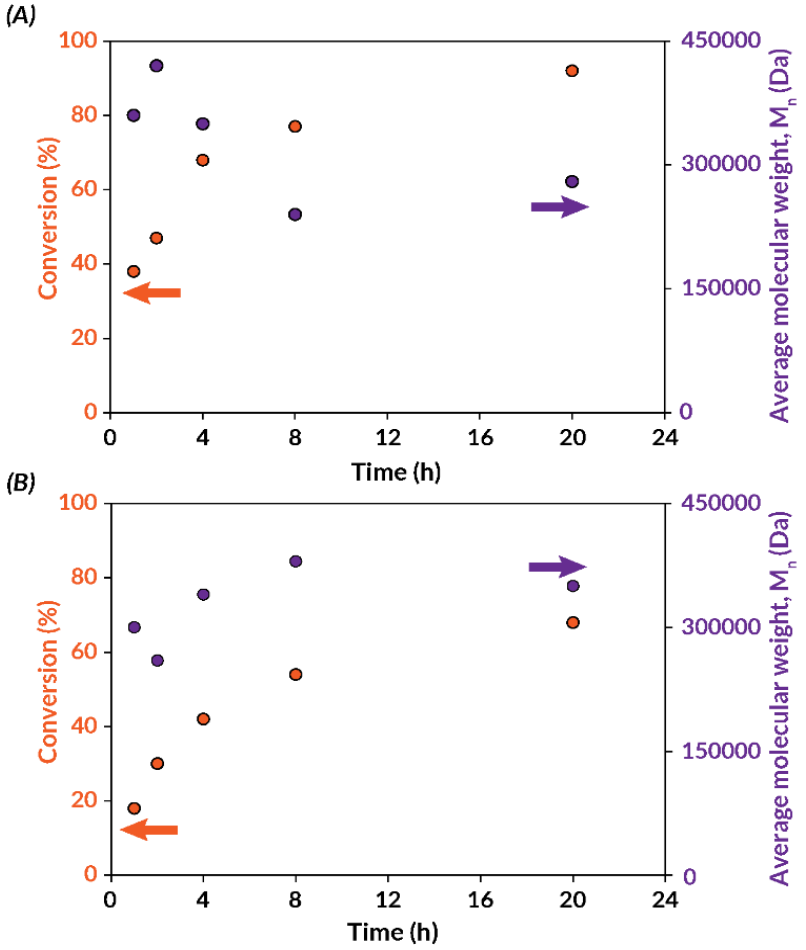

Figure 2.8 Conversion and molar mass progression during US-mechanoredox *t*BA polymerizations under optimized conditions (see Table 2.7): **(A)** with $BaTiO_3$ (7 wt%) in DMF; **(B)** with ZnO (7 wt%) in DMAc.

Table 2.8: US-mechanoredox FRP controls: conversion of (meth)acrylate in the absence of US.

Entry	Monomer	Nanoparticle	Solvent	Conversion[d] (%)
1[a]	*t*BA	$BaTiO_3$	DMF	<5
2[a]	*t*BA	ZnO	DMAc	<5
3[[a]	BA	$BaTiO_3$	DMF	<5
4[a]	BA	ZnO	DMAc	<5
5[b]	EA	$BaTiO_3$	DMF	<5
6[b]	EA	ZnO	DMAc	<5
7[c]	MA	$BaTiO_3$	DMF	<5
8[c]	MA	ZnO	DMAc	<5
9[b]	MMA	$BaTiO_3$	DMF	<5
10[b]	MMA	ZnO	DMAc	<5

Reaction conditions: $[monomer]_0$:$[DPIHP]_0$ = 100:1. [a] [monomer] = 7.3 M, [DPIHP] = 0.073 M; [b] [monomer] = 9.3 M, [DPIHP] = 0.093 M; [c] [monomer] = 10.9 M, [DPIHP] = 0.109 M. [d] Conversion was determined by ^{1}H NMR spectroscopy. PNP loading: 7 wt%. Reaction time: 20 h, 20 °C.

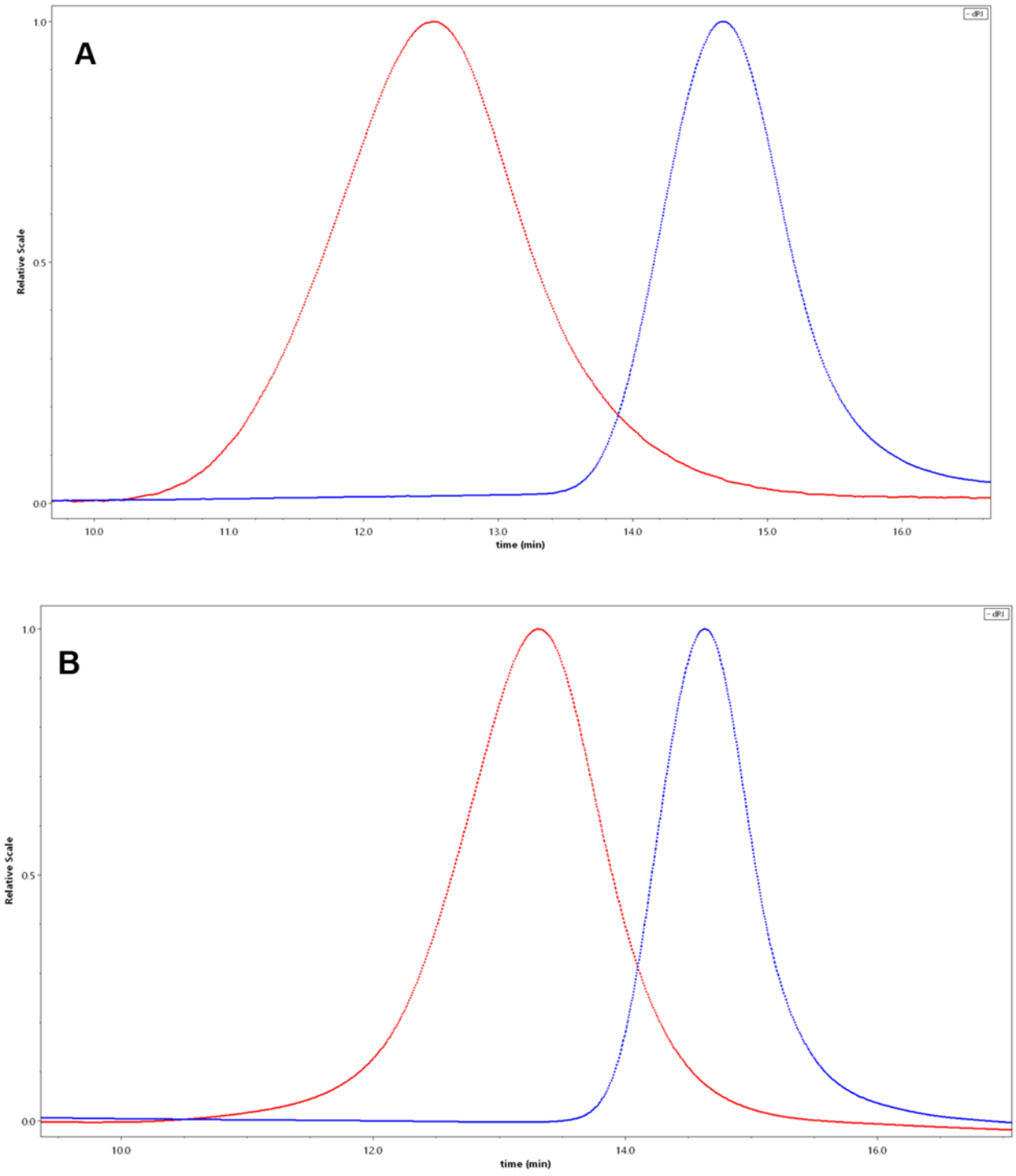

Figure 2.9: GPC-RI traces of (A) poly(tBA) before (M_n – 170 kDa, Đ – 1.7, red) and after (M_n – 21 kDa, Đ – 1.3, blue) and (B) poly(MMA) before (M_n – 110 kDa, Đ – 1.6, red) and after (M_n – 20 kDa, Đ – 1.1, blue) sonication in DMF (2.1 M) for 24 h. US-mediated polymer chain scission is observed for both types of polymers as assessed by change in retention time and measurement of absolute molar masses by GPC-MALS.

Additionally, an "on-off" experiment was conducted to assess the role of US on the FRP reaction profile (Figure 2.10). As assessed by ^{1}H NMR spectroscopy, *t*BA conversion reached 35% after 1 h of US and remained stagnant (< 5% further conversion) during the first "off" period of 2 h. During the second 2 h "on" period, monomer conversion increased to 57%. Interestingly, after a longer "off" period (15 h), monomer conversion increased to 73%. These data collectively suggest that while FRP rates are higher in the presence of US, likely due to continuous mechanoredox generation of initiating radicals and/or thermal cavitation effects under US irradiation, propagating chain ends still remain active even in the absence of US.

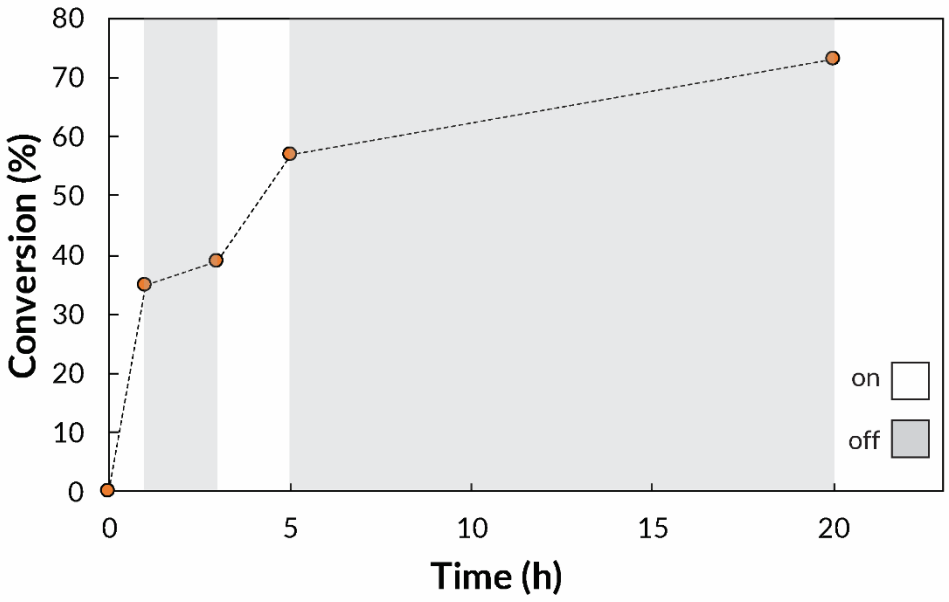

Figure 2.10: On/Off US-mechanoredox FRP of *t*BA. Reaction conditions: $[t\text{BA}]_0$:$[\text{DPIHP}]_0$ = 100:1. [*t*BA] = 7.3 M in DMF, Ultrasonic bath (40 kHz, 70 W, 20 °C).

2.3 Ball milling (BM) Mechanoredox Polymerizations

As the diaryl iodonium chemistry evolved in solution using ultrasound, we were intrigued to find out if mechanoredox FRP could transition into the ball mill. The advantages of ball milling, including reducing solvent usage, mitigating reagent insolubility,[72] and facilitating the use of incompatible and/or immiscible reagents,[73] are apparent from prior solid state step-growth,[74] ring-opening,[75] and iterative[76] polymerizations. Although poly(meth)acrylates have been synthesized under ball milling conditions via mechanochemical

radical generation on quartz surfaces[77] and a recapitulated solid-state ATRP process,[78] the use of a tuneable mechanoredox pathway has remained unrealized under ball mill grinding conditions prior to our work.

To begin, we translated our optimized US-mechanoredox FRP conditions for *t*BA (50:1 *t*BA:DPIHP, 7 wt% $BaTiO_3$) into the ball mill using minimal DMF (0.12 mL, 0.030% v/w = volume of DMF relative to total mass of all other reaction components) as is required for liquid assisted grinding (LAG).[79] LAG is a procedure that enhances mechanochemical reactivity through the addition of small quantities of a solvent.[3] Upon initial investigation, >95% monomer conversion was observed by ^{1}H NMR spectroscopy (Figure 2.11) after only ***3 h*** in the ball mill (30 Hz) compared to 20 h in solution with US; the resulting material in the stainless steel milling jar was a visibly viscous material (Figure 2.12) with a high molecular weight (M_n = 165 kDa) as determined by GPC-MALS. Without the addition of the LAG solvent, little monomer conversion was observed (Table 2.11). Unlike the US-mediated reactions, ball mill grinding was tolerant of oxygen and *rigorous exclusion of air was not required*. Our observations are in stark contrast to Bielawski's recent work on solid-state ATRP[78] where polymerization only occurred in an inert atmosphere. Other common acrylates also showed high conversions (Table 2.12) under our BM-mechanoredox FRP conditions, but importantly, monomer conversion was seen only when samples were subjected to ball mill grinding. As with the US processes, both iodonium salt and PNP were required; when DPIHP and/or $BaTiO_3$ were removed from the reaction mixture, no monomer conversion was observed (Table 2.9 entries 3-5). Similarly, when the PNP was replaced with ZnO or TiO_2, no conversion was seen after ball mill grinding for 3 h (Table 2.10, entries 1 & 2).

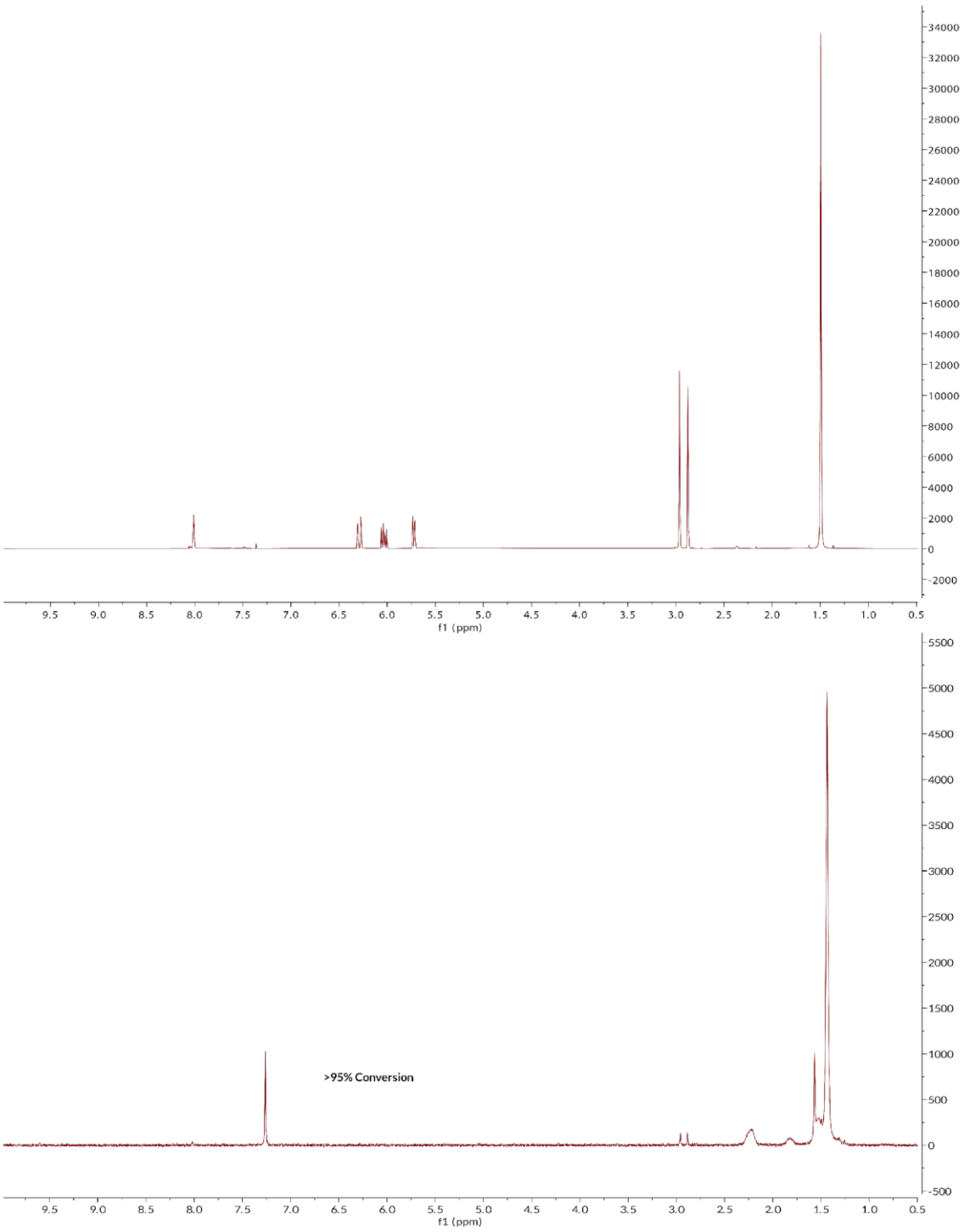

Figure 2.11: Representative ^{1}H NMR spectum of poly(*t*BA) synthesized using BM-mechanoredox FRP from which >95% monomer conversion was determined (bottom). Representative ^{1}H NMR spectrum of reaction mixture prior to ball mill grinding is shown on top. Polymer sample was synthesized using conditions from entry 1 of Table 2.9: *t*BA = 0.026 g, 2.0 mmol; DPIHP = 0.017 g, 0.040 mmol; $BaTiO_3$ = 0.14 g, 0.60 mmol; DMF (LAG) = 0.12 mL; 0.030% v/w. Milled for 180 minutes at 30 Hz.

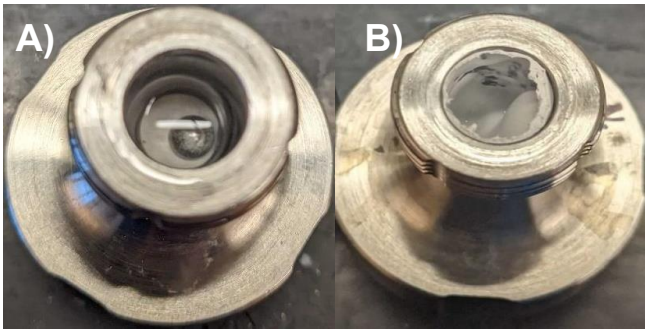

Figure 2.12: Photographs of a typical BM-mediated FRP reaction before and after ball mill grinding. Photograph **(A)** is before milling and Photograph **(B)** is after milling with >95% monomer conversion.

Table 2.9: Control experiment results for ball milling and PNP mediated polymerization of acrylate monomers.

Entry	Deviation from Standard Conditions	Conversion[a] (%)
1	None	>95
2	Without DMF	<5
3	Without $BaTiO_3$	<5
4	Without DPIHP	14
5	Without $BaTiO_3$ and DMF	7
6	Without ball	<5

Reaction conditions: Standard Conditions: *t*BA = 0.26 g, 2.0 mmol; DPIHP = 0.14 g, 0.040 mmol; $BaTiO_3$ = 0.14 g, 0.60 mmol; DMF (for LAG) = 0.12 mL, 0.030% v/w. Ball mill (1.5 mL stainless steel jar, 5 mm stainless steel grinding ball, 30 Hz). Reaction time: 3 h. [a] Conversion was determined by ^{1}H NMR spectroscopy.

Table 2.10: BM-mechanoredox controls: ball milling *t*BA with different nanoparticles.

Entry	Nanoparticle	Conversion[a] (%)
1	ZnO	<5
2	TiO_2	<5
3	None	<5

Reaction conditions: *t*BA = 0.26 g, 2.0 mmol; DPIHP = 0.14 g, 0.040 mmol; PNP = 0.60 mmol; DMF (for LAG) = 0.12 mL, 0.030% v/w. Ball mill (1.5 mL stainless steel jar, 5 mm stainless steel grinding ball, 30 Hz). Reaction time: 3 h. [a] Conversion was determined by ^{1}H NMR spectroscopy.

We then investigated the kinetics of BM-mechanoredox FRP due to their expedited rates compared to our US-mediated FRP. Interestingly, these studies revealed that there is an incubation period; no conversion is observed prior to 140 minutes (Figure 2.13). Since these reactions are conducted under air in sealed vessels, we hypothesized that the limited oxygen would eventually be removed from the atmosphere, potentially through reduction under mechanoredox conditions. Once the atmosphere is "scrubbed" of oxygen, nearly quantitative monomer conversion is quickly observed after just an additional ca. 10 min. To test this hypothesis, we set up a *t*BA BM-mechanoredox FRP reaction under an inert N_2 atmosphere in a glovebox and observed that FRP proceeded without a noticeable incubation period (Table 2.11). 14% conversion was observed after just 10 minutes while nearly 70% conversion was observed after 90 minutes. Oxygen seems to perturb the onset of monomer conversion but does not significantly affect the overall time to full conversion (ca. 150 min). We surmise that mixing is the rate limiting factor under inert conditions; in the presence of oxygen, sufficient mixing becomes competitive with atmosphere scrubbing so monomer consumption appears to be nearly instantaneous once all oxygen is removed from the system.

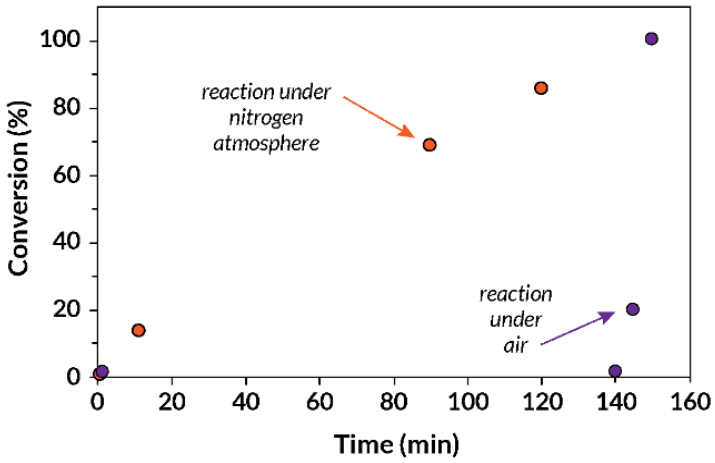

Figure 2.13. Comparison of BM-mechanoredox kinetics (*t*BA conversion) in an inert atmosphere and under air.

Table 2.11: BM-mechanoredox controls: ball milling *t*BA under nitrogen at different time points.

Entry[a]	Time	Conversion (%)	M_n (kDa)	Đ
1	10	14	525	1.3
2	90	69	561	1.3
3	120	86	520	1.3

Reaction conditions: *t*BA = 0.26 g, 2.0 mmol; DPIHP = 0.14 g, 0.040 mmol; $BaTiO_3$ = 0.14 g, 0.60 mmol; DMF (for LAG) = 0.12 mL, 0.030% v/w. Ball mill (1.5 mL stainless steel jar, 5 mm stainless steel grinding ball, 30 Hz). Reaction time: 3 h. [a] Conversion was determined by ^{1}H NMR spectroscopy.

Table 2.12: Ball milling mechanoredox acrylate polymerizations.

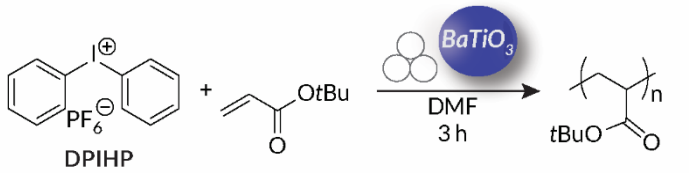

Entry	Monomer	Conversion[a] (%)	M_n (kDa) [b]	Đ[b]
1	*t*BA	>95	416	1.3
2	BA	90	556	1.6
3	EA	>95	751	1.4
4	MA	>95	937	1.2
5	MMA	86	56	1.7

Reaction conditions: Monomer = 2.0 mmol, DPIHP = 0.040 mmol, $BaTiO_3$ = 0.60 mmol, DMF (for LAG) = 0.12 mL (0.030% v/w). [a] Conversion was determined by ^{1}H NMR spectroscopy. [b] M_n and Đ were determined by GPC-MALS. Ball mill (1.5 mL stainless steel jar, 5 mm stainless steel grinding ball, 30 Hz). Reaction time: 3 h.

The overall physical data collected from GPC-MALS analysis (Table 2.12 and Figure 2.14) of BM-mechanoredox FRP polymers show similar trends to what was measured for US-mechanoredox FRP. Importantly, the similarities in M_n and Đ between the two methods suggest that ball mill grinding leads to uniform rate enhancements (i.e. rates of initiation,

propagation, and termination) relative to US; drastic disparities in M_n and/or Đ would suggest non-uniform rate enhancements in the ball mill. Under an inert atmosphere, >85% monomer consumption for all monomers is achieved in under 3 h via ball milling conditions, while almost a full day (20 h) reaction is needed under ultrasonic irradiation conditions. Hence, solvating conditions (i.e. US-mechanoredox FRP) slow the overall rate of monomer consumption compared to that of BM-mechanoredox FRP, but do not significantly alter the makeup of the final poly(meth)acrylates. Interestingly, resubjection of BM-mechanoredox polymers (e.g., poly(*t*BA), poly(MMA)) to the original reaction conditions (0.030% v/w DMF, ball mill grinding at 30 Hz, 3 h) led to only a small decrease in molar mass as assessed by GPC-MALS (Figures 2.15 & 2.16). Hence, while mechanochemical chain scission pathways were operative under ultrasonication conditions, they were less prevalent, at least on this shorter time scale, under ball milling conditions.

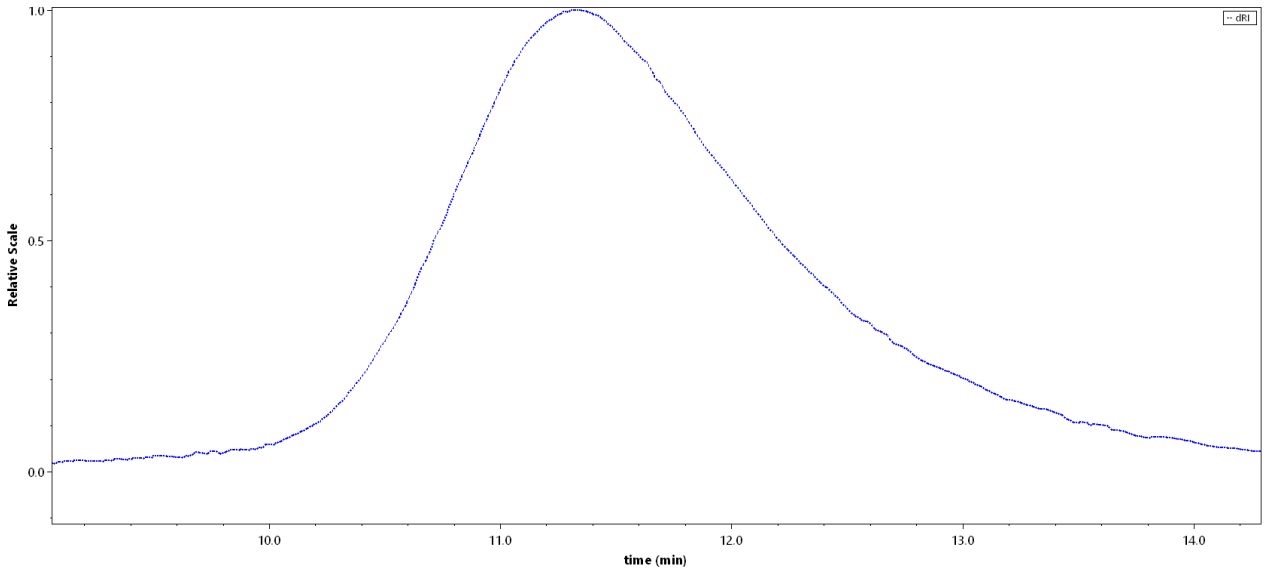

Figure 2.14: Representative of GPC-RI trace of poly(*t*BA). M_n (GPC-MALS): 475 kDa. Synthesized by ball milling for 3 h with conditions as follows: *t*BA = 0.26 g, 2.0 mmol; DPIHP = 0.017 g, 0.040 mmol; $BaTiO_3$ = 0.14 g, 0.60 mmol; DMF (LAG) = 0.12 mL; 0.030% v/w.

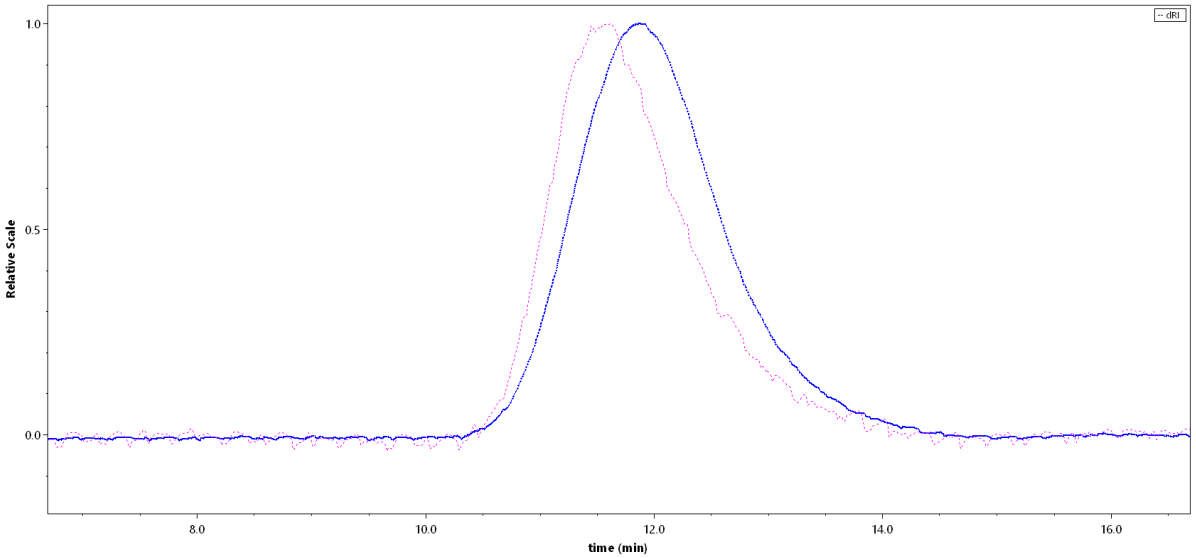

Figure 2.15: GPC-RI traces of poly(*t*BA) before (M_n – 290 kDa, Đ – 1.4, pink) and after (M_n – 260 kDa, Đ – 1.4, blue) ball mill grinding in DMF (61 mg of polymer in 0.018 mL solvent) for 3 h as determined by GPC-MALS.

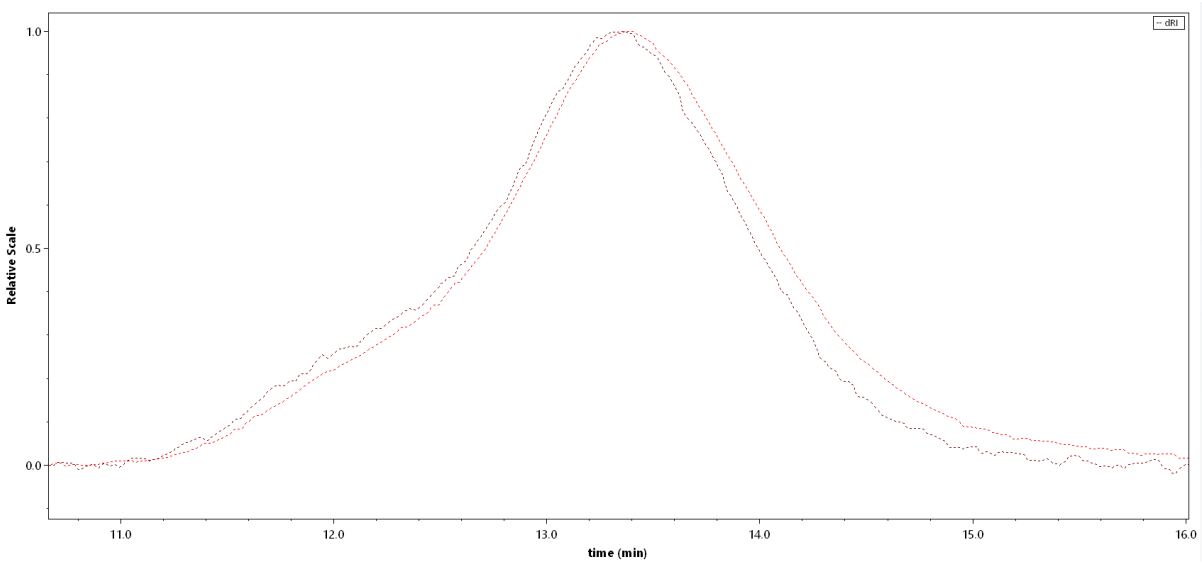

Figure 2.16: GPC-RI traces of poly(MMA) before (M_n – 95 kDa, Đ – 1.7, brown) and after (M_n – 75 kDa, Đ – 1.8, red) ball mill grinding in DMF (61 mg of polymer in 0.018 mL solvent) for 3 h as determined by GPC-MALS.

Based on work from the ultrasonic irradiation reactions, we hypothesized that PNP identity may also influence polymerization efficiency. Upon testing this hypothesis, we determined that the difference in reactivity between the two PNPs in ball milling is much more significant than with US. Under otherwise identical conditions (Table 2.12, entry 1), no conversion was observed when $BaTiO_3$ was replaced with ZnO (Table 2.10, entry 1). These results parallel the trends observed in C-H borylation and arylation reactions studied by Kubota

and Ito;[48] the specific mechanistic underpinnings behind such a stark reactivity difference is unclear at this time.

2.4 Mechanoredox FRP of Ionic Liquids

Expanding the monomer scope of the mechanoredox FRP, we transitioned to polymerizing ionic liquids with the intention of demonstrating compatibility with additive manufacturing curing. Working with the ionic liquid, 1-butyl-3-vinylimidazolium bis(trifluoromethane)sulfonimide, force was applied by a sonicator bath or a ball mill. When force was applied in a sonicator bath, 50% monomer conversion was observed (Table 2.13, entry 1). Interestingly, no monomer conversion was observed in the ball mill (Table 2.13, entries 2-3). While challenges exist in effectively applying force to 3D printed materials that are regularly produced with the ionic liquids this proof-of-concept study clearly demonstrates the ability for our mechanoredox chemistry to transfer to other monomer classes, including those that are regularly utilized in additive manufacturing.[80]

Table 2.13: Force induced mechanoredox polymerization of ionic liquids.

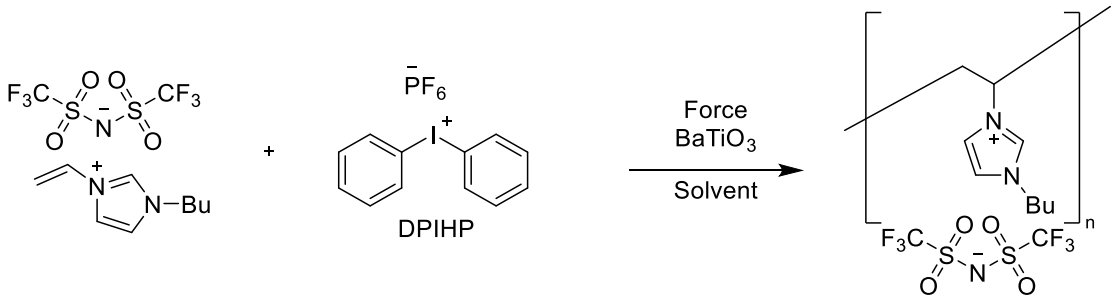

Entry	Solvent	Type of Force	Conversion[a]
1[b]	none	Sonicator	50%
2[c,d]	DMF	Ball mill	<5%
3[c]	none	Ball mill	<5%

Reaction conditions: Monomer = 12.5 mmol, DPIHP = 0.0050 mmol, $BaTiO_3$ = 3.5 mmol. [a] Conversion was determined by ^1H NMR spectroscopy. [b] Reaction time: 3 h. [c] Reaction time: 20 h. Ball mill (1.5 mL stainless steel jar, 5 mm stainless steel grinding ball, 30 Hz). [d] DMF (for LAG) = 0.018 mL (0.030% v/w)

2.5 Synthesis and Mechanical Property Testing of $BaTiO_3$/PMMA Composite Materials

To further demonstrate the utility of this mechanoredox chemistry, we synthesized composite materials containing PMMA and $BaTiO_3$ nanoparticles in the ball mill. Such composites are traditionally synthesized by emulsion polymerization to encapsulate the nanoparticles or the incorporation of nanoparticles after polymerization.[81,82] By conducting mechanoredox FRP in the ball mill to form composite materials, the incorporation of the $BaTiO_3$ occurs in the polymerization process in one pot without the need for surfactants.[81]

Initially, attempts were made to form crosslinked materials containing the $BaTiO_3$ nanoparticles. By conducting mechanoredox FRP via ball mill grinding in the presence of a crosslinker, diethylene glycol diacrylate, insoluble crosslinked acrylate-based materials were formed. Different amounts of crosslinker and $BaTiO_3$ nanoparticles were incorporated to change the consistency of the materials (Table 2.14), and the nanoparticles were trapped within the networks, forming a composite material. Unfortunately, due to the nature of ball mill grinding, inconsistent shapes of the produced and non-processable networks made mechanical testing of material properties nearly impossible.

Table 2.14: Ball milling mechanoredox acrylate crosslinked materials.

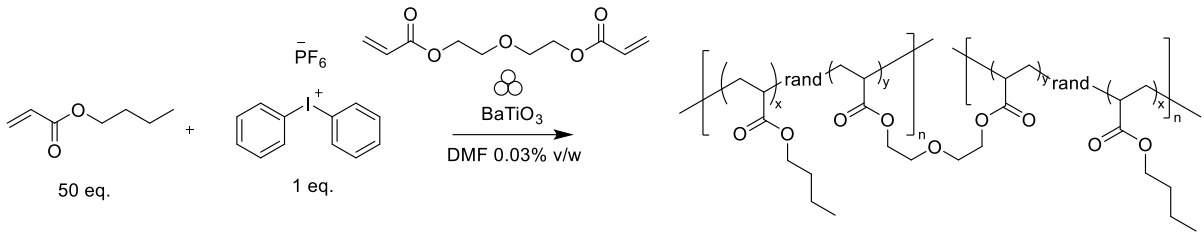

Entry	DHIP (mmol)	Monomer (mmol)	$BaTiO_3$ (mmol)	Crosslinker (%)	Qualitative Observation
1	0.04	2	0.60	10	Crosslinked - very brittle
2	0.08	4	0.60	3	Crosslinked - brittle
3	0.08	4	0.24	5	Crosslinked - ductile
4	0.08	4	0.24	2	Crosslinked - very ductile
5	0.08	4	0.08	1	No crosslinking
6	0.08	4	0.24	1	Crosslinked - ductile but inconsistent shape

Reaction conditions: Ball mill (1.5 mL stainless steel jar, 5 mm stainless steel grinding ball, 30 Hz). Reaction time: 3 h.

To overcome the processing challenges, vortexing was also presented as a feasible force source to crosslink materials in a consistent shape. Because of the versatility provided by the vortexers, reactions were set up in glass vials instead of milling jars. Glass vials allow for access to a consistently shaped material as the vial itself can be broken after each use to extract a consistent shaped material formed to the walls of the vessel. The only shortcoming to the materials formed in vials via vortexing remained the need for the milling ball to achieve conversion. The milling ball was then trapped within the material and altered the internal structure of the crosslinked material, making an alternative method for synthesizing composite materials desirable.

It was determined that the $BaTiO_3$ nanoparticles could be adequately incorporated into films without a crosslinker. To test the mechanical properties of the ball milled composite materials were drop casted to form films for mechanical testing. These films were directly

compared to composites formed via traditional processes sonicating commercial PMMA with $BaTiO_3$ nanoparticles in solution and solution casting the mixture and are currently being characterized via dynamic mechanical analysis.

2.6 Summary

In summary, we developed mechanoredox methodology for the synthesis of poly(meth)acrylates under complementary reaction conditions. The fields of self-healing and strain-strengthening materials will undoubtedly benefit from fundamental processes that can forge chemical bonds in response to mechanical inputs. In fact, several examples of mechanoredox polymer crosslinking[83–85] already exist, providing compelling arguments for accessing thermoset materials that may be inaccessible under thermal conditions. Furthermore, as photons are readily absorbed by chromophores or scattered by insoluble additives[86,87], the ability to spatially focus mechanical energy will allow for the development of advanced, responsive macromolecular networks. The diversity of mechanical inputs provides the opportunity for divergent applications as the field evolves. Additional mechanistic studies are ongoing in our lab to probe experimental differences observed in these mechanoredox FRP studies and the exact identity of initiating species.

2.7 Experimental

2.7.1 Materials

All chemicals were obtained from commercial sources and used as received unless otherwise stated. *Tert*-butyl acrylate (*t*BA), butyl acrylate (BA), ethyl acrylate (EA), methyl acrylate (MA), and methyl methacrylate (MMA) were purchased from Tokyo Chemical Industry (TCI). Styrene was purchased from Acros. All monomers were purified by passing through basic alumina immediately before use. Diphenyl iodonium hexafluorophosphate (DPIHP) and 4-bromobenzenediazonium tetrafluoroborate (BBDT) were obtained from TCI. Cubic $BaTiO_3$ nanoparticles (<100 nm size) and ZnO nanoparticles (18 nm) were purchased

from Sigma-Aldrich and US Research Nanomaterials, respectively. Anhydrous TiO_2 powder was obtained from Fisher Chemical. All ultrasound reactions were carried out in 4 mL vials (ChemGlass #CG-4904-05) unless otherwise stated. Large scale (5 g) polymerization reactions were carried out in 10 mL round bottom flasks. Unless otherwise noted, reaction solvents, dimethylformamide (DMF), dimethylacetamide (DMAc), dimethylsulfoxide (DMSO), toluene, dioxane, and anisole, were sourced from commercially available sources and used without further purification.

Acrylate monomers used in glovebox experiments were dried over molecular sieves, degassed via freeze-pump-thaw, and filtered through basic alumina. Anhydrous dimethylformamide (DMF) used in glovebox experiments was obtained from a JC Meyer solvent purification system.[88]

All air-sensitive free radical polymerization (FRP) reactions were performed under inert atmosphere (nitrogen) using standard Schlenk technique or, when indicated, in an Innovative Technology PureLab HE glovebox.

Ultrasonication (US) experiments were performed in a Branson Ultrasonic Cleaner (model 1510R-MT, 70 W, 40 kHz) equipped with an immersed coil of copper tubing connected to a ThermoScientific recirculating chiller for temperature control (see Figure 2.2 for a photograph of the experimental setup). Ball milling (BM) experiments were performed using a Retsch Mixer Mill (MM 400) ball mill instrument in 1.5 mL stainless steel screw-top jars (Verder Scientific #014620230) with a single 5 mm stainless steel grinding ball (Verder Scientific #224550003).

2.7.2 Characterization

All ^{1}H nuclear magnetic resonance (^{1}H NMR) spectra were obtained on a Bruker AVANCE-300, Bruker AVANCE-301, or Bruker AVANCE-500 NMR spectrometer at 25 °C. ^{1}H NMR spectra samples were prepared in chloroform-*d* ($CDCl_3$) and referenced to Me_4Si

(TMS chemical shift, δ, at 0.00 ppm), unless otherwise stated. All ^{1}H NMR spectra were analyzed using Bruker TopSpin or MestreNova processing software. Chemical shifts are represented in parts per million (ppm). Integration values of the sidechains from monomers (and their corresponding polymers) were used as internal standards and compared to the decreasing integration values of the olefinic (ca. 5.5 – 6.5 ppm) protons of each monomer to calculate monomer conversion. See Figure 2.17 for a graphical example.

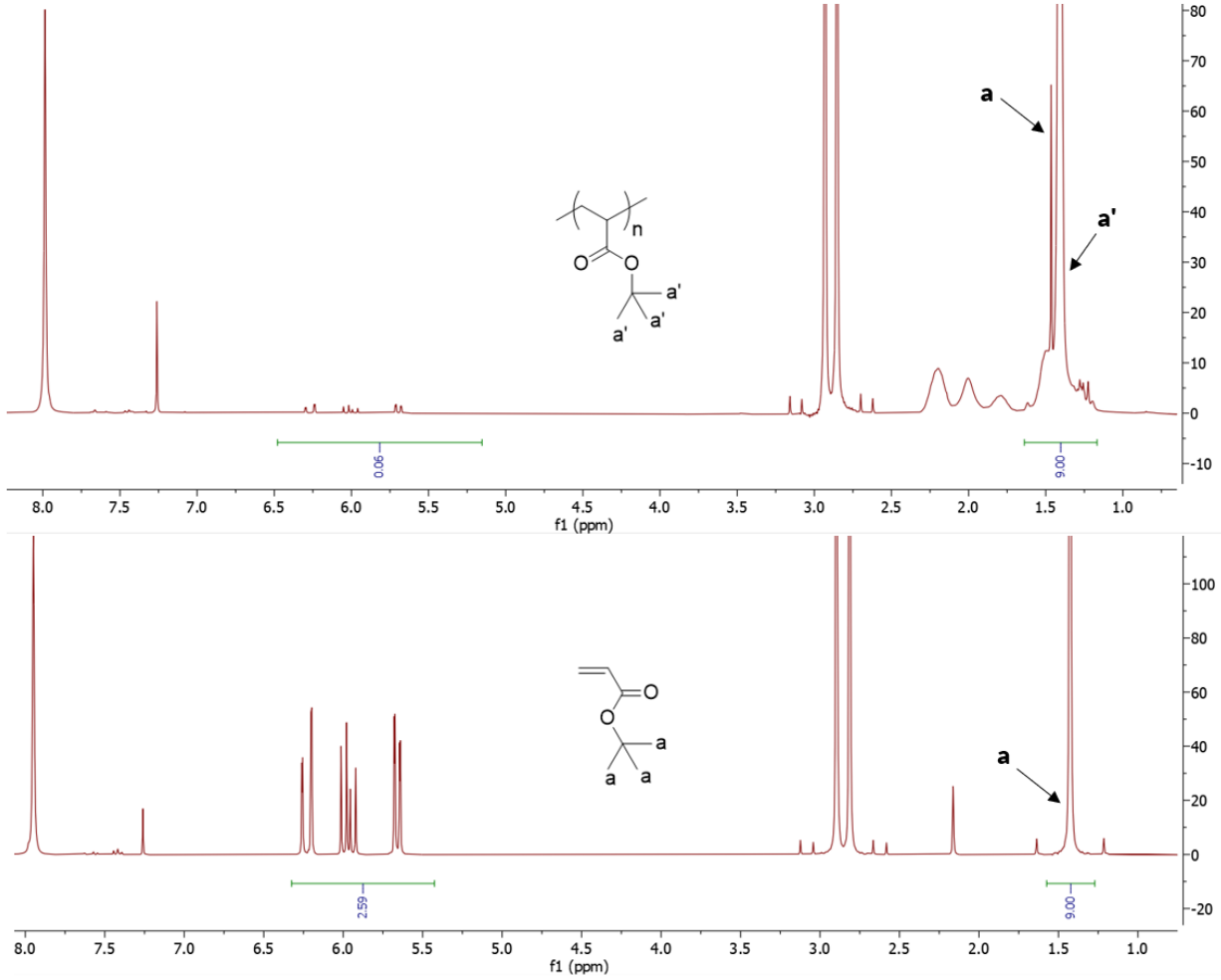

Figure 2.17: Representative crude ^{1}H NMR spectra of *t*BA US-mechanoredox FRP at time = 0 h (bottom) and time = 20 h (top). Reaction conditions: $[t\text{BA}]_0$:$[\text{DPIHP}]_0$ = 100:1. [*t*BA] = 7.3 M in DMF. Ultrasonic bath (40 kHz, 70W, 20 °C). >90% monomer conversion is measured by the disappearance of olefinic protons (ca. 5.5 – 6.5 ppm) relative to methyl internal standard peaks (a and a') on the *tert*-butyl groups present in the monomer and polymer.

Gel permeation chromatography (GPC) data were obtained on an Agilent 1260 HPLC equipped with a Wyatt 8-angle DAWN NEON light-scattering detector, ViscoStar NEON viscometer, and Optilab NEON refractive index detector. GPC samples were analyzed at a flow

rate of 1 mL/min in chloroform stabilized with 0.5%-1.0% ethanol through two Agilent PLgel MIXED-C columns at 35 °C. GPC samples were prepared at ca. 10 mg/mL in chloroform and were filtered through 0.2 μm PTFE filters before analysis. The following dn/dc values were used; they were measured by the 100% mass recovery method using Wyatt Astra 7.3 software: **poly(*t*BA)**: 0.024; **poly(BA)**: 0.033; **poly(EA)**: 0.029; **poly(MA)**: 0.039; **poly(MMA)**: 0.053

2.7.3 Synthetic and Experimental Procedures

Synthesis of 4-methoxybenzenediazoium tetrafluoroborate (MBDT):

Following the literature procedure from Kubota and Ito,[48] 4-methoxyaniline (1.2 g, 10 mmol) was added to tetrafluoroboric acid (50%, 5.0 mmol, 3.5 mL) and water (4.0 mL) and stirred at 0 °C. Sodium nitrite (700 mg, 10 mmol) was dissolved into water (1.5 mL) and added into the aniline mixture (portion wise in 0.25 mL aliquots). The reaction mixture stirred for 30 minutes at 0 °C. The mixture was then filtered, and the resulting solid was dissolved in acetone. Diethyl ether was added to precipitate the target diazonium salt. The precipitate was filtered, washed with diethyl ether, and dried under vacuum to afford MBDT as a white solid (1.5 g, 68%). The purity of the compound was confirmed by ^{1}H NMR spectroscopy and was in agreement with the literature.

^{1}H NMR (300 MHz, $(CD_3)_2CO$): δ(ppm) 8.65 (d, J = 10 Hz, 2H), 7.42 (d, J = 10 Hz, 2H), 4.04 (s, 3H).

Representative experimental procedure for US-mechanoredox FRP:

In a typical polymerization experiment, DPIHP (0.017 g, 0.039 mmol, 1 equiv.) and dimethylformamide (0.50 g) were loaded into a 4 mL glass vial and thoroughly mixed until all DPIHP was fully dissolved. Then, $BaTiO_3$ nanoparticles (0.072 g, 7 wt% relative to total mass of reactants) were added into that solution. Finally, *tert*-butyl acrylate (0.50 g, 3.9 mmol, 100 equiv.) was added and the vial was capped with a rubber septum (Sigma #Z167258) and sealed with electrical tape. The reaction mixture was then degassed by sparging with N_2 for 40

minutes. After the completion of sparging, vials were then immersed into the ultrasonic bath (20 °C, 70 W, 40 kHz) via clamps and sonicated for 20 h (see Figure 2.2 for setup). Afterwards, samples were diluted with chloroform and passed through a column of neutral alumina for ^{1}H NMR and GPC sample preparation.

Representative kinetics experiment procedure for US-mechanoredox FRP ($BaTiO_3$/DMF):

In a typical kinetics experiment, DPIHP (0.017 g, 0.039 mmol, 1 equiv.) and dimethylformamide (0.50 g) were loaded into a 4 mL glass vial and thoroughly mixed until all DPIHP was fully dissolved. Then, $BaTiO_3$ nanoparticles (0.072 g, 7 wt%, relative to total mass of reactants) were added into that solution. Finally, *tert*-butyl acrylate (0.50 g, 3.9 mmol, 100 equiv.) was added and the vial was capped with a rubber septum (Sigma #Z167258) and sealed with electrical tape. Reaction mixtures were prepared for each time point of the kinetics experiment. The reaction mixtures were then degassed by sparging with N_2 for 40 minutes and then immersed into the ultrasonic bath (20 °C, 70 W, 40 kHz) via clamps and sonicated for the target time (see Figure 2.2 for setup). Afterwards, samples were diluted with chloroform and passed through a column of neutral alumina. Afterwards, samples were diluted with chloroform and passed through a column of neutral alumina for ^{1}H NMR and GPC sample preparation.

Representative kinetics experiment procedure for US-mechanoredox FRP (ZnO/DMAc):

In a typical kinetics experiment, DPIHP (0.017 g, 0.039 mmol, 1 equiv.) and dimethylacetamide (0.50 g) were loaded into a 4 mL glass vial and thoroughly mixed until all DPIHP was fully dissolved. Then, ZnO nanoparticles (0.072 g, 7 wt% relative to total mass of reactants) were added into that solution. Finally, *tert*-butyl acrylate (0.50 g, 3.9 mmol, 100 equiv.) was added and the vial was capped with a rubber septum (Sigma #Z167258) and sealed with electrical tape. Reaction mixtures were prepared for each time point of the kinetics experiment. The reaction mixtures were then degassed by sparging with N_2 for 40 minutes and

then immersed into the ultrasonic bath (20 °C, 70 W, 40 kHz) via clamps and sonicated for the target period of time (see Figure 2.2 for setup). Afterwards, samples were diluted with $CHCl_3$ and passed through a column of neutral alumina. Afterwards, samples were diluted with chloroform and passed through a column of neutral alumina for ^{1}H NMR and GPC sample preparation.

Representative experiment procedure for DPIHP addition kinetic study:

In a typical kinetics experiment, butyl acrylate (0.50 g, 3.9 mmol) and dimethylformamide (0.50 g) were loaded into a 4 mL glass vial and thoroughly mixed. Then, $BaTiO_3$ nanoparticles (0.072 g, 7 wt%%, relative to total mass of reactants) were added into that solution and the vial was capped with a rubber septum (Sigma #Z167258) and sealed with electrical tape. In a separate vial, DPIHP (0.017 g, 0.039 mmol) was dissolved in dimethylformamide (0.10 g). Reaction mixtures were then degassed by sparging with N_2 for 40 minutes and the vial containing butyl acrylate was immersed into the ultrasonic bath (20 °C, 70 W, 40 kHz) via clamps and sonicated for 8 h. Afterwards, the previously prepared DPIHP solution was added into the reaction vial using a syringe/needle; the reaction mixture was then sonicated for an additional 12 h. Afterwards, samples were diluted with chloroform and passed through a column of neutral alumina. Afterwards, samples were diluted with chloroform and passed through a column of neutral alumina for ^{1}H NMR and GPC sample preparation.

Representative procedure for monitoring poly(meth)acrylate degradation by US:

A poly(*t*BA) or poly(MMA) sample was synthesized by the standard US-mechanoredox FRP procedure described above and was isolated by precipitation in cold methanol/water (50%/50%). Following removal of solvent under vacuum, a white polymer was obtained. The polymer was dissolved in dimethylformamide (final concentration = 2.1 M) in a 4 mL glass vial. The vial was capped with a rubber septum (Sigma #Z167258) and sealed with electrical tape. The mixture was degassed by sparging with N_2 for 40 minutes. Finally, the

sparged mixture was placed in an ultrasonic bath (20 °C, 70 W, 40 kHz). A GPC sample was taken after 24 h (Figure 2.9).

Representative procedure for BM-mechanoredox FRP of *t*BA:

To a 1.5 mL stainless steel milling jar charged with a 5 mm stainless steel milling ball was added DPIHP (0.017 g, 0.04 mmol), dimethylformamide (0.12 mL, 0.030% v/w = volume of DMF relative to total mass of all other reaction components) for liquid-assisted grinding (LAG), *tert*-butyl acrylate (0.26 g, 2 mmol), and $BaTiO_3$ (0.14 g, 0.60 mmol). The jar was sealed under air, secured in the ball mill, and shaken at 30 Hz for the desired amount of time. Then, a small aliquot was extracted from the ball mill jar with a spatula and dissolved in an appropriate solvent for ^{1}H NMR and GPC characterization.

Representative procedure for "air-free" BM-mechanoredox FRP of *t*BA:

"Air-free" ball mill grinding experiments were set up in an identical fashion to those described above except the milling jars were charged with all reagents and sealed in the glovebox before securing in the ball mill. Note that all liquid reagents (DMF and acrylate monomer) were degassed via the freeze-pump-thaw method prior to transferring into the glovebox.

Representative procedure for monitoring poly(meth)acrylate degradation by ball milling:

To a 1.5 mL stainless steel milling jar charged with a 5 mm stainless steel milling ball was added freshly synthesized poly(*t*BA) or poly(MMA) (61 mg) and dimethylformamide (0.018 mL, 0.030% v/w = volume of DMF relative to total mass of all other reaction components). The jar was sealed under air, secured in the ball mill, and shaken at 30 Hz for 3 h. Then, a small aliquot was extracted from the ball mill jar with a spatula and dissolved in chloroform for GPC characterization.

Representative procedure for mechanoredox US-FRP of 1-butyl-3-vinylimidazolium bis(trifluoromethane)sulfonimide:

DPIHP (0.009 g, 0.02 mmol, 1 equiv.) was loaded into a 4 mL glass vial with $BaTiO_3$ nanoparticles (0.031 g, 7 wt% relative to total mass of reactants) and 1-butyl-3-vinylimidazolium bis(trifluoromethane)sulfonimide (0.431 g, 1 mmol, 50 equiv.) added. The vial was capped with a rubber septum (Sigma #Z167258) and sealed with electrical tape, and the reaction mixture was then degassed by sparging with N_2 for 40 minutes. After the completion of sparging, vials were then immersed into the ultrasonic bath (20 °C, 70 W, 40 kHz) via clamps and sonicated for 20 h (see Figure 2.2 for setup). Afterwards, samples were diluted with chloroform and passed through a column of neutral alumina for ^{1}H NMR and GPC sample preparation.

Representative procedure for mechanoredox BM-FRP of 1-butyl-3-vinylimidazolium bis(trifluoromethane)sulfonimide:

To a 1.5 mL stainless steel milling jar charged with a 5 mm stainless steel milling ball was added DPIHP (0.021 g, 0.05 mmol), dimethylformamide (0.12 mL, 0.030% v/w = volume of DMF relative to total mass of all other reaction components) for liquid-assisted grinding (LAG), 1-butyl-3-vinylimidazolium bis(trifluoromethane)sulfonimide (0.54 g, 1.25 mmol), and $BaTiO_3$ (0.039 g, 0.35 mmol). The jar was sealed under air, secured in the ball mill, and shaken at 30 Hz for the desired amount of time. Then, a small aliquot was extracted from the ball mill jar with a spatula and dissolved in an appropriate solvent for ^{1}H NMR and GPC characterization.

Representative procedure for BM-mechanoredox crosslinking FRP:

To a 1.5 mL stainless steel milling jar charged with a 5 mm stainless steel milling ball was added DPIHP (0.051 g, 0.12 mmol), dimethylformamide (0.27 mL, 0.30% v/w = volume of DMF relative to total mass of all other reaction components) for liquid-assisted grinding

(LAG), n-butyl acrylate (0.769 g, 6 mmol), diethylene glycol diacrylate, and $BaTiO_3$. The jar was sealed under air, secured in the ball mill, and shaken at 30 Hz for the desired amount of time. Then, the sample was extracted from the jar for observations.

2.8 Acknowledgements and Publications

This mechanoredox FRP methodology was conducted in collaboration with Dr. Progya Chakma. The ionic liquid additive manufacturing force-curing work is being conducted in collaboration with Dr. Julian Smith-Jones, Nathan Ballinger, Rowina Bell under the direction of Prof. Alshakim Nelson. The mechanical testing of the $BaTiO_3$-PMMA composite films is being conducted with the assistance of Brian Sun.

This chapter was adapted from the publication below publication(s):

- **S. Zeitler**,* P. Chakma,* M. Golder, *Chem. Sci.,* 2022, **13**, 4131–4138, *co-first author
- **S. Zeitler,**** M. Skala, R. Bell, J. Smith-Jones, T. Masmeijer, E. Habtour, A. Nelson, M. Golder, *manuscript in preparation*. **author order to be determined
- **S. Zeitler,**** B. Sun, M. Golder, *manuscript in preparation.* **author order to be determined

2.9 References

1 J. L. Howard, Q. Cao and D. L. Browne, *Chem. Sci.*, 2018, **9**, 3080–3094.

2 J. A. Leitch and D. L. Browne, *Chem. – A Eur. J.*, 2021, **27**, 9721–9726.

3 T. Friščić, C. Mottillo and H. M. Titi, *Angew. Chem. Int. Ed.*, 2019, 2–14.

4 R. T. O'Neill and R. Boulatov, *Nat. Rev. Chem.*, 2021, **5**, 148–167.

5 J. L. Do and T. Friščić, *ACS Cent. Sci.*, 2017, **3**, 13–19.

6 M. M. Caruso, D. A. Davis, Q. Shen, S. A. Odom, N. R. Sottos, S. R. White and J. S. Moore, *Chem. Rev.*, 2009, **109**, 5755–5798.

7 D. A. Davis, A. Hamilton, J. Yang, L. D. Cremar, D. Van Gough, S. L. Potisek, M. T. Ong, P. V. Braun, T. J. Martínez, S. R. White, J. S. Moore and N. R. Sottos, *Nature*, 2009, **459**, 68–72.

8 M. E. McFadden and M. J. Robb, *J. Am. Chem. Soc.*, 2019, **141**, 11388–11392.

9 Z. Chen, J. A. M. Mercer, X. Zhu, J. A. H. Romaniuk, R. Pfattner, L. Cegelski, T. J. Martinez, N. Z. Burns and Y. Xia, *Science*, 2017, **357**, 475–479.

10 C. L. Brown and S. L. Craig, *Chem. Sci.*, 2015, **6**, 2158–2165.

11 C. E. Diesendruck, G. I. Peterson, H. J. Kulik, J. A. Kaitz, B. D. Mar, P. A. May, S. R. White, T. J. Martínez, A. J. Boydston and J. S. Moore, *Nat. Chem.*, 2014, **6**, 623–628.

12 T. G. Hsu, J. Zhou, H. W. Su, B. R. Schrage, C. J. Ziegler and J. Wang, *J. Am. Chem. Soc.*, 2020, **142**, 2100–2104.

13 Y. Lin, T. B. Kouznetsova and S. L. Craig, *J. Am. Chem. Soc.*, 2020, **142**, 2105–2109.

14 X. Hu, T. Zeng, C. C. Husic and M. J. Robb, *ACS Cent. Sci.*, 2021, **7**, 1216–1224.

15 M. B. Larsen and A. J. Boydston, *J. Am. Chem. Soc.*, 2013, **135**, 8189–8192.

16 M. B. Larsen and A. J. Boydston, *Macromol. Chem. Phys.*, 2016, **217**, 354–364.

17 M. A. Ghanem, A. Basu, R. Behrou, N. Boechler, A. J. Boydston, S. L. Craig, Y. Lin, B. E. Lynde, A. Nelson, H. Shen and D. W. Storti, *Nat. Rev. Mater.*, 2021, **6**, 84–98.

18 Z. Shi, J. Wu, Q. Song, R. Göstl and A. Herrmann, *J. Am. Chem. Soc.*, 2020, **142**, 14725–14732.

19 Y. Zhang, J. Yu, H. N. Bomba, Y. Zhu and Z. Gu, *Chem. Rev.*, 2016, **116**, 12536–12563.

20 K. S. Suslick, *Science*, 1990, **247**, 1439–1445.

21 G. Cravotto, E. C. Gaudinoa and P. Cintas, *Chem. Soc. Rev*, 2013, **42**, 7521–7534.

22 K. Kooiman, H. J. Vos, M. Versluis and N. De Jong, *Adv. Drug Deliv. Rev.*, 2014, **72**, 28–48.

23 S. Ibsen, A. Tong, C. Schutt, S. Esener and S. H. Chalasani, *Nat. Commun.*, 2015, **6**, 8264.

24 Y. Pan, S. Yoon, J. Sun, Z. Huang, C. Lee, M. Allen, Y. Wu, Y. J. Chang, M. Sadelain, K. Kirk Shung, S. Chien and Y. Wang, *Proc. Natl. Acad. Sci. U. S. A.*, 2018, **115**, 992–997.

25 P. N. T. Wells, *Phys. Med. Biol.*, 2006, **51**, R83.

26 J. Gonzales, R. K. Nair, S. J. Madsen, T. Krasieva and H. Hirschberg, *J. Biomed. Opt.*, 2016, **21**, 078002.

27 I. Lentacker, S. C. De Smedt and N. N. Sanders, *Soft Matter*, 2009, **5**, 2161–2170.

28 S. Dabral, H. Wotruba, J. G. Hernández and C. Bolm, *ACS Sustain. Chem. Eng.*, 2018, **6**, 3242–3254.

29 A. Stolle, T. Szuppa, S. E. S. Leonhardt and B. Ondruschka, *Chem. Soc. Rev.*, 2011, **40**, 2317–2329.

30 H. Staudinger, W. Heuer. *Ber. Dtsch. Chem*. Ges., A/B 1934, **67**, 1159.

31 J. Li, C. Nagamani and J. S. Moore, *Acc. Chem. Res.*, 2015, **48**, 2181–2190.

32 J. Ayarza, Z. Wang, J. Wang, C.-W. Huang and A. P. Esser-Kahn, *ACS Macro Lett.*, 2020, 1237–1248.

33 S. Tu, Y. Guo, Y. Zhang, C. Hu, T. Zhang, T. Ma and H. Huang, *Adv. Funct. Mater.*, 2020, **30**, 1–31.

34 M. B. Starr and X. Wang, *Nano Energy*, 2015, **14**, 296–311.

35 M. Wang, B. Wang, F. Huang and Z. Lin, *Angew. Chem. Int. Ed.*, 2019, **58**, 7526–7536.

36 A. Cafarelli, A. Marino, L. Vannozzi, J. Puigmartí-Luis, S. Pané, G. Ciofani and L. Ricotti, *ACS Nano*, 2021, **15**, 11066–11086.

37 P. Christen, K. Ito, R. Ellouz, S. Boutroy, E. Sornay-Rendu, R. D. Chapurlat and B. Van Rietbergen, *Nat. Commun.*, 2014, **5**, 4855.

38 R. J. Nims, L. Pferdehirt, N. B. Ho, A. Savadipour, J. Lorentz, S. Sohi, J. Kassab, A. K. Ross, C. J. O'conor, W. B. Liedtke, B. Zhang, A. L. Mcnulty and F. Guilak, *Sci. Adv*, 2021, **7**, 9858–9885.

39 S. Li, Z. Zhao, J. Zhao, Z. Zhang, X. Li and J. Zhang, *ACS Appl. Nano Mater.*, 2020, **3**, 1063–1079.

40 M. B. Starr, J. Shi and X. Wang, *Angew. Chem. Int. Ed.*, 2012, **51**, 5962–5966.

41 Z. Liang, C. F. Yan, S. Rtimi and J. Bandara, *Appl. Catal. B Environ.*, 2019, **241**, 256–269.

42 J. M. Wu, Y.-G. Sun, W.-E. Chang and J.-T. Lee, *Nano Energy*, 2018, **46**, 372-382.

43 R. Caliò, U. Rongala, D. Camboni, M. Milazzo, C. Stefanini, G. de Petris and C. Oddo, *Sensors*, 2014, **14**, 4755–4790.

44 H. Mohapatra, M. Kleiman and A. P. Esser-Kahn, *Nat. Chem.*, 2017, **9**, 135–139.

45 Z. Wang, J. Ayarza and A. P. Esser-Kahn, *Angew. Chem. Int. Ed.*, 2019, **58**, 12023–12026.

46 Z. Wang, X. Pan, L. Li, M. Fantin, J. Yan, Z. Wang, Z. Wang, H. Xia and K. Matyjaszewski, *Macromolecules*, 2017, **50**, 7940–7948.

47 Z. Wang, X. Pan, J. Yan, S. Dadashi-Silab, G. Xie, J. Zhang, Z. Wang, H. Xia and K. Matyjaszewski, *ACS Macro Lett.*, 2017, 546–549.

48 K. Kubota, Y. Pang, A. Miura and H. Ito, *Science*, 2019, **366**, 1500–1504.

49 Y. Pang, J. W. Lee, K. Kubota and H. Ito, *Angew. Chem. Int. Ed.*, 2020, **59**, 22570–22576.

50 C. Schumacher, J. G. Hernández and C. Bolm, *Angew. Chem. Int. Ed.*, 2020, **59**, 16357–16360.

51 N. Kvasovs and V. Gevorgyan, *Chem. Soc. Rev.*, 2021, **50**, 2244–2259.

52 I. Ghosh, L. Marzo, A. Das, R. Shaikh and B. König, *Acc. Chem. Res.*, 2016, **49**, 1566–1577.

53 P. P. Romańczyk and S. S. Kurek, *Electrochim. Acta*, 2020, 136404.

54 M. M. Chehimi, A. Lamouri, M. Picot and J. Pinson, *J. Mater. Chem. C*, 2014, **2**, 356–363.

55 R. Steeno, M. C. Rodríguez González, S. Eyley, W. Thielemans, K. S. Mali and S. De Feyter, *Chem. Mater.*, 2020, **32**, 5246–5255.

56 K. Matyjaszewski and J. Xia, *Chem. Rev.*, 2001, **101**, 2921–2990.

57 J. Chiefari, Y. K. Chong, F. Ercole, J. Krstina, J. Jeffery, T. P. T. Le, R. T. A. Mayadunne, G. F. Meijs, C. L. Moad, G. Moad, E. Rizzardo and S. H. Thang, *Macromolecules*, 1998, **31**, 5559–5562.

58 G. Moad, E. Rizzardo and S. H. Thang, *Aust. J. Chem*, 2009, **62**, 1402–1472.

59 H. Zhou and J. A. Johnson, *Angew. Chem. Int. Ed.*, 2013, **52**, 2235–2238.

60 M. Chen, M. Zhong and J. A. Johnson, *Chem. Rev.*, 2016, **116**, 10167–10211.

61 T. G. McKenzie, Q. Fu, M. Uchiyama, K. Satoh, J. Xu, C. Boyer, M. Kamigaito and G. G. Qiao, *Adv. Sci.*, 2016, 1–9.

62 J. Xu, K. Jung, A. Atme, S. Shanmugam and C. Boyer, *J. Am. Chem. Soc.*, 2014, **136**, 5508–5519.

63 E. A. Merritt and B. Olofsson, *Angew. Chem. Int. Ed.*, 2009, **48**, 9052–9070.

64 B. M. Teo, M. Ashokkumar and F. Grieser, *J. Phys. Chem. B*, 2008, **112**, 5265–5267.

65 B. M. Teo, F. Grieser and M. Ashokkumar, *Macromolecules*, 2009, **42**, 4479–4483.

66 T. G. McKenzie, F. Karimi, M. Ashokkumar and G. G. Qiao, *Chem. - Eur. J.*, 2019, 1–18.

67 J. Collins, T. G. McKenzie, M. D. Nothling, S. Allison-Logan, M. Ashokkumar and G. G. Qiao, *Macromolecules*, 2018, **52**, 185–195.

68 J. Collins, T. G. McKenzie, M. D. Nothling, M. Ashokkumar and G. G. Qiao, *Polym. Chem.*, 2018, **9**, 2562–2568.

69 T. G. McKenzie, E. Colombo, Q. Fu, M. Ashokkumar and G. G. Qiao, *Angew. Chem. Int. Ed.*, 2017, **56**, 12302–12306.

70 Z. Z. Z. Wang, Z. Z. Z. Wang, X. Pan, L. Fu, S. Lathwal, M. Olszewski, J. Yan, A. E. Enciso, Z. Z. Z. Wang, H. Xia and K. Matyjaszewski, *ACS Macro Lett.*, 2018, 275–280.

71 J. Collins, T. G. McKenzie, M. D. Nothling, S. Allison-Logan, M. Ashokkumar and G. G. Qiao, *Macromolecules*, 2019, **52**, 185–195.

72 J. B. Ravnsbæk and T. M. Swager, *ACS Macro Lett.*, 2014, **3**, 305–309.

73 G. S. Lee, B. R. Moon, H. Jeong, J. Shin and J. G. Kim, *Polym. Chem.*, 2019, **10**, 539–545.

74 S. Grätz and L. Borchardt, *RSC Adv.*, 2016, **6**, 64799–64802.

75 N. Ohn, J. Shin, S. S. Kim and J. G. Kim, *ChemSusChem*, 2017, **10**, 3529–3533.

76 O. Maurin, P. Verdié, G. Subra, F. Lamaty, J. Martinez and T. X. Métro, *Beilstein J. Org. Chem.*, 2017, **13**, 2087–2093.

77 M. Hasegawa, Y. Akiho and Y. Kanda, *J. Appl. Polym. Sci.*, 1995, **55**, 297–304.

78 H. Y. Cho and C. W. Bielawski, *Angew. Chem. Int. Ed.*, 2020, **59**, 13929–13935.

79 G. A. Bowmaker, *Chem. Commun.*, 2013, **49**, 334–348.

80 H. Nulwala, A. Mirjafari, X. Zhou, *Eur. Polym. J.,* 2018, **108**, 390-398.

81 K. Brandt, C. Neusel, S. Behr, G. A. Schneider, *J. Mater. Chem. C.*, 2013, **1**, 3129-3137.

82 R. K. Goyal, S. S. Katkade, D.M. Mule, *Comp. B*., 2013, **44**, 128-132.

83 H. Mohapatra, J. Ayarza, E. Sanders, A. M. Scheuermann, P. Griffin and A. P. Esser-Kahn, *Angew. Chem. Int. Ed.*, 2018, 11208–11212.

84 Z. Wang, J. Wang, J. Ayarza, T. Steeves, Z. Hu, S. Manna and A. P. Esser-Kahn, *Nat. Mater.*, 2021, **20**, 869–874.

85 J. Ayarza, Z. Wang, J. Wang and A. P. Esser-Kahn, *ACS Macro Lett.*, 2021, **10**, 799–804.

86 A. Bagheri and J. Jin, *ACS Appl. Polym. Mater.*, 2019, **1**, 593–611.

87 M. H. Shaw, J. Twilton and D. W. C. MacMillan, *J. Org. Chem.*, 2016, **81**, 6898–6926.

88 A. B. Pangborn, M. A. Giardello, R. H. Grubbs, R. K. Rosen and F. J. Timmers, *Organometallics*, 1996, **15**, 1518–1520.

Chapter 3: Mechanochemical Reversible-Addition Fragmentation Chain Transfer Polymerization

3.1 Introduction

The term mechanochemistry, first coined by Ostwald in 1887, utilizes chemical transformations driven by mechanical force for applications in materials science, inorganic, and organic synthesis.[1-5] Force induced transformations offer unique advantages over traditional methods of activation (e.g., heat, light, and electrochemistry) by avoiding thermally induced by-products or limited photochemical surface penetration.[3,6,7] Oftentimes, mechanochemical reactions can also be performed in nearly solvent-free conditions where the use of toxic bulk reaction media is avoided.[8, 9] This paradigm provides a greener alternative to traditional solution-phase chemistry. In the context of macromolecular science, mechanochemistry has almost exclusively been used for destruction of soft matter where applied mechanical stress, often from ultrasound cavitation bubbles, is used to degrade polymers into smaller fragments.[10-13] More recently, work pioneered by Moore and others utilizes mechanical force in a constructive manner to *selectively* cleave backbone linkages, release cargo, and/or modulate optical/mechanical properties within designer macromolecules.[1,14-18] In particular, polymeric materials imbued with force responsive units called mechanophores have seen significant utility in applications spanning catalysis, self-healing, and sensing.[1]

A variety of recent reports couple the advantages of mechanochemistry with constructive synthetic redox processes. This burgeoning field, appropriately termed mechanoredox catalysis,[14,19] involves the polarization of piezoelectric materials in response to mechanical stimuli that then initiate redox events via single electron transfer.[19-21] The piezoelectric effect has historically found utility in diverse engineering applications, such as water splitting and treatment, energy harvesting, and biomedicine.[21-24] In synthetic organic

chemistry, mechanoredox catalysis has been employed as an alternative to photoredox catalysts for small molecule construction.[20] Recently, piezoelectric nanoparticles (PNPs) such as ZnO and $BaTiO_3$ have been utilized to initiate small molecule arylation, borylation, atom-transfer radical addition, and trifluoromethylation reactions under ball milling (BM) conditions.[25-27] In addition to small molecule transformations, mechanoredox catalysis is utilized in polymer science to facilitate step growth, free radical polymerization (FRP), and atom transfer radical polymerization (ATRP) under ultrasonic (US) irradiation.[14,28-32] Similar chemistry within related thermosets provides preliminary evidence for utilizing mechanoredox catalysis in force-responsive "living" materials.[33,34]

Despite significant progress in mechanoredox catalyzed polymerizations, there are still not well-established direct routes to the sustainable synthesis of materials with complex architectures. The development of mechanoredox catalyzed reversible-addition fragmentation chain transfer (RAFT) polymerization methodology offers the potential to bridge this gap in synthetic methodology; RAFT is a living and user-friendly polymerization technology with broad functional group tolerance.[35] Only one previous report exists on the development of mechanoredox RAFT. Zhao recently reported a solution-state process regulated by ultrasonic stimulation and ZnO (Figure 3.1A).[34] Alkyl radicals generated from piezoelectric reduction of an activated alkyl bromide (i.e., ATRP initiator) triggered S-S bond scission of a bis(trithiocarbonate) disulfide RAFT agent.[36] The development of related processes with conventional RAFT agents under ball milling conditions would enable more sustainable implementation with broader applications.

Building upon the transition metal-free mechanoredox FRP process facilitated by diaryliodonium salts and PNPs[31] to access high molar mass poly(meth)acrylates described in the previous chapter, we postulated that addition of a chain transfer agent may enable RAFT polymerization. Notably, we envisioned not only gaining control over molar mass, dispersity,

and degree of polymerization,[37-42] but also more importantly, sustainably accessing complex architectures that are difficult to synthesize under traditional solution-state RAFT conditions.

We hypothesized that in a typical mechanoredox RAFT polymerization, mechanically-polarized PNPs could reduce diphenyl iodonium hexafluorophosphate (DPIHP) to form phenyl radicals to commence the RAFT equilibrium (*vide infra*). Herein, we demonstrate an efficient mechanoredox RAFT polymerization process facilitated by diaryliodonium salts and piezoelectrically active $BaTiO_3$. This process was achieved using a conventional RAFT agent with complementary US irradiation, BM, and vortex mechanical stimuli without the need of exogenous additives.

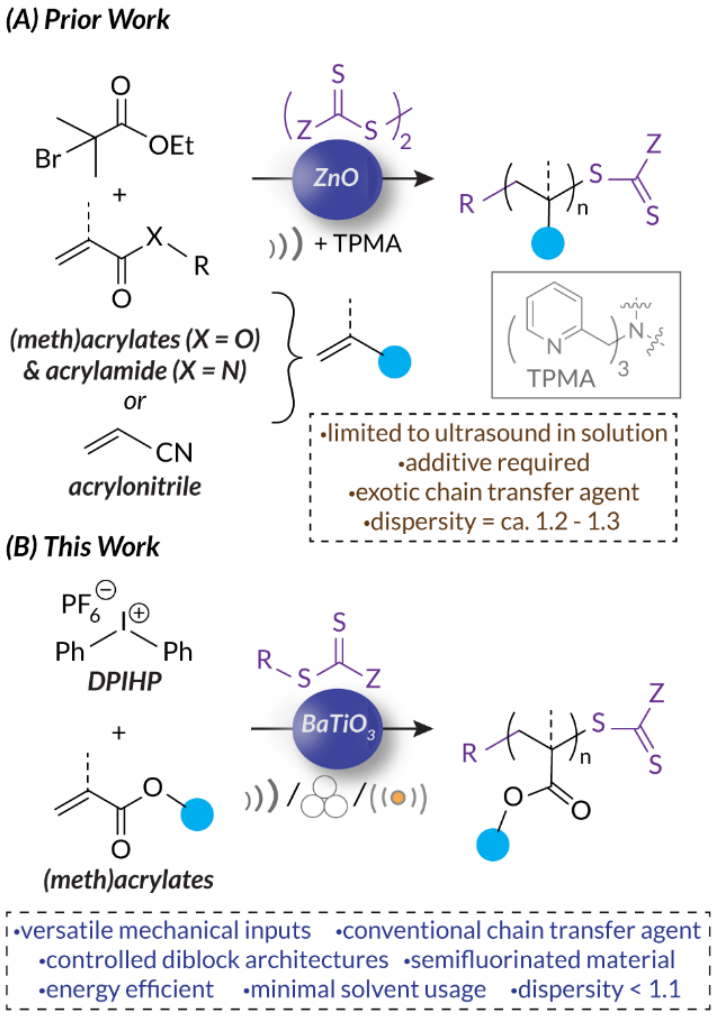

Figure 3.1. Evolution of mechanoredox RAFT leading to this work.

Described in this chapter, mechanoredox RAFT polymerizations were carried out using DPIHP as the initiator and 2-(dodecylthiocarbonothioylthio)-2-methylpropionic acid (DDMAT) as the chain transfer agent. Because of our prior success with $BaTiO_3$ in FRP[31], $BaTiO_3$ was used as the PNP in all mechanoredox RAFT studies.

3.2 Mechanoredox RAFT: Ultrasonic Irradiation

We began our initial studies in solution under low frequency (ca. 40 kHz) US irradiation. It is well known that the high frequency (ca. 490 kHz) US treatment of organic solvents such as DMF and DMAc leads to bond homolysis and formation of organic radicals that can initiate sonochemical RAFT (sonoRAFT) of (meth)acrylates.[43] To study whether similar sonoRAFT occurs at low frequency, a potential background process in mechanoredox RAFT, RAFT polymerization was carried out with butyl acrylate (BA) in various organic solvents using DDMAT as a chain transfer agent. Interestingly, moderate to high conversion was observed with DMF (65% by ^{1}H NMR spectroscopy) and DMAc (40% by ^{1}H NMR spectroscopy) with very good control over dispersity (1.05) (Figure 3.2A). On the other hand, no polymerization was observed with DMSO, MeCN, anisole, and PhMe (Table 3.1). These results are consistent with our previously reported mechanoredox FRP system; amide-based solvents are capable of non-inconsequential homolytic cleavage under low frequency US conditions. These conditions also afford little control over initiation and are not amenable to the synthesis of more architecturally complex materials. The control afforded by discrete initiators motivated us to develop suitable mechanoredox methodology.

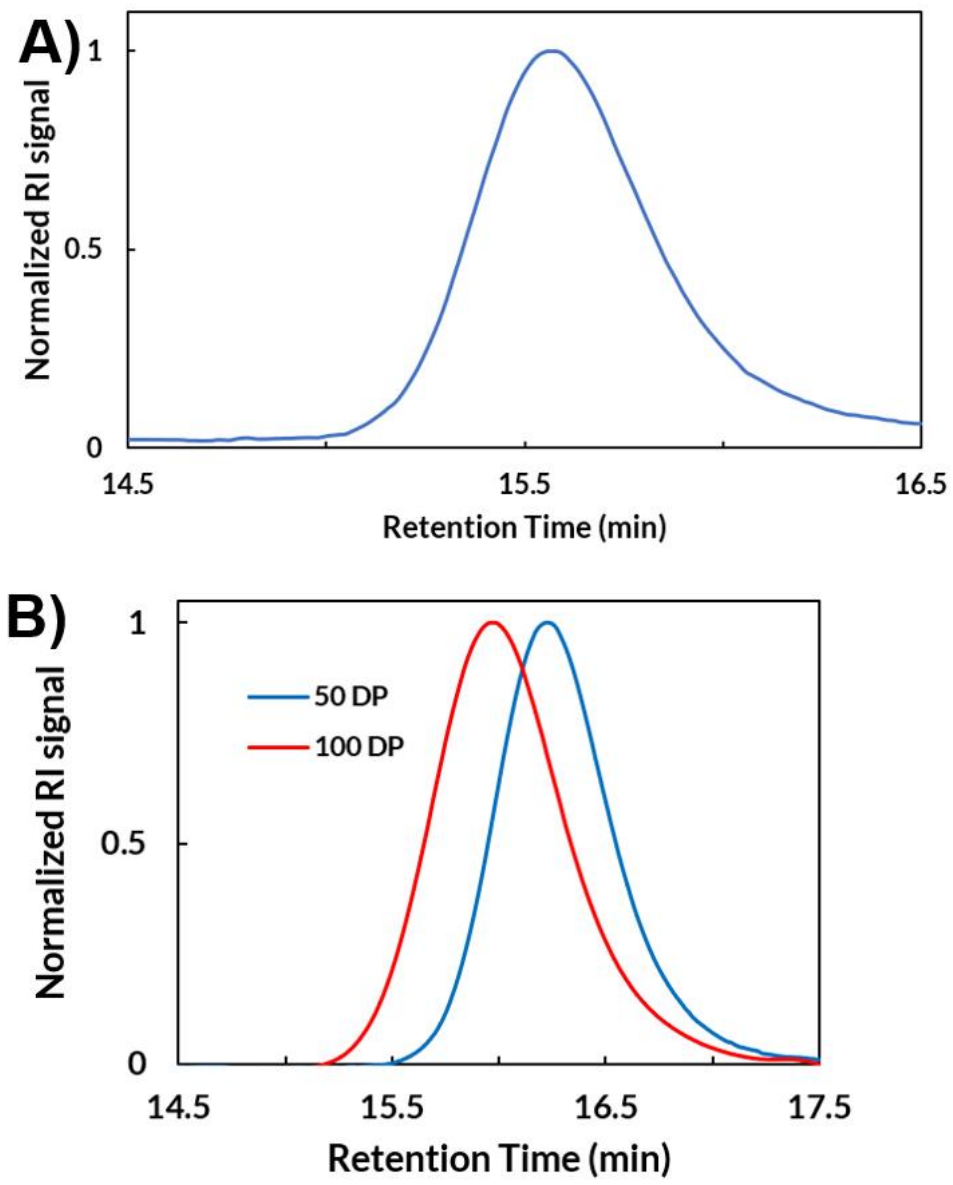

Figure 3.2. GPC-RI traces of PBA synthesized by A) sonoRAFT with DMF as solvent at target DP = 50 (Entry 1, Table 3.1) and B) mechanoredox RAFT (US irradiation) with DMSO as solvent at target DP = 50 and 100 (Entries 1 and 2, Table 3.3).

Table 3.1: SonoRAFT of BA (US irradiation without $BaTiO_3$) in different organic solvents.

Entry[a]	Solvent	Conv. (%) [b]	$M_{n,\,theo}$ (kDa)	$M_{n,\,GPC}$ (kDa)[c]	Đ [c]
1	DMF	65	4.5	4.2	1.05
2	DMAc	40	3.5	3.0	1.02
3	DMSO	<5	-	-	-
4	Acetonitrile	<5	-	-	-
5	Anisole	<5	-	-	-
7	Toluene	<5	-	-	-

Reaction conditions: [a] [BA] = 7.3 M, target DP = 50, Ultrasonic bath (40 kHz, 70 W, 20 °C). Reaction time - 24 h. [b] Conversion was determined by ^{1}H NMR spectroscopy, [c] M_n and Đ were determined by GPC-MALS.

Focusing on solvents that did not lead to polymerization under low frequency sonoRAFT (i.e., DMSO, MeCN, PhMe), we attempted mechanoredox RAFT through addition of $BaTiO_3$ and DPIHP to the reaction mixture. Moderate conversion (ca. 50%) was observed only in DMSO (Table 3.2) while no polymerization was observed in MeCN and PhMe, likely due to poor solubility of DPIHP and/or DDMAT. Mechanoredox RAFT of a range (meth)acrylate monomers was then carried out in DMSO (7 wt% $BaTiO_3$). Monomer conversion (measured by ^{1}H NMR spectroscopy) was moderate with *tert*-butyl acrylate (*t*BA), BA, and methyl acrylate (MA), and much lower with methyl methacrylate (MMA) (Table 3.3). Number-average molecular weight (M_n) and dispersity (Đ = M_w/M_n) measured by gel permeation chromatography coupled with a multi-angle light scattering detector (GPC-MALS) reveals decent correlation of theoretical and experimental molar mass with relatively well controlled dispersity in *t*BA, BA, and MA (Table 3.3 and Figure 3.2B). PMMA shows a significant difference in theoretical and experimental molar mass, perhaps due to slow propagation and/or chain scission under ultrasound irradiation.[43] Despite these initial promising results, polymerization reactions were quite slow (Figure 3.3) with only moderate

monomer conversion (up to 50%) after 24 h (Table 3.3). Interestingly, when mechanoredox RAFT of BA was carried out *without* DPIHP (Table 3.3, Entry 2), approximately 15% conversion was observed. We hypothesize that this result could be due to direct reduction of DDMAT by polarized $BaTiO_3$ leading to RAFT polymerization, akin to similar mechanisms proposed for PET-RAFT or *e*RAFT.[44-46]

Table 3.2: Mechanoredox RAFT of BA (US irradiation with $BaTiO_3$) in different organic solvents.

Entry[a]	Solvent	Conv. (%) [b]	$M_{n,\,theo}$ (kDa)	$M_{n,\,GPC}$ (kDa)[c]	Đ [c]
1	DMSO	50	3.6	4.2	1.12
2[d]	DMSO	<5	-	-	-
3	Acetonitrile	<5	-	-	-
4	Anisole	<5	-	-	-
5	Toluene	<5	-	-	-

Reaction conditions: [a] [BA] = 7.3 M, target DP = 50, 7 wt% $BaTiO_3$, ultrasonic bath (40 kHz, 70 W, 20 °C). Reaction time - 24 h. [b] Conversion was determined by ^{1}H NMR spectroscopy, [c] M_n and Đ were determined by GPC-MALS. [d] Reaction carried out in absence of $BaTiO_3$.

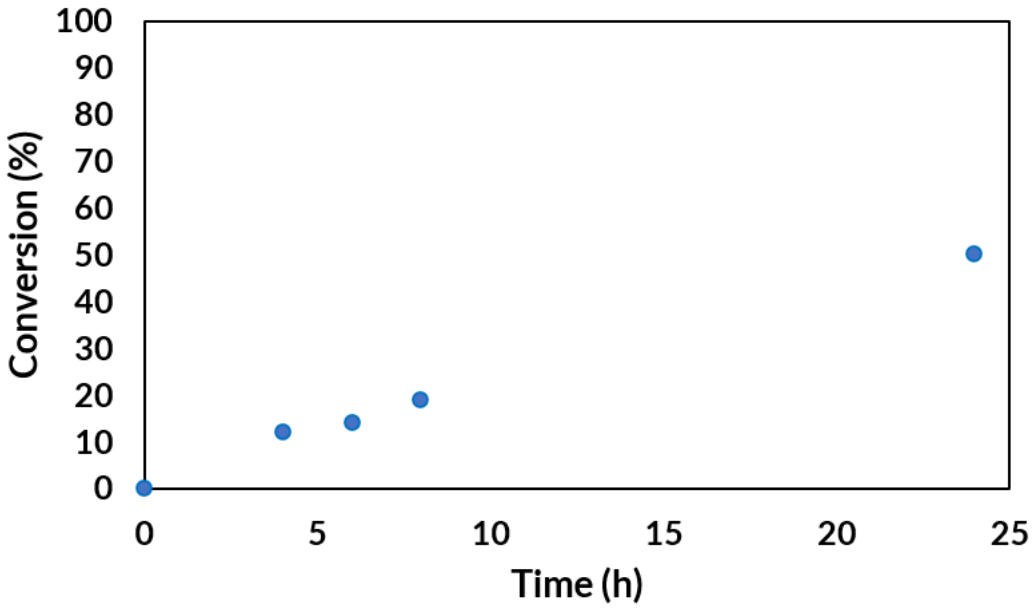

Figure 3.3. Monomer conversion progression in mechanoredox RAFT of BA (US irradiation) with target DP = 50.

Table 3.3: Mechanoredox RAFT polymerization of (meth)acrylates in an ultrasonication bath.

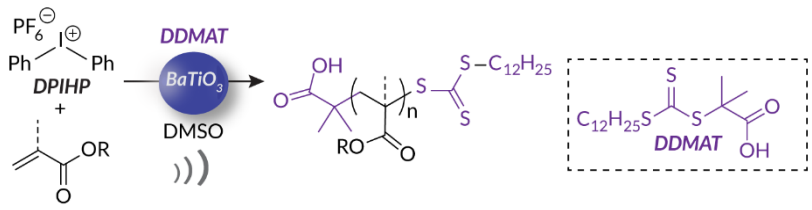

Entry[a]	Monomer	Target DP	Conversion (%) [b]	$M_{n,\,theo}$ (kDa)	$M_{n,\,GPC}$ (kDa) [c]	Đ[c]
1	BA	50	50	3.6	4.2	1.12
2[d]	BA	50	15	1.4	3.9	1.40
3	BA	100	38	5.2	6.3	1.16
4	*t*BA	45	45	3.3	4.5	1.20
5	MA	50	50	2.6	4.3	1.22
6	MMA	50	20	1.3	5.4	1.45

Reaction condition: [a] [monomer] = 7.3 M in DMSO, target DP = 50, $[DDMAT]_0$: $[DPIHP]_0$ = 1:1. 7 wt% $BaTiO_3$, ultrasonic bath (40 kHz, 70 W, 20 °C). Reaction time - 24 h. [b] Conversion was determined by ^1H NMR spectroscopy, [c] M_n and Đ were determined by GPC-MALS. [d] Reaction carried out in absence of DPIHP.

3.3 Mechanoredox RAFT: Ball Milling

3.3.1 Homopolymer synthesis

Our initial mechanoredox RAFT results using low frequency ultrasound suffered from slow reactions and moderate control over dispersity. Based on previous success in translating processes into a ball mill, we hypothesized we could solve these challenges and prepare for more complex systems (e.g., diblock copolymers) under revised conditions.[31] In addition, BM is a greener synthetic method as only trivial amounts of solvent are needed.[47] BM is also more energy efficient compared to conventional solution-state systems.[2] Initial mechanoredox RAFT polymerizartion (Table 3.4) was carried out with *t*BA in the presence of $BaTiO_3$, DPIHP, and DDMAT. A small amount of DMF (η = 0.060 μL/mg) was used for liquid assisted grinding (LAG); it is well accepted that $0 < \eta < 1$ defines a LAG process.[2] Here, η equals the mass ratio

of solvent used (in volume) to the total mass of other materials in the reaction mixture.[48] Using standard reaction (SR) conditions under an inert atmosphere, quantitative monomer conversion was observed in only 3 h (Table 3.4, Entry 1). GPC analysis of the resulting P*t*BA reveals narrow dispersity (Đ = 1.04) and good correlation between theoretical and experimental M_n (Figure 3.4). In contrast to our previous mechanoredox FRP studies[31], when the polymerization reaction was carried out in the presence of air, no monomer conversion was observed (Table 3.4, Entry 2) within 3 h. In addition, when control reactions were carried out without applying force or by excluding DPIHP or $BaTiO_3$ (or both), no polymerization was observed, confirming the importance of the mechanoredox process for effective polymerization (Table 3.4, Entries 5 – 6). The importance of LAG is exemplified when exogenous DMF is removed and no monomer conversion is observed (Table 3.4, Entry 7). Results from this initial study established reaction conditions for subsequent processes (Figure 3.5).

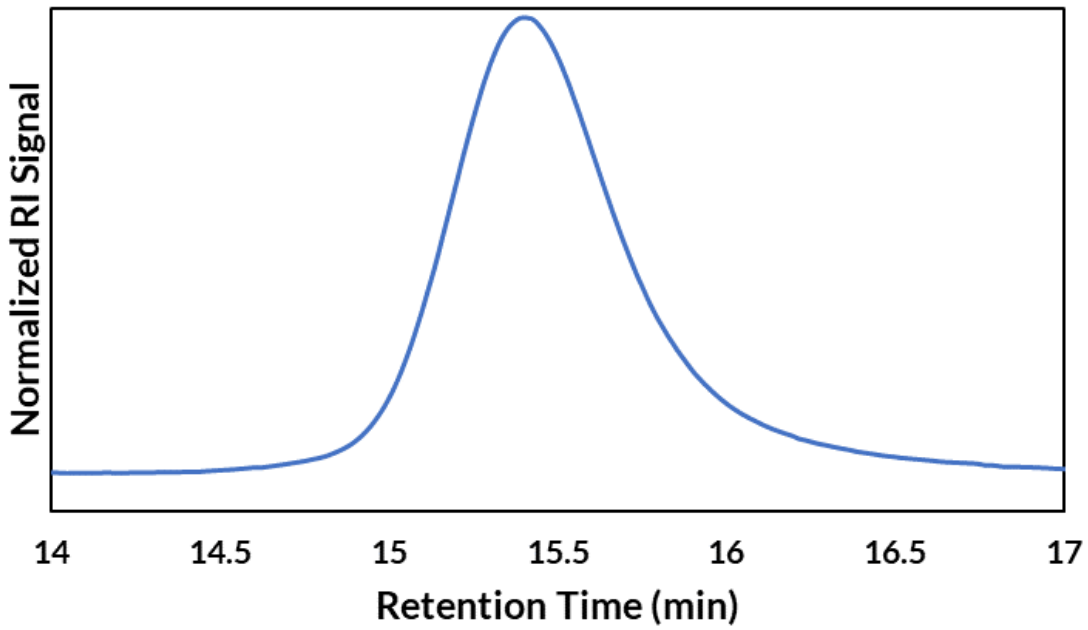

Figure 3.4. GPC-MALS-RI trace of P*t*BA with target DP = 50 synthesized by mechanoredox RAFT in ball mill. $M_{n,\,theo}$ = 6.4 kDa, $M_{n,\,GPC}$ = 6.2 kDa, Đ = 1.04.

Table 3.4: Controls for mechanoredox RAFT polymerization in a ball mill.

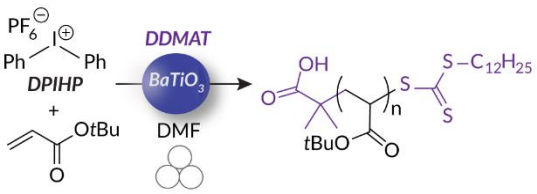

Entry[a]	Conditions	Conversion (%) [b]
1	Standard reaction	>95
2	In air	<5
3	Without force	<5
4	Without DPIHP	<5
5	Without $BaTiO_3$	<5
6	Without DMF	<5
7	Without $BaTiO_3$ and DPIHP	<5

Reaction conditions: [a] Target DP = 50, LAG (η = 0.060 μL/mg) with DMF. $[DDMAT]_0$: $[DPIHP]_0$ = 1:1. Ball mill (1.5 mL stainless steel jar, 5 mm stainless steel grinding ball, 30 Hz). 15 wt% $BaTiO_3$, reaction time - 3 h. [b] Conversion was determined by ^1H NMR spectroscopy.

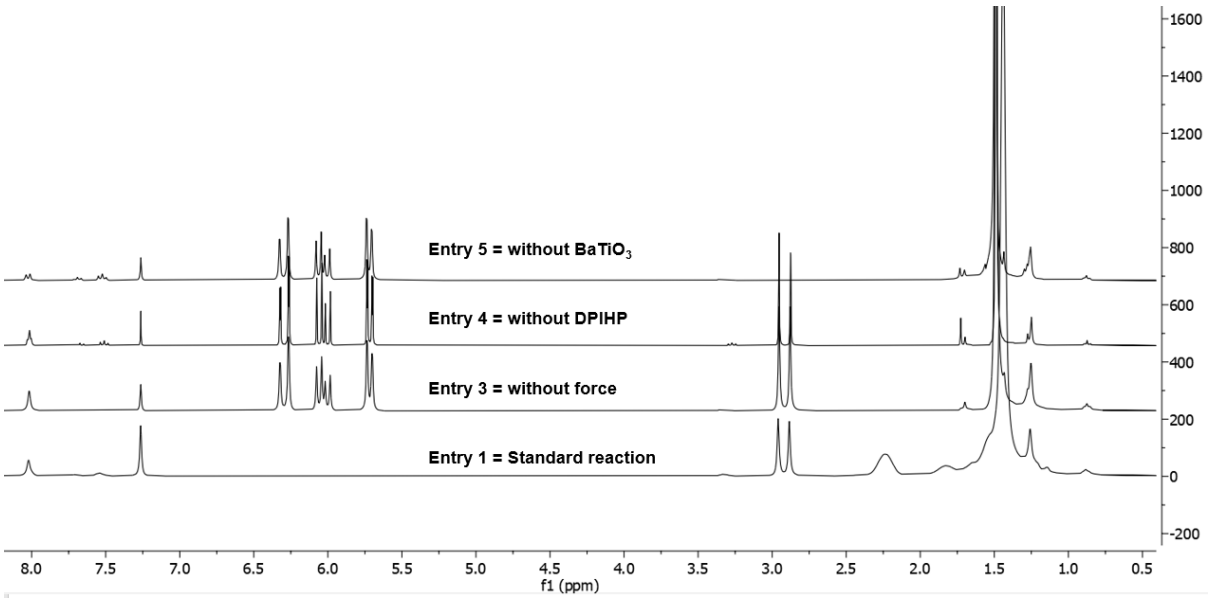

Figure 3.5. ^1H NMR spectra of mechanoredox RAFT of *t*BA under various conditions (see Table 3.4).

Next, to study the viability of mechanoredox RAFT in a ball mill, a range of (meth)acrylate monomers were evaluated at various target DP values (Table 3.5). Quantitative conversion was achieved with BA and di(ethylene glycol) ethyl ether acrylate (DEGEEA); GPC analysis reveals narrow dispersity and excellent correlation between theoretical and experimental molar mass. MA also exhibits high conversion (80%) with good control over molar mass. Mechanoredox RAFT of MMA, however, was found to be slow and less controlled with the experimental molar mass diverging significantly from theoretical values. This result is consistent with our findings in FRP; low conversion and broader dispersity is likely due to slow propagation compared to other acrylate-based monomers and mechanochemical chain cleavage of higher T_g (glass transition temperature) PMMA during the polymerization process.[49]

Additionally, $BaTiO_3$ used in this mechanoredox BM process can be easily recovered by centrifugation and be recycled at least three time. Subsequent reactions do not show deviations in monomer conversion (Figure 3.6). Compared to an analogous solution-state RAFT polymerization (see SI), BM is at least three-times more energy efficient to achieve full conversion (Figure 3.7). Combined, these data confirm that there are green chemistry advantages to mechanoredox RAFT over traditional solution-state processes.

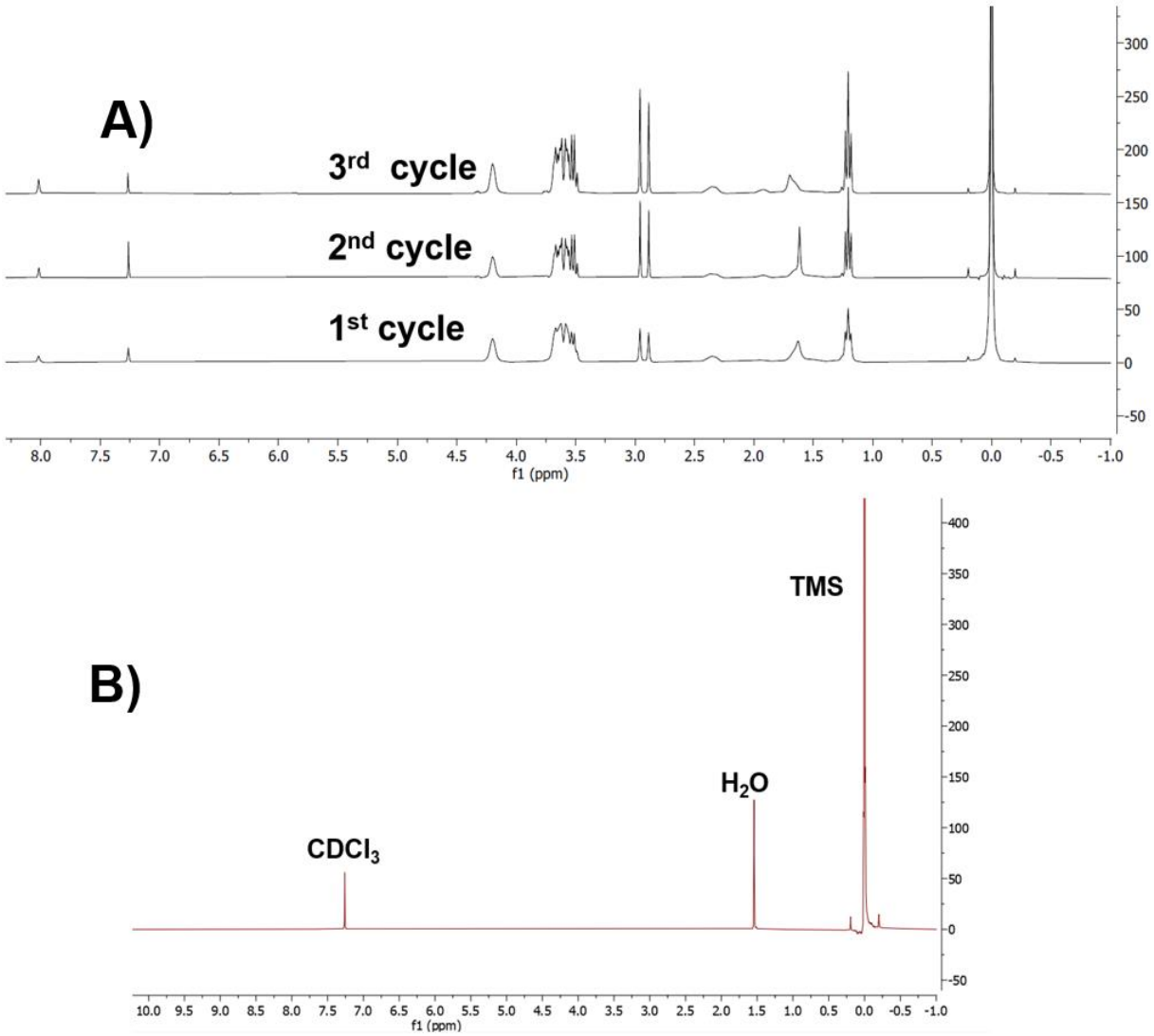

Figure 3.6. A) ^{1}H NMR spectra of PDEGEEA synthesized via mechanoredox RAFT using "recycled" $BaTiO_3$. >95% monomer conversion is obtained even after two rounds of recycling (3rd reaction cycle). B) ^{1}H NMR spectrum of suspended "recovered $BaTiO_3$" after drying in a vacuum oven.

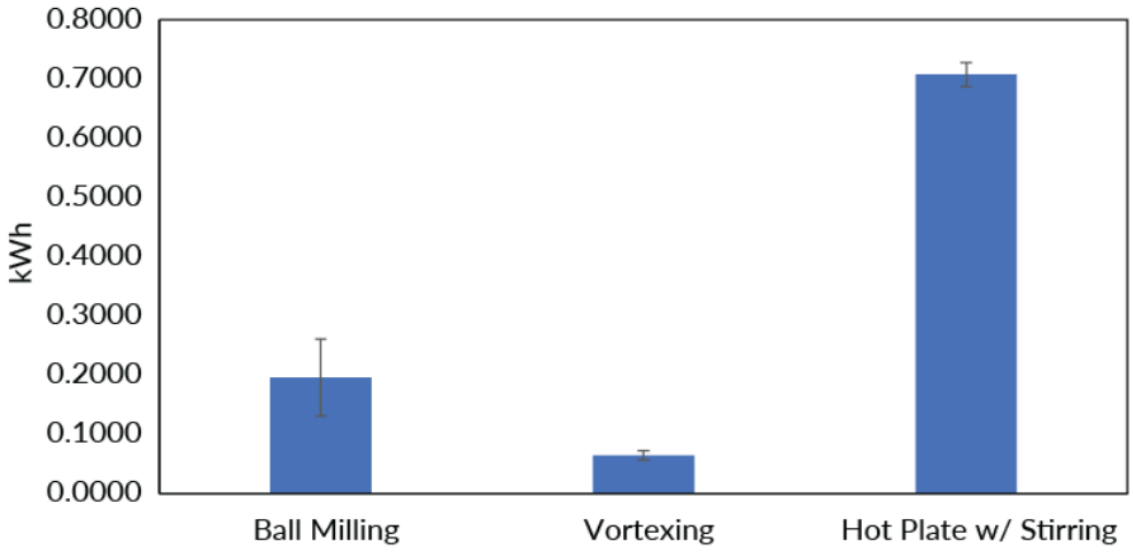

Figure 3.7. Energy consumption of *t*BA RAFT polymerizations under mechanoredox RAFT conditions (ball mill or vortexer) compared to a "traditional" thermal RAFT in solution on a heated stir plate. Ball milling, vortexing, and "traditional" thermal processes were carried out for 3 h, 8 h, and 20 h respectively. All experiments were run triplicate (n = 3). Error bars represent standard deviations for each set of experiments.

Kinetic analysis of BA polymerization (target DP = 100) using our standard mechanoredox RAFT conditions was carried out in a ball mill and characterized by ^{1}H NMR spectroscopy and GPC-MALS; the collective data reveals a faster reaction profile compared to our US system. When plotted on a semilogarithmic scale, a linear increase in M_n with conversion was observed (Figure 3.8A). A narrow dispersity is maintained at all time points as would be expected for a RAFT process (Figure 3.8B). Additionally, all GPC peaks are symmetrical and shifted monomodally to lower retention time with increased conversion (Figure 3.8C). Interestingly, while monitoring the polymerization of BA at target DP = 50, an incubation period of 80 minutes was observed. After the incubation period, linear conversion was observed before reaching quantitative conversion in 3 h (Figure 3.9). We postulate that this initial incubation period is due to slower solvation of DDMAT and DPIHP; larger quantities of these reagents are required for target DP = 50 compared to target DP = 100.

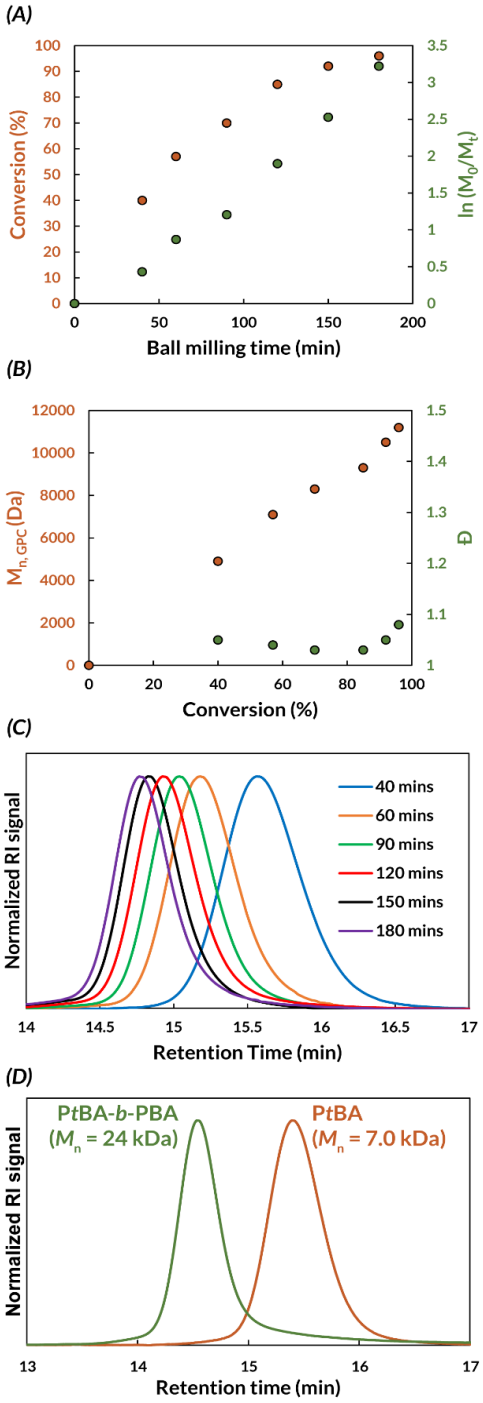

Figure 3.8. Kinetic data of mechanoredox RAFT polymerization of BA (target DP = 100) in a ball mill showing kinetic profile with respect to A) conversion and B) molecular weight and dispersity, C) GPC traces as a function of reaction time, D) GPC traces for P*t*BA-*b*-PBA polymer synthesized from chain extension of P*t*BA macroinitiator via mechanoredox RAFT in a ball mill.

3.3.2 Evidence of Living Polymerizations

To confirm living behavior of the polymers synthesized by mechanoredox RAFT, we performed one–pot chain extension experiments. Initially a P*t*BA macroinitiator with target DP = 50 was synthesized using standard mechanoredox RAFT conditions in a ball mill (3 h, M_n = 7.0 kDa, Đ = 1.07) (Figure 3.8D) and was used for chain extension studies without isolation. BA was then added into the milling jar, in addition to $BaTiO_3$, DPIHP, and DMF, before milling for an additional 3 h. GPC-MALS characterization of the resulting polymer shows a monomodal shift to lower retention time (M_n = 24 kDa) while preserving a narrow dispersity (Figure 3.8D). These results confirm chain-end fidelity of the polymers synthesized by mechanoredox RAFT in a ball mill.

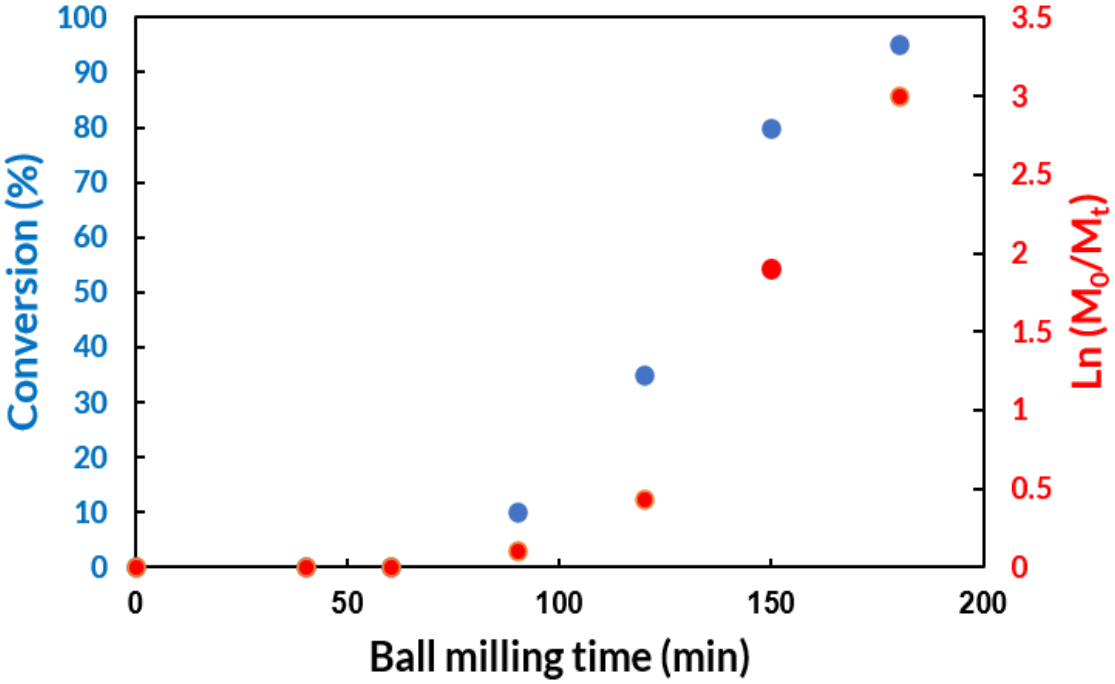

Figure 3.9. Kinetic data for mechanoredox RAFT polymerization of BA (target DP = 50) in a ball mill.

To explore the versatility of mechanoredox RAFT in a ball mill, two telechelic polymers were synthesized. Telechelic polymers contain two reactive end groups leading to bidirectional polymer growth and are often used as building blocks for adaptable macromolecular structures.[50,51] First, telechelic P*t*BA was synthesized using the telechelic RAFT agent S, S′-Bis (R, R′-dimethyl-R″-acetic acid)-trithiocarbonate (ATTC) (Figure 3.10A) using standard mechanoredox RAFT conditions. GPC-MALS analysis of the resulting polymer reveals good correlation between theoretical and experimental M_n values (M_n = 21.5 kDa) based on the target DP with a narrow dispersity (Figure 3.11). To validate the formation of a telechelic polymer, aminolysis was used to cleave the trithiocarbonyl group. The resulting polymer shifted to longer retention time (Figure 3.10B) and was approximately half of the original telechelic P*t*BA molar mass (M_n = 10.6 kDa), matching the expectation of cleavage at the bidirectional chain transfer agent. Only telechelic polymer growth, as opposed to unidirectional polymerization, can explain this experimental result. Similar results were observed for a second telechelic RAFT agent (bi-DDMAT), further showcasing the flexibility of this system (Figure 3.12). We envision that the construction of complex soft materials derived from telechelic systems will be further enabled by mechanoredox RAFT technology.

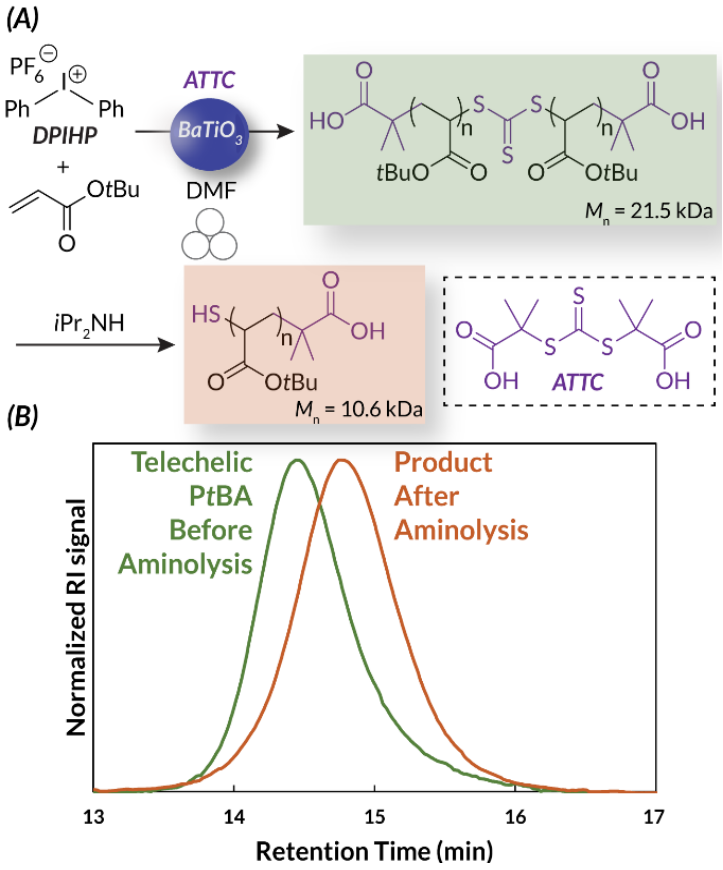

Figure 3.10. A) Synthesis of telechelic P*t*BA via mechanoredox RAFT in a ball mill and aminolysis of the resulting telechelic polymer, B) GPC traces of telechelic P*t*BA before and after aminolysis.

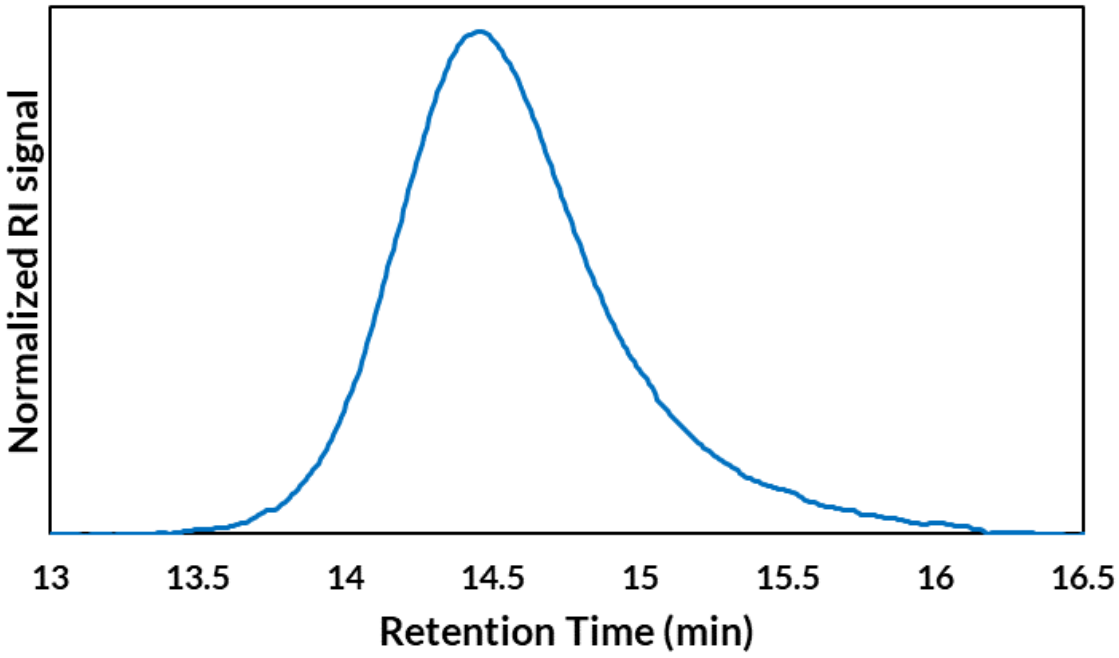

Figure 3.11. GPC-MALS-RI trace of telechelic P*t*BA synthesized by mechanoredox RAFT using ATTC as the chain transfer agent in a ball mill. $M_{n,\,theo}$ = 23.0 kDa, $M_{n,\,GPC}$ = 21.5 kDa, Đ = 1.04.

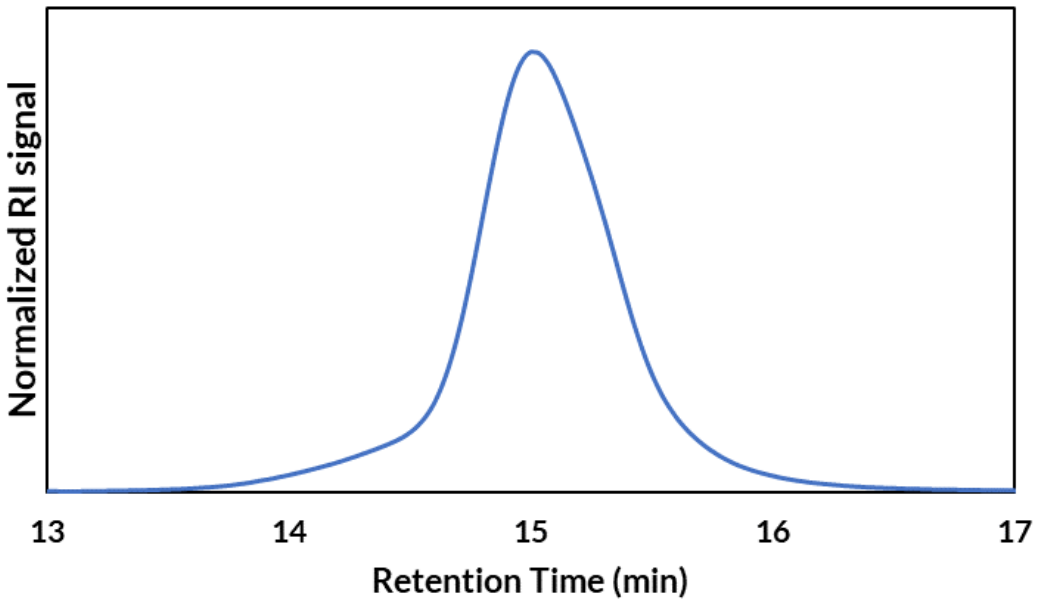

Figure 3.12. GPC-MALS-RI trace of the resulting telechelic polymer (> 95% BA conversion). $M_{n,\,theo}$ = 12.9 kDa, $M_{n,\,GPC}$ = 11.1 kDa, Đ = 1.1.

Table 3.5: Mechanoredox RAFT polymerization of (meth)acrylates in a ball mill.

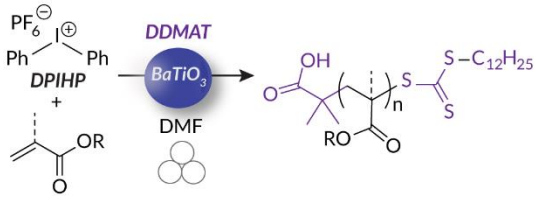

Entry[a]	Monomer	Target DP	Conversion (%) [b]	$M_{n,\,theo}$ (kDa)	$M_{n,\,GPC}$ (kDa) [c]	Đ[c]
1	BA	50	>95	6.5	6.6	1.03
2	BA	100	>95	13.1	12.5	1.07
3	BA	200	>95	24.7	24.1	1.08
4	DEGEEA	50	>95	9.3	9.6	1.08
5	MA	100	80	7.3	7.2	1.03
6	MMA	100	65	6.9	16.1	1.45

Reaction condition: [a] LAG (η = 0.060 μL/mg) with DMF. [DDMAT]: [DPIHP] = 1:1. Ball mill (1.5 mL stainless steel jar, 5 mm stainless steel grinding ball, 30 Hz). 15 wt% $BaTiO_3$, reaction time - 3 h. [b] Conversion was determined by ^{1}H NMR spectroscopy. [c] M_n and Đ were determined by GPC-MALS

3.3.3 Semi Fluorinated Diblock Synthesis

Based on the efficiency demonstrated for mechanoredox RAFT processes in a ball mill, we envisioned polymers that are challenging to synthesize with traditional solution-state reversible deactivation radical polymerization (RDRP) methods could be realized using our developed system, as growth in the field of polymer synthesis has expanded the desire for more complex structures. Block copolymers have become of interest, particularly for their self-assembly properties.[52-53] Biologically synthesized polymers (i.e. DNA, proteins) are highly ordered in their

addition; newly developed routes to block copolymers approach the ability to synthetically create such orderly materials. Most commonly, RDRP are utilized to make block copolymers as chain end fidelity is maintained in the living polymerization, but others have attempted to accomplish the synthesis of block copolymers through other routes as well.[54] For example, ring opening metathesis polymerization (ROMP), in which polymer synthesis occurs via cross metathesis of olefins, has been used as a route to block copolymers but requires metal additives to conduct the polymerization, presenting potential purification challenges.[54,55] Alternatively, ionic block copolymer polymerizations have been conducted; however, harsh conditions are often required and significant air and water sensitivity lead to restrictions in the relevancy of the method.[54,56] The directive control of block order, chain length, and dispersity makes RDRP the optimum path for making block copolymers.

RAFT is a uniquely advantageous RDRP option for the synthesis of block copolymers as it allows for well-defined block lengths, continuous addition of monomer due to chain end fidelity, and a significant library of chain transfer agents available to tune the system to the reactivity of the desired monomers.[54,57] Additionally, RAFT does not require metal additives to conduct polymerization, unlike other RDRP methods, which makes purification of polymers for biological applications straightforward. A myriad of modifications to this well-known technique have been developed to increase the utility of the chemistry, including nanoparticle-centered polymer growth and aqueous-based chemistry.[58,59] Traditionally, when used for block copolymer synthesis, heat or light have been used as stimulus to induce reactivity.

A particularly difficult system to copolymerize via tradition RAFT solution-based methods is immiscible monomers due to lack of a shared compatible solvent; recent work from Kim et al.

on mechanochemical ring-opening metathesis polymerization exemplifies these issues.[60] The synthesis of well-defined semifluorinated polymers using conventional CRP methods often suffer from broad molar mass distribution and/or use of expensive fluorinated solvent (>$15/g) as recently demonstrated by Chen and Hawker.[61-65] Additional advances have been made using photoredox CRP methods with exotic fluorinated chain transfer agents.[66] Only recently have semifluorinated polymers become available under photoRAFT conditions using conventional CTAs and solvents.[67] With an emphasis on sustainability and the possibility of future advanced applications (e.g., manufacturing opaque composites, nanoparticle synthesis)[34], we envisioned that mechanoredox RAFT could fill a fundamental gap in synthetic polymer methodology.

To demonstrate the power of our developed RAFT technology, we targeted a semifluorinated diblock copolymer containing an immiscible hydrophilic PDEGEEA block. Using standard mechanoredox RAFT conditions in a ball mill, quantitative conversion of DEGEEA into the first block was achieved in 3 h (Figure 3.13A).

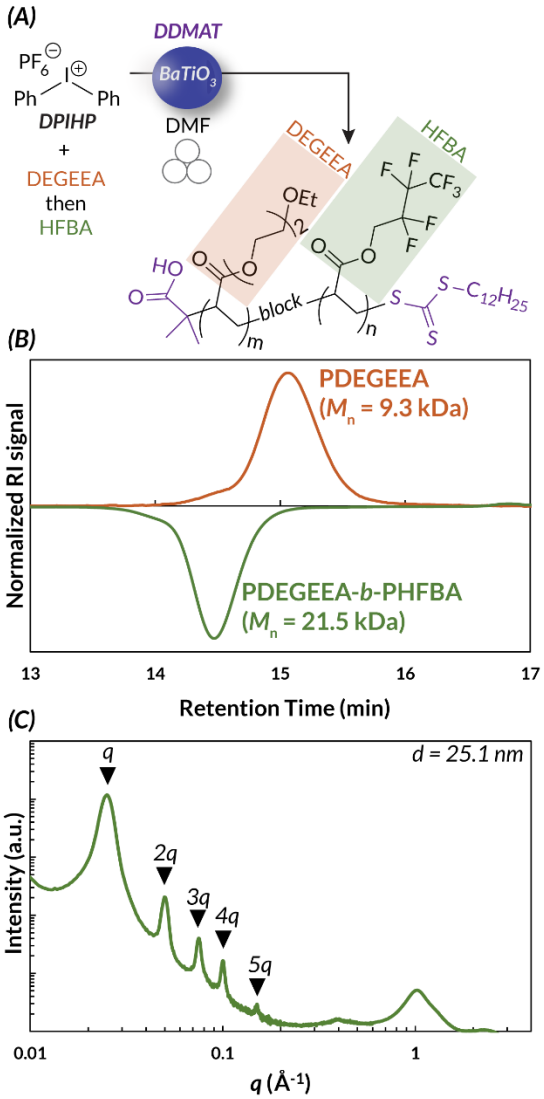

Figure 3.13. A) Synthesis of PDEGEEA-*b*-PHFBA by mechanoredox RAFT, B) GPC trace for PDEGEEA-*b*-PHFBA, C) 1D SAXS curve of PDEGEEA-*b*-PHFBA.

GPC-MALS (Table 3.5) analysis revealed narrowly disperse PDEGEEA with excellent correlation between theoretical and experimental molar mass (M_n = 9.3 kDa, Đ = 1.02) based on the target DP. Without precipitating the first block, heptafluorobutyl acrylate (HFBA), along with additional portions of DPIHP and $BaTiO_3$, were added into the milling jar; chain extension commenced upon milling.

Within 3 h, full conversion of HFBA was observed by ^{1}H and ^{19}F NMR spectroscopy (Figure 3.14). A monomodal GPC shift to lower retention time is observed with a narrowly dispersed PDEGEEA-*b*-PHFBA peak (M_n = 21.5 kDa, Đ = 1.04). The refractive index of the fluorine-rich diblock copolymer is lower than that of the GPC mobile phase (chloroform), leading to a characteristic negative *d*RI signal (Figure 3.13B).[68]

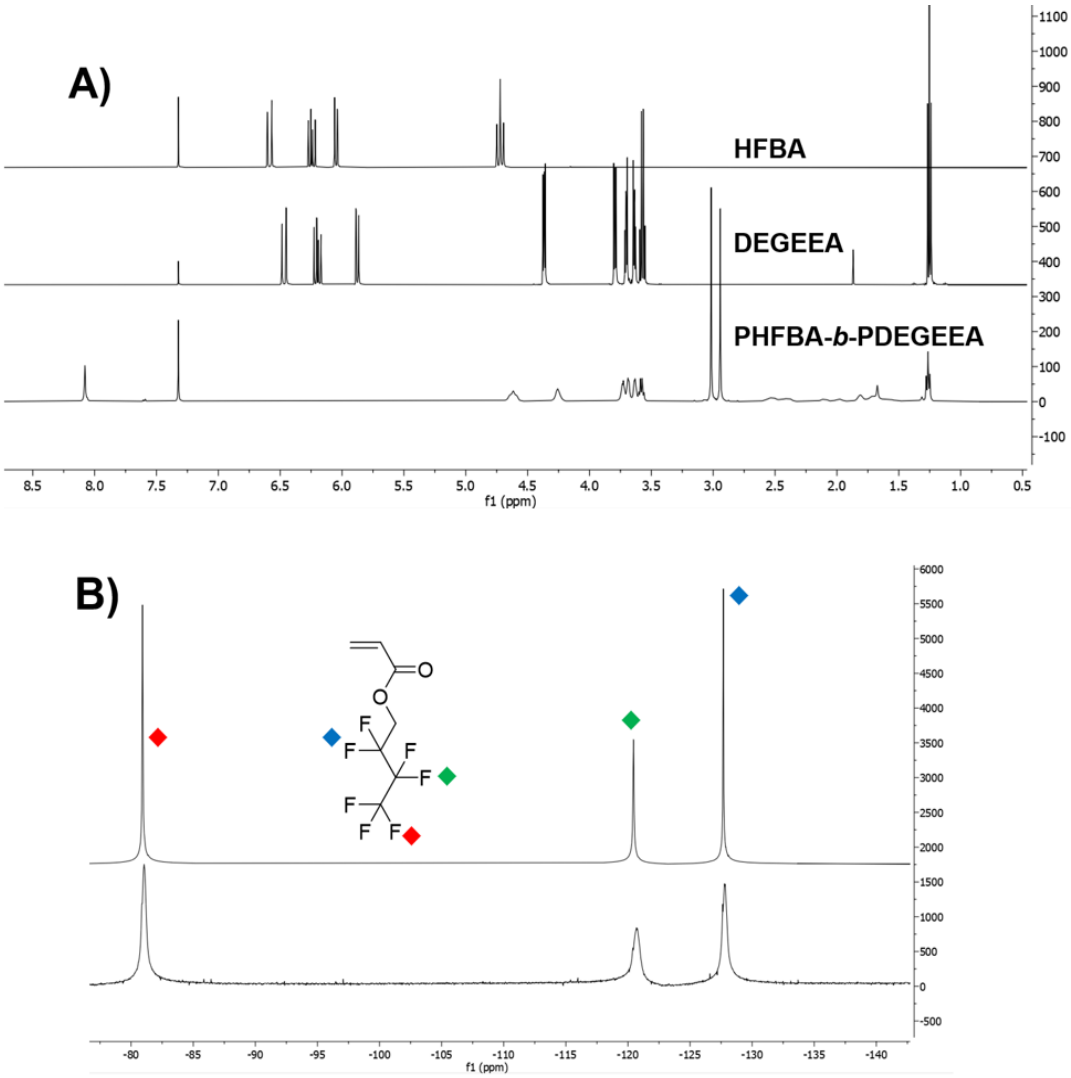

Figure 3.14. A) Stacked ^{1}H NMR spectra of DEGEEA, HFBA and crude PDEGEEA-*b*-PHFBA after mechanoredox RAFT polymerization. Full monomer conversion led to disappearance of olefinic proton peaks, and B) ^{19}F NMR spectra of HFBA monomer (top) and PDEGEEA-*b*-PHFBA (bottom). Full monomer conversion (chain extension) led to peak broadening in the bottom ^{19}F NMR spectrum.

To confirm the putative diblock copolymer structure, self-assembly of a purified bulk sample was probed using small-angle x-ray scattering (SAXS). A sharp principal peak at q = 0.025 $Å^{-1}$ (*d* = 25.1 nm) is observed (Figure 3.13C) in addition to sharp higher order reflections corresponding to integer values of q (1q, 2q, 3q, 4q, 5q); this pattern is characteristic of a lamellar morphology.[69] When an analogous SAXS measurement was carried out on a PDEGEEA-*b*-PHFBA sample embedded with $BaTiO_3$ (i.e., unpurified diblock copolymer), a single broad principal peak at q = 0.028 $Å^{-1}$ (d = 22.4 nm) is observed. The sharp peaks present in the high-q region (q > 1 $Å^{-1}$) correspond to the crystalline structure of $BaTiO_3$ (Figure 3.15). We propose that higher order reflections are not clearly visible because most of the features are dominated by strongly scattering $BaTiO_3$ nanoparticles. The formation of this mesophase material with a similar domain spacing to the purified diblock copolymer demonstrates that self- assembly can occur during ball milling. The precise polymer sequence accessed using mechanoredox RAFT is essential for productive self-assembly; SAXS of an analogous random copolymer (i.e., PDEGEEA-*r*-PHFBA) does not show any features indicative of self-assembly (Figure 3.16).

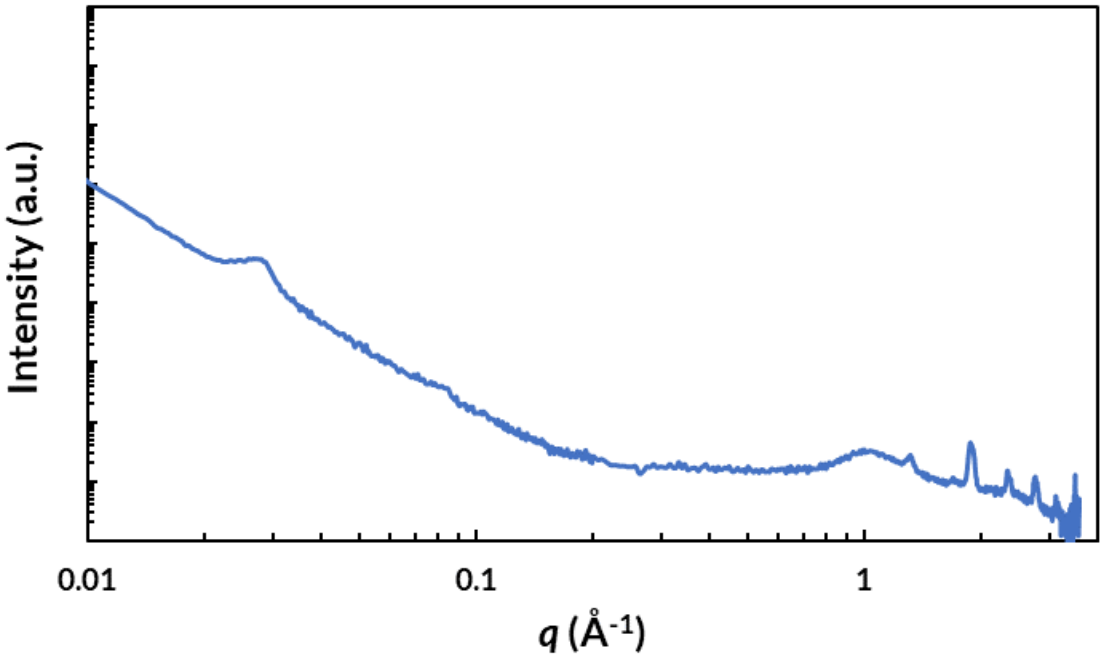

Figure 3.15. 1D SAXS curve of PDEGEEA-*b*-PHFBA with embedded $BaTiO_3$.

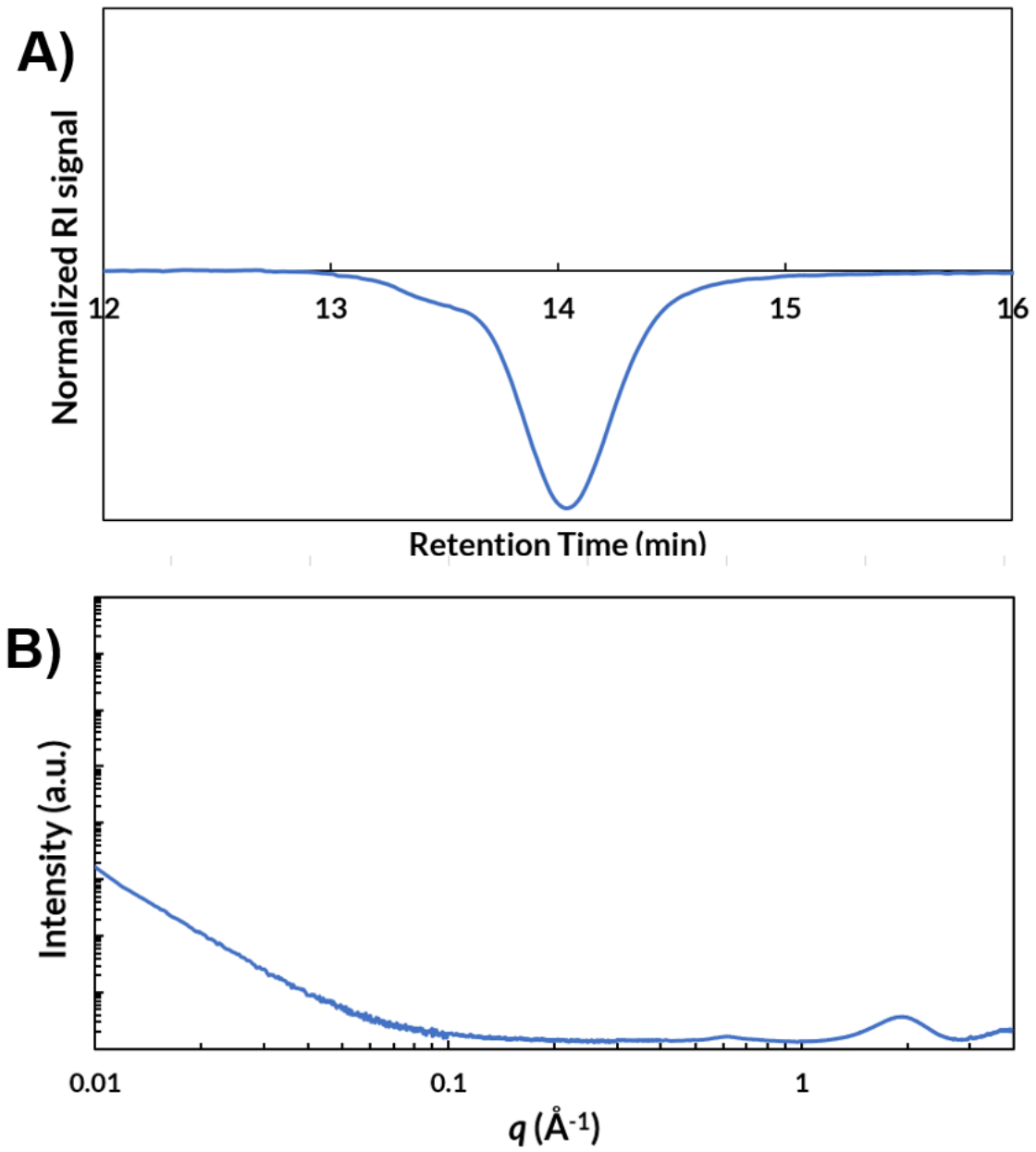

Figure 3.16. A) GPC-MALS-RI trace of PDEGEEA-*r*-PHFBA (>95% each monomer conversion). $M_{n,\,theo}$ = 24.7 kDa, $M_{n,\,GPC}$ = 26.1 kDa, Đ = 1.08. B) 1D SAXS curve of PDEGEEA-*r*-PHFBA.

Finally, thermal properties of PDEGEEA-*b*-PHFBA were studied using differential scanning calorimetry (DSC). Two separate T_gs at –50 °C and –18 °C correspond to the two separate blocks of PDEGEEA and PHFBA, respectively (Figure 3.17). These values are similar to the T_g

values of PDEGEEA and PHFBA homopolymers previously reported.[70, 71] On the other hand, DSC analysis of PDEGEEA-*rand*-PHFBA reveals a single glass transition at –35 °C (Figure 3.18). These collective bulk data unequivocally demonstrate that mechanoredox RAFT can form diblock architectures without any appreciable mechanochemical backbone degradation and/or sequence erosion.

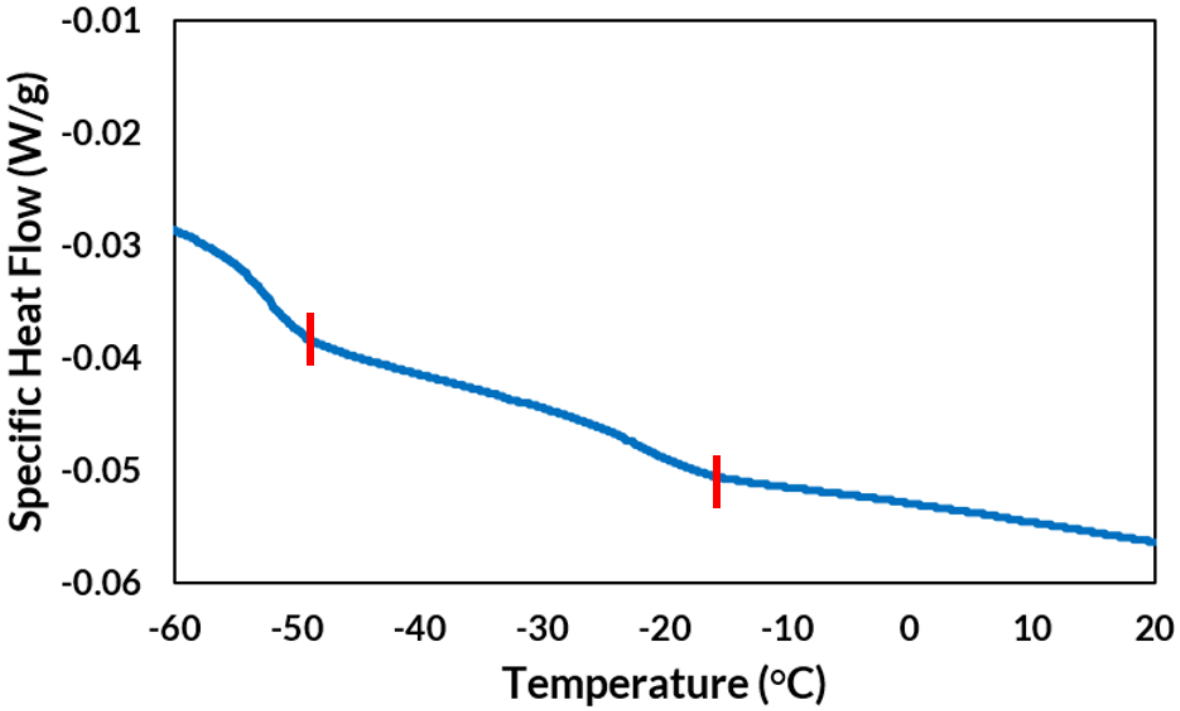

Figure 3.17. DSC trace (2nd heating) of PDEGEEA-*b*-PHFBA (3.0 mg). T_gs are observed at –50 °C and –18 °C.

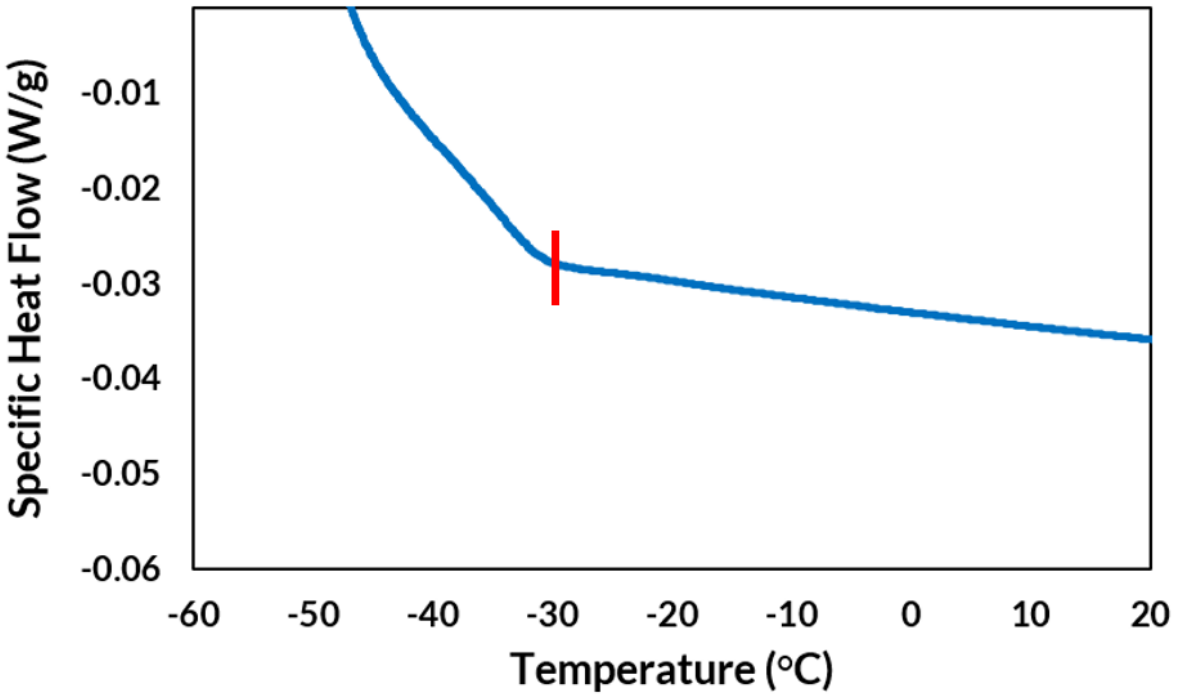

Figure 3.18. DSC trace (2nd heating) of PDEGEEA-*r*-PHFBA (3.0 mg). T_g is observed at –35 °C.

To allow for extensive self-assembly studies of the high χ polymers in solution, the synthesis of the polymers was scaled up to produce sufficient amounts of testable material. To do so, the milling jar size was increased from 1.5 mL to 5 mL, and the number of 5 mm stainless steel milling balls was increased from one to three milling balls. In addition to increasing the scale of these reactions, we also expanded the library of block ratios to demonstrate how changes in composition of high χ polymers can rapidly change the properties of the polymers. We varied the block ratios targeting from 50:25 to 50:75 ratios and achieving these blocks close to targeted DPs (Table 3.6); the various block ratios also highlight the control that is achieved via our synthetic method. Characterization was conducted using a combination of GPC MALS to calculate the M_n of the first block and ^{1}H NMR to calculate the ratio of the second block and thus determine a total molecular weight (Figures 3.19-3.24). With blocks synthesized from both short polyethylene

glycol methyl ether acrylates (DEGEEA) and long chain polyethylene glycol methyl ether acrylates (PEGMEA) and HFBA, the developed RAFT chemistry allowed for the synthesis of well-defined blocks of each monomer (Table 3.6). In particular, the PEGMEA also expanded the library of monomers we have used to include macromonomers and presents a block with expected unique self-assembly properties. The self-assembly studies were conducted external to the group with results forthcoming.

Table 3.6: Scaled up syntheses of high χ diblock copolymers.

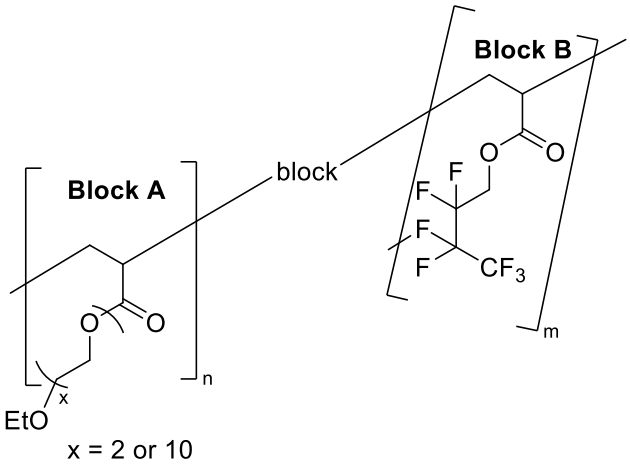

Entry[a]	B1 Monomer	B1 - Target DP	B1- Exper. DP[b]	B2 - Target DP	B2- Exper. DP[b]	Total Target M_n (kDa)	Total Exper. M_n (kDa)[c]
1	DEGEEA	50	43	50	46	22.1	19.8
2	DEGEEA	50	42	25	28	15.8	15.1
3	DEGEEA	50	44	75	74	28.5	27.1
4	PEGMEA	50	40	25	33	30.4	27.6
5	PEGMEA	50	57	50	57	36.7	41.5

Reaction condition: [a] LAG (η = 0.060 μL/mg) with DMF. [DDMAT]: [DPIHP] = 1:1. Ball mill (5 mL stainless steel jar, 3 5 mm stainless steel grinding ball, 30 Hz). 15 wt% $BaTiO_3$, reaction time - 3 h per block. [b] Block composition was determined by ^1H NMR spectroscopy. [c] M_n was determined by GPC-MALS.

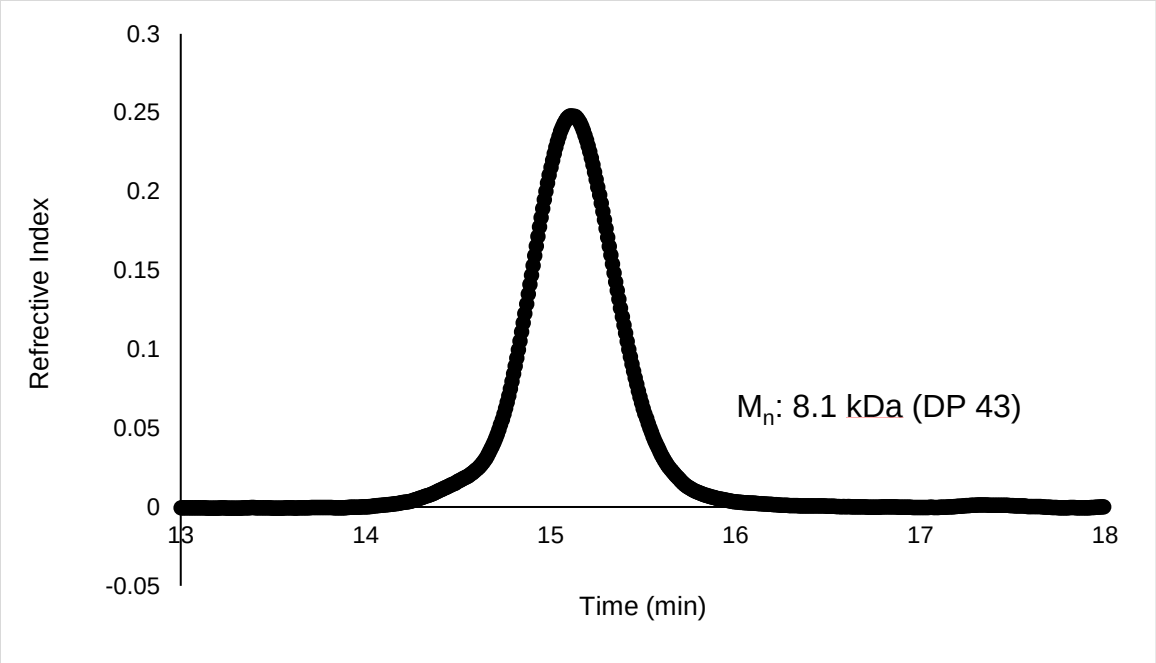

Figure 3.19. A) Representative GPC-MALS-RI trace of poly(DEGEEA) (>95%) used to calculate the with a targeted DP 50 and experimental DP 43. [a] M_n was determined by GPC-MALS. [b] Conversion was determined by ^{1}H NMR spectroscopy.

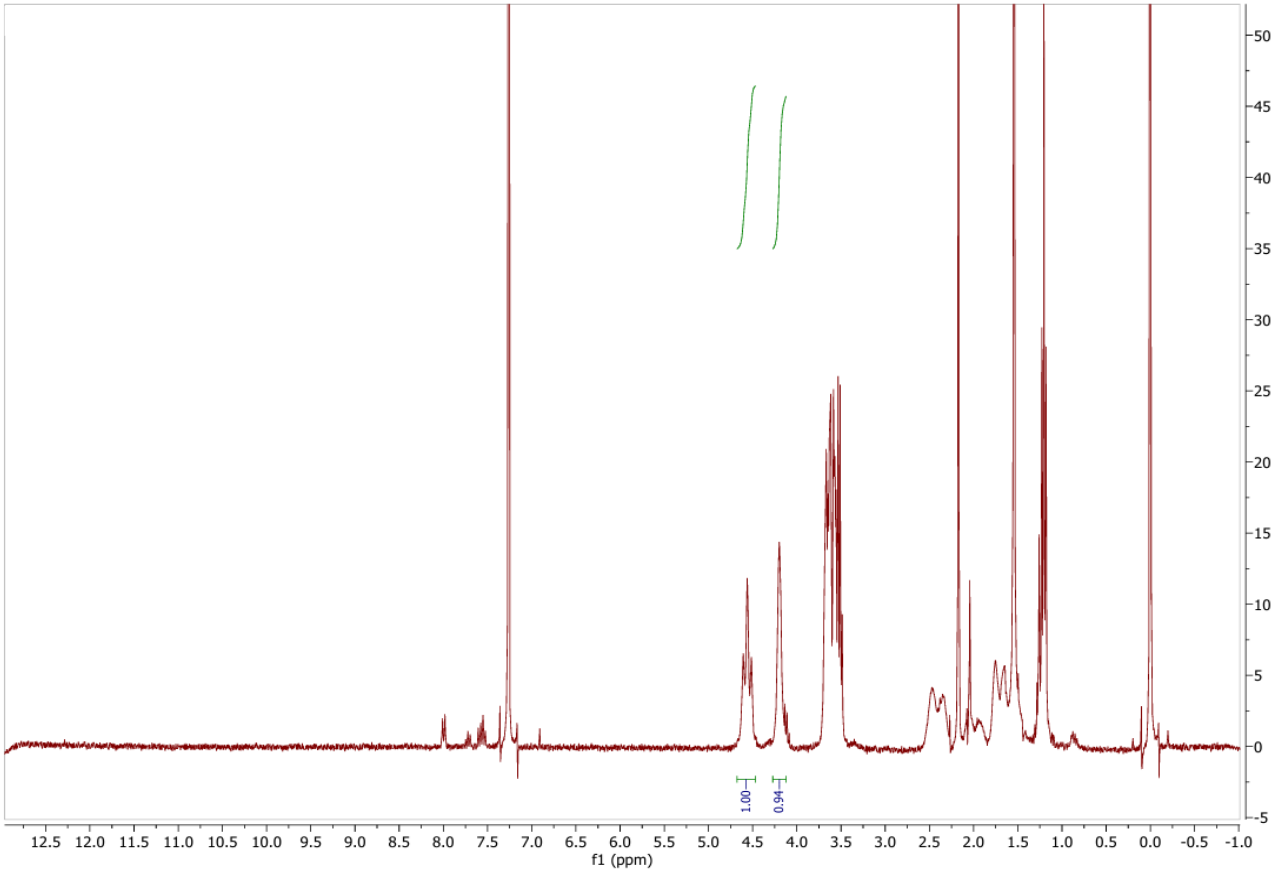

Figure 3.20. ^{1}H NMR spectra of mechanoredox RAFT of PDEGEEA-b-PHFBA used to calculate the block ratios: DEGEEA DP: 43 and HFBA DP: 46.

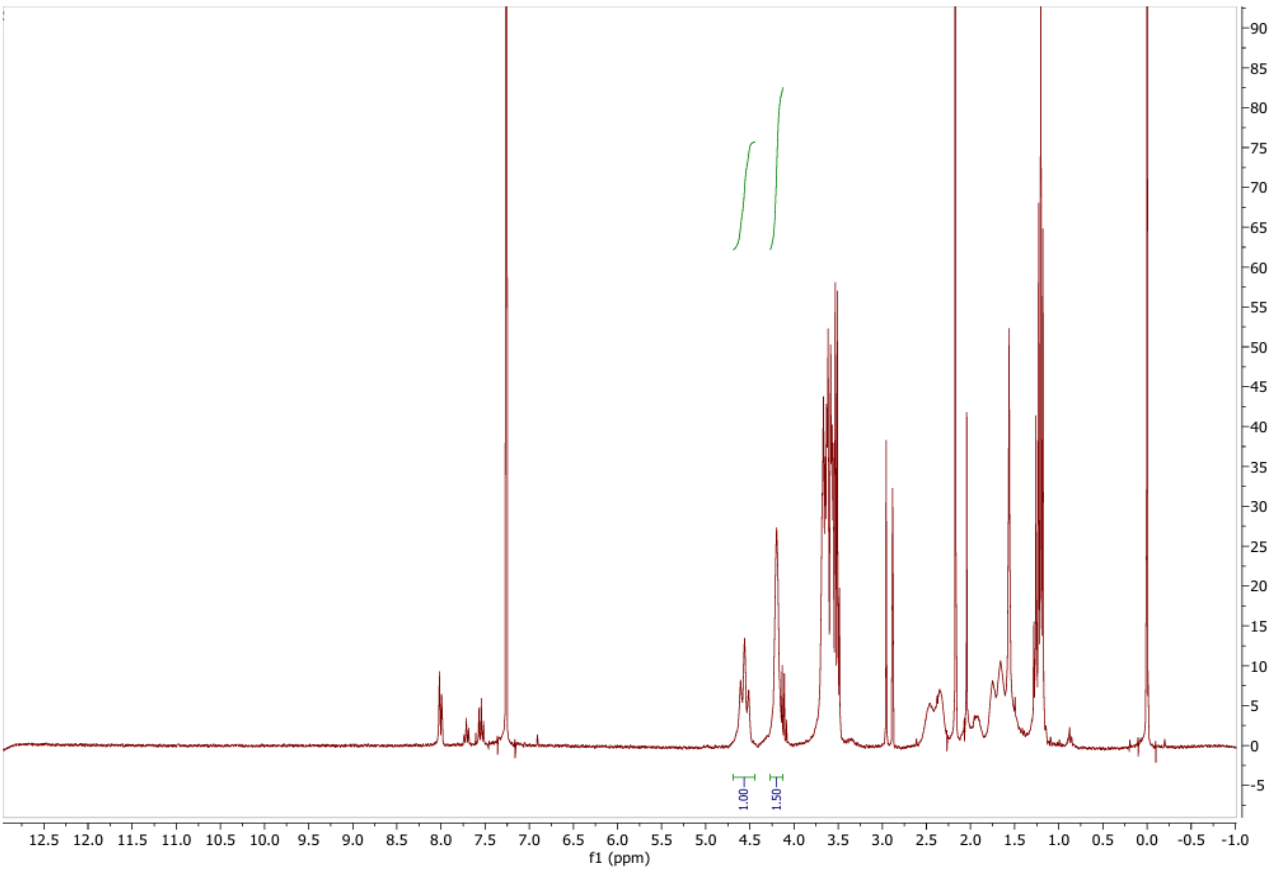

Figure 3.21. ^{1}H NMR spectra of mechanoredox RAFT of PDEGEEA-b-PHFBA used to calculate the block ratios: DEGEEA DP: 42 and HFBA DP: 28.

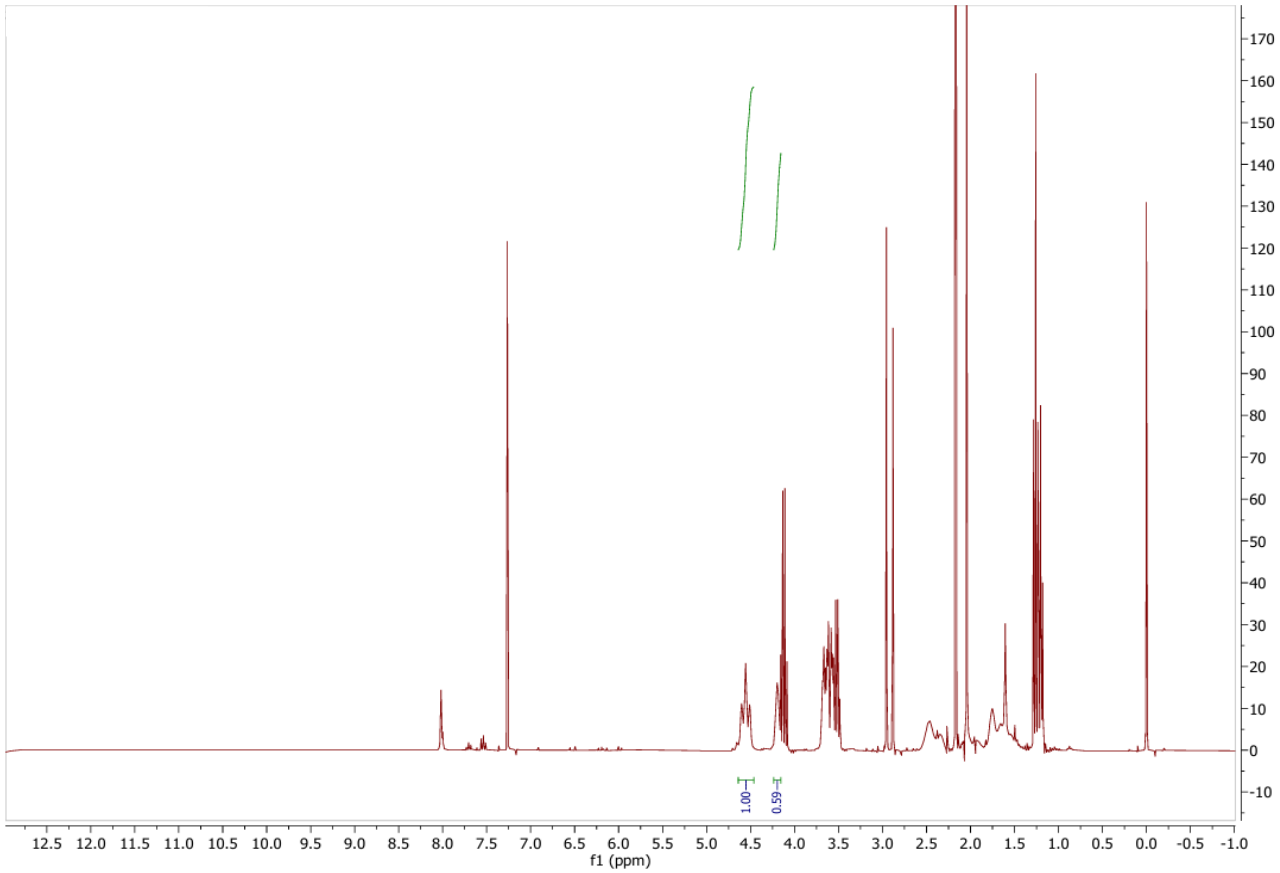

Figure 3.22. ^{1}H NMR spectra of mechanoredox RAFT of PDEGEEA-b-PHFBA used to calculate the block ratios: DEGEEA DP: 44 and HFBA DP: 74.

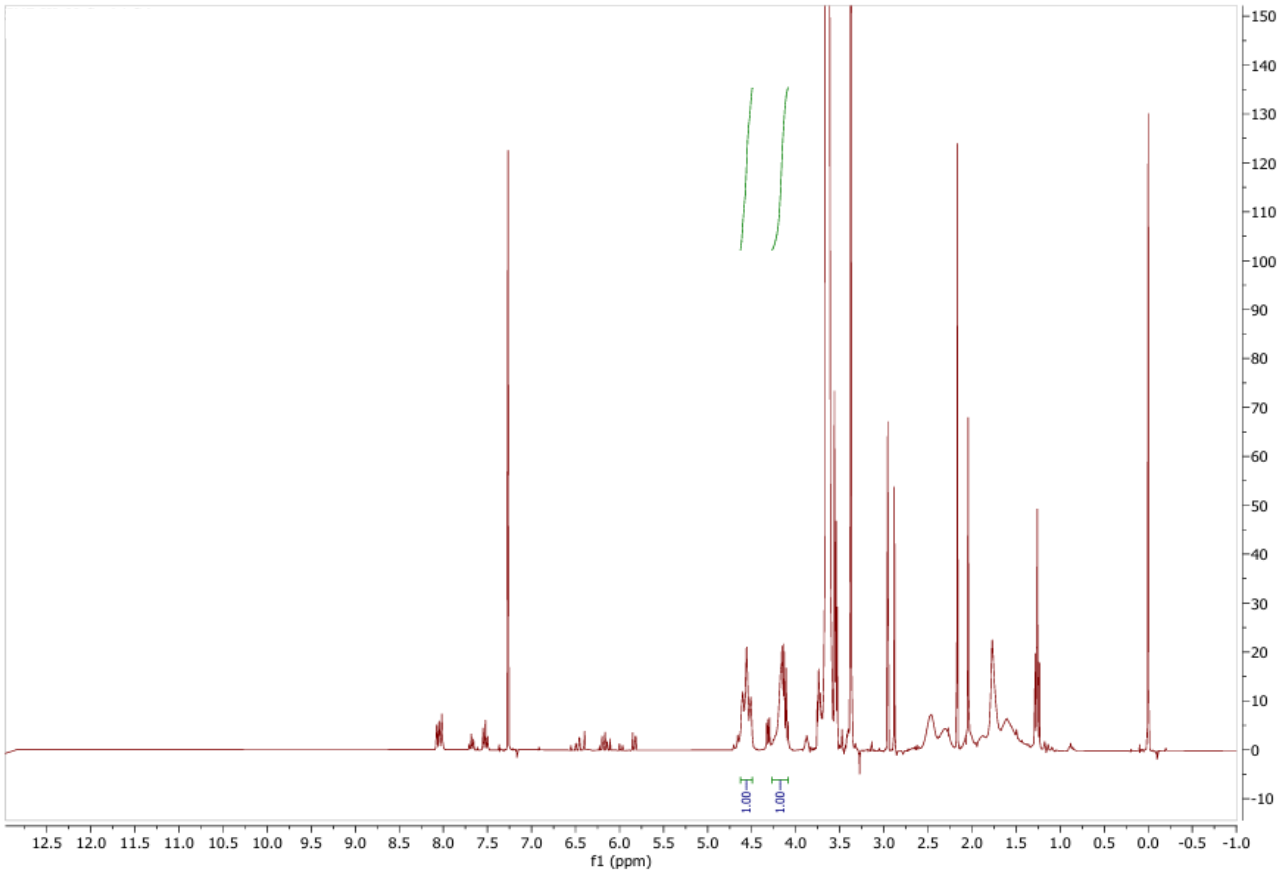

Figure 3.23. ^{1}H NMR spectra of mechanoredox RAFT of PPEGMEA-b-PHFBA used to calculate the block ratios: PEGMEA DP: 57 and HFBA DP: 57.

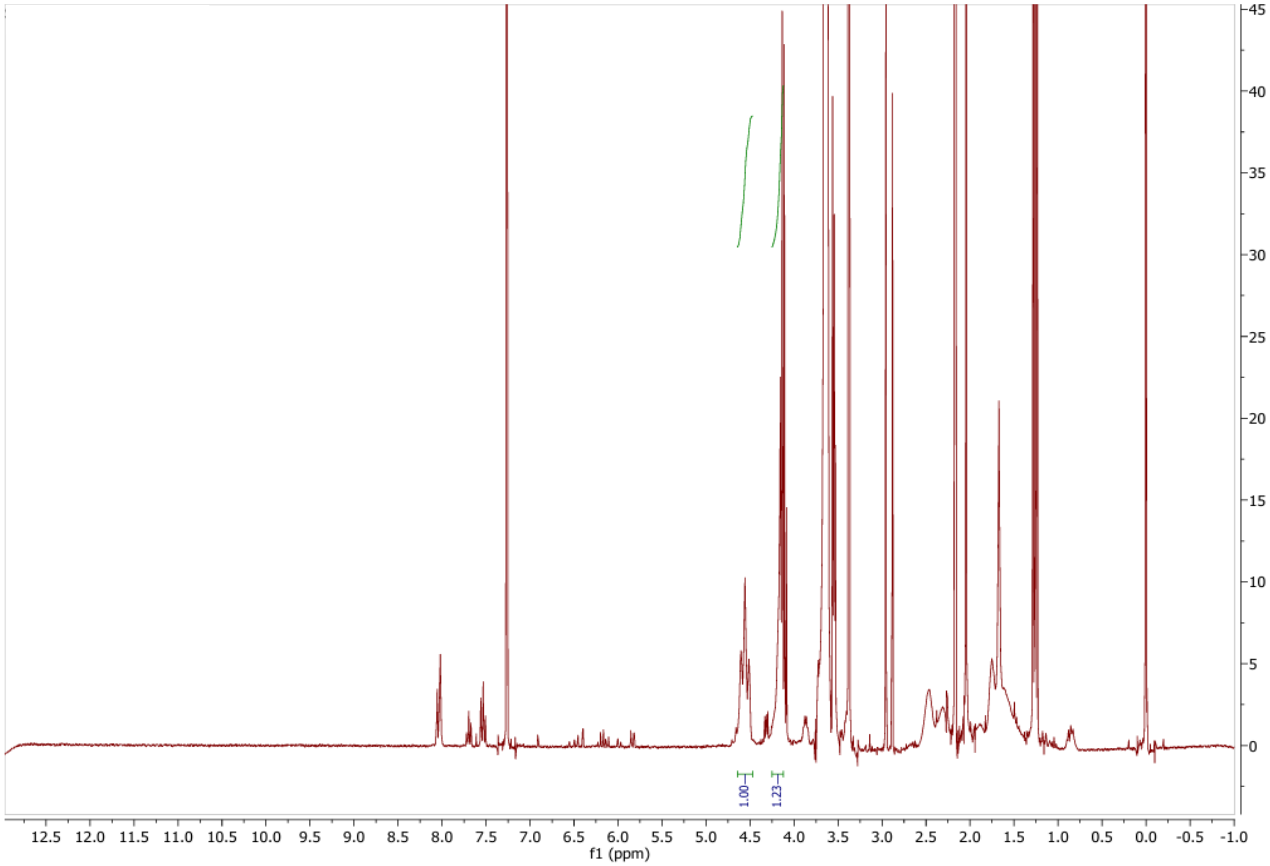

Figure 3.24. ^{1}H NMR spectra of mechanoredox RAFT of PPEGMEA-b-PHFBA used to calculate the block ratios: PEGMEA DP: 40 and HFBA DP: 33.

3.3.4 Synthesis of Triblock Copolymers with Compatible Monomers

Building upon the exciting proof of concept for using force to build block copolymers, we were inspired to conduct multiblock copolymer synthesis via mechanoredox RAFT. Initially, we investigated extending polymer growth beyond diblocks; the chain end should retain viability to allow for further chain extension. However, we wanted to confirm that we could successfully achieve additional blocks while maintaining high control of polymer chain length and dispersity.

In order to demonstrate this extension, we first polymerized a triblock copolymer, poly(BA)-co-poly(EA)-co-poly(MA). The monomers BA, EA, and MA, were selected due to their high compatibility with one another and extensively studied with mechanoredox chemistry previously,

thus making them the ideal choice for exclusively showing the desired chain end fidelity. After ball milling for 4 hours per segment, each block was analyzed by ^{1}H-NMR and GPC to quantify monomer consumption and dispersity. Each block had nearly complete monomer conversion (>95%) with low dispersity retained for each additional block (Figure 3.25, Table 3.7).

Table 3.7: Triblock copolymer synthesis.

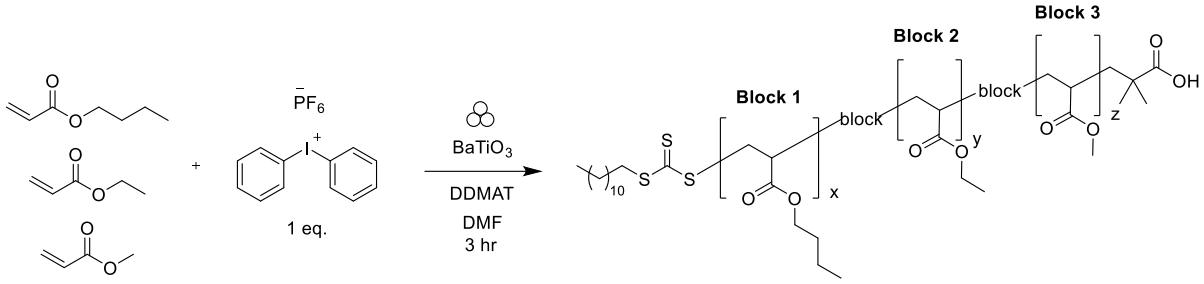

Polymer Block	Conversion (%)[a]	Đ[b]
1	>95	1.37
2	>95	1.24
3	>95	1.03

Reaction condition: [a] LAG (η = 0.060 μL/mg) with DMF. [DDMAT]: [DPIHP] = 1:1. Ball mill (1.5 mL stainless steel jar, 1 5 mm stainless steel grinding ball, 30 Hz). 15 wt% $BaTiO_3$, reaction time - 3 h per block. [b] Block composition was determined by ^{1}H NMR spectroscopy. [c] Đ was determined by GPC-MALS.

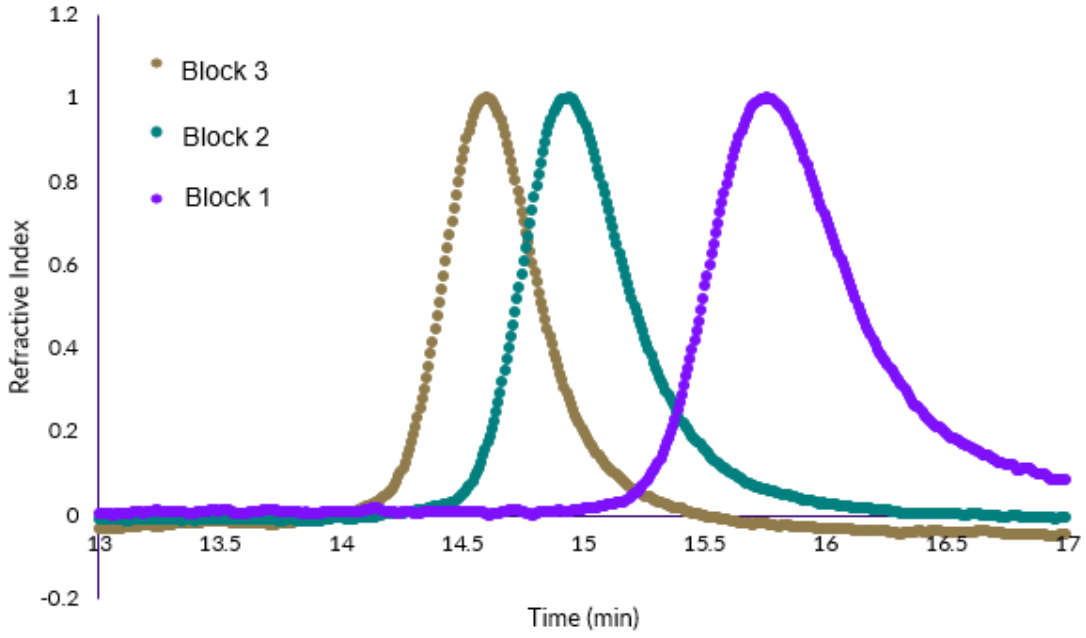

Figure 3.25. A) GPC-MALS-RI trace of poly(butyl acrylate)-co-poly(ethyl acrylate)-co-poly(methyl acrylate) (>95% each monomer conversion). [a] Đ was determined by GPC-MALS. [b] Conversion was determined by ^{1}H NMR spectroscopy.

3.4 Mechanoredox RAFT: Vortexing

In addition to ball milling, we envisioned that more readily available lab equipment (e.g., vortexer) could be used to drive mechanoredox polymerizations.[72] Reactions were carried out in a vortexer (3000 rpm) using analogous BM conditions (LAG with DMF, η = 0.060 μL/mg, 1.5 mL stainless-steel milling vial). Moderate conversion (ca. 70%) was observed with BA over 8 h when one milling ball was used. However, when two millling balls were used conversion increased to 89% in the same time period. When either DPIHP or $BaTiO_3$ was excluded from the reaction mixture, no polymerization was observed (Table 3.8). Quantitative conversion was observed with *t*BA following the same conditions. GPC analysis of PBA and P*t*BA at different target DP reveals narrow dispersity and overall good correlation between theoretical and experimental molar mass

(Table 3.9). Similar to the BM system, slow and less controlled polymerization of MMA was observed.

Table 3.8: Mechanoredox RAFT of BA (vortexer).

Entry[a]	Conditions	Conv. (%) [b]
1	Standard reaction	>95
2	Without DPIHP	<5
3	Without $BaTiO_3$	<5

Reaction conditions: [a] LAG (η = 0.060 μL/mg) with DMF. [DDMAT]: [DPIHP] = 1:1. 1.5 mL stainless steel vial, two 5 mm stainless steel grinding ball, 3000 rpm. 15 wt% $BaTiO_3$, reaction time - 8 h. [b] Conversion was determined by ^{1}H NMR spectroscopy.

Table 3.9: Mechanoredox RAFT polymerization of (meth)acrylates in a vortexer.

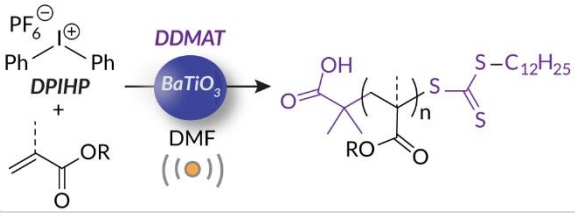

Entry[a]	Monomer	Target DP	Conversion (%) [c]	$M_{n,\,theo}$ (kDa)	$M_{n,\,GPC}$ (kDa) [d]	Đ[d]
1	BA	100	89	11.7	11.1	1.01
2[b]	BA	100	71	9.4	8.2	1.02
3	tBA	100	>95	13.2	10.4	1.05
4	MMA	100	45	4.7	35.1	1.38
5	BA	300	83	32.2	27.8	1.01
6	tBA	300	>95	37.3	29.0	1.12

Reaction condition: [a] LAG (η = 0.060 μL/mg) with DMF. [DDMAT]: [DPIHP] = 1:1. Vortexer (1.5 mL stainless steel vial, two 5 mm stainless steel grinding balls, 3000 rpm). 15 wt% $BaTiO_3$, reaction time - 8 h. [b] One 5 mm stainless steel grinding balls [c] Conversion was determined by ^{1}H NMR spectroscopy. [d] M_n and Đ were determined by GPC-MALS.

A simple kinetic analysis of BA polymerization (target DP = 100) using optimized conditions was carried out in a vortexer and monitored by ^{1}H NMR spectroscopy and GPC-MALS. These data reveal a slower kinetic profile compared to the BM system (Figure 3.26). I attribute these lower reaction rates to weaker shear forces and less efficient mixing compared to a ball mill system. The longer reaction times are complemented by decreased energy consumption relative to BM (Figure 3.7). Nonetheless, a narrow dispersity is maintained at all time points indicating an efficient RAFT process (Figure 3.27). Despite extended reaction times, I anticipate that these findings will make mechanoredox RAFT a more accessible process to a broader scientific audience. Overall, both vortexting and ball milling provide more energy efficient inputs to drive RAFT polymerization compared to traditional thermal solution-state processes (Figure 3.7).

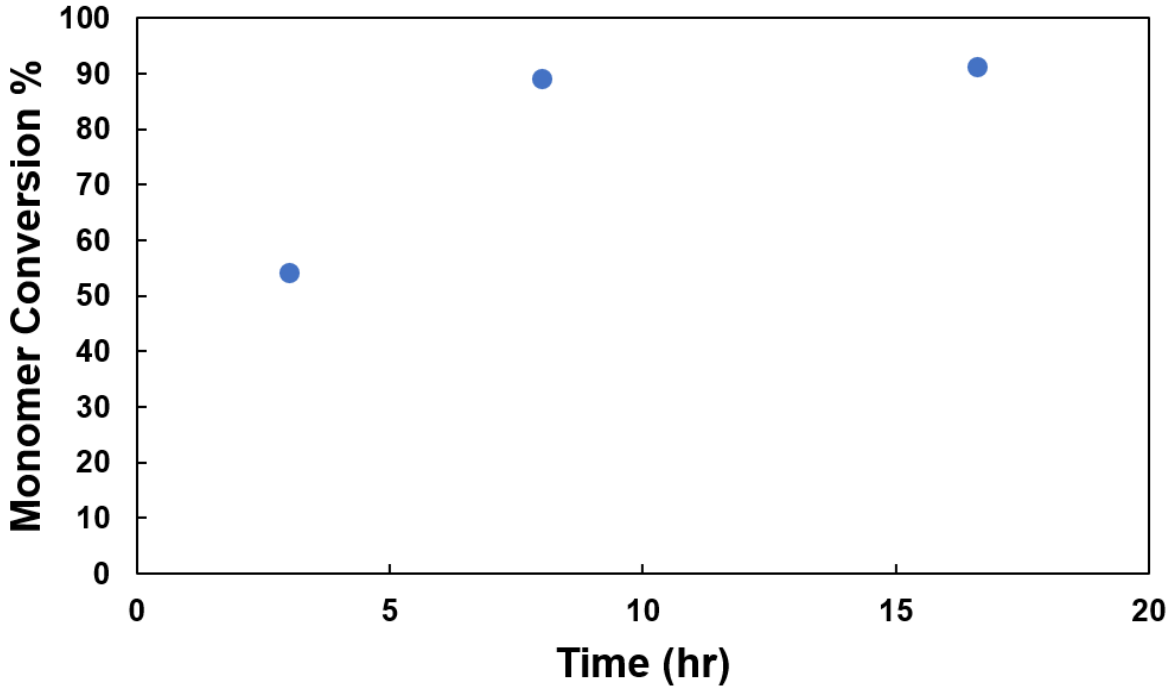

Figure 3.26. Kinetic data for mechanoredox RAFT polymerization of BA (target DP = 100) in a vortexer.

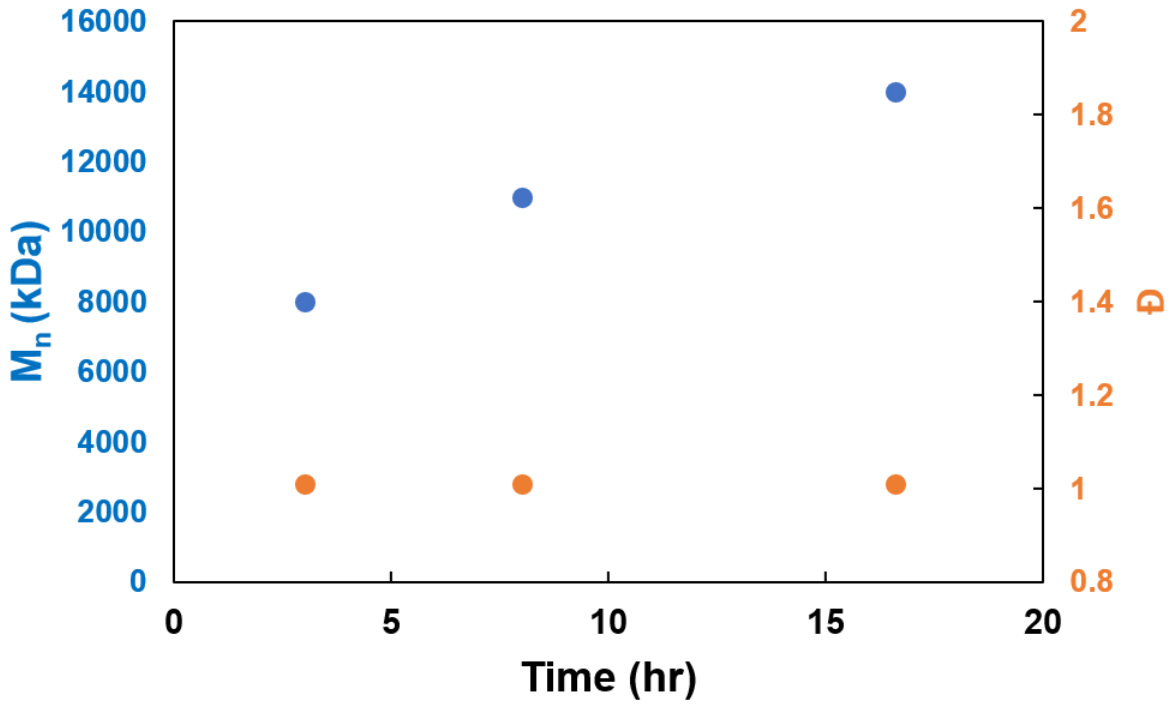

Figure 3.27. Kinetic data for mechanoredox RAFT polymerization of BA (target DP = 100) in a vortexer showing the kinetic profile with respect to dispersity and molar mass evolution.

3.5 Mechanistic Study of Mechanoredox RAFT

We proposed a mechanism in which a phenyl radical is formed from DPIHP upon mechanoredox reduction; therefore, we conducted radical trapping experiments to support this mechanistic hypothesis (Scheme 3.1A). DPIHP was ball milled (3 h) in the presence of $BaTiO_3$ and an H-atom donor, cyclohexane thiol (CySH).[73] Reduction of DPIHP, homolytic cleavage of a C-I bond, and subsequent H-atom transfer would generate a 1:1 mixture of benzene and iodobenzene; these species were indeed identified by GC-MS and quantified by ^{1}H NMR spectroscopy (yields: 30% benzene and 45% iodobenzene at 50% DPIHP consumption) (Figures 3.28-3.30). When $BaTiO_3$ is omitted from the reaction mixture, neither benzene nor iodobenzene were observed (Figure 3.31). These results confirm the importance of mechanoredox processes for effective radical initiation (Scheme 3.1B).

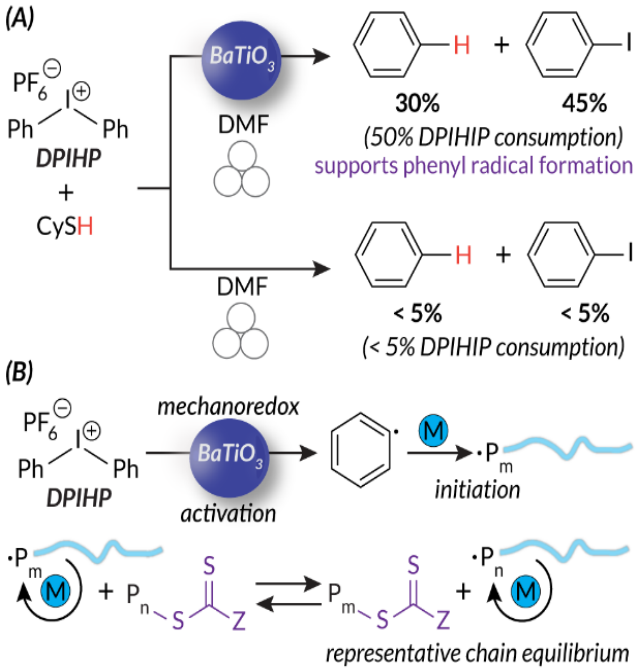

Scheme 3.1. A) Mechanistic H-atom transfer experiments supporting the formation of phenyl radicals in mechanoredox RAFT initiation. Ball milling experiments (30 Hz) were run for 3 h, B) Abbreviated RAFT mechanism.

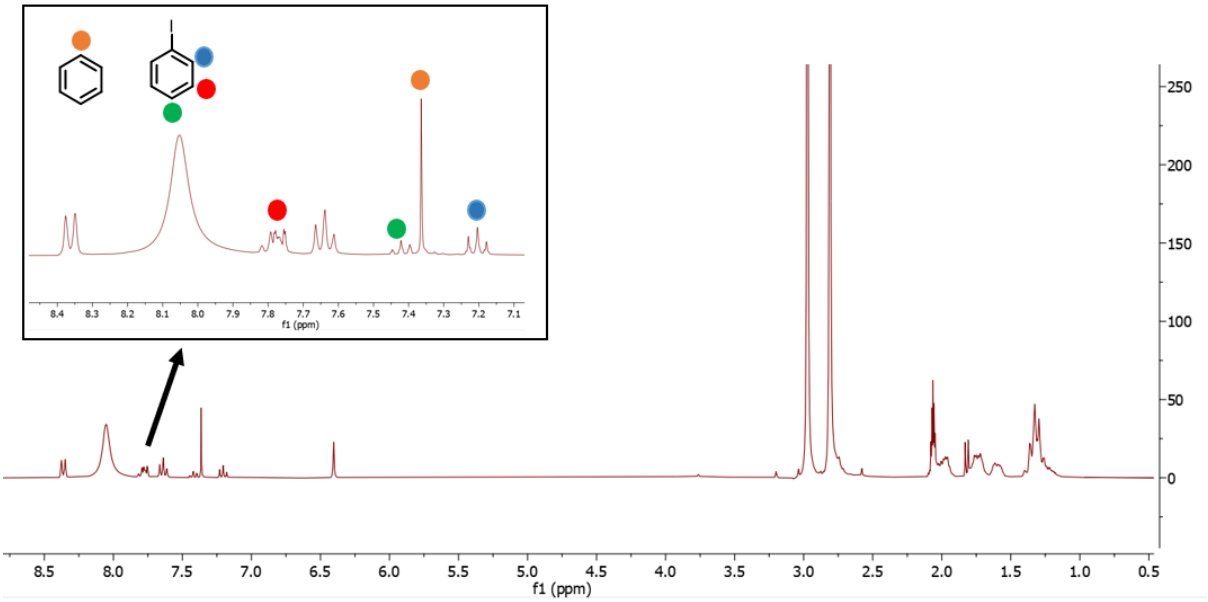

Figure 3.28. Crude ^{1}H NMR spectrum of radical trapping experiments in presence of $BaTiO_3$

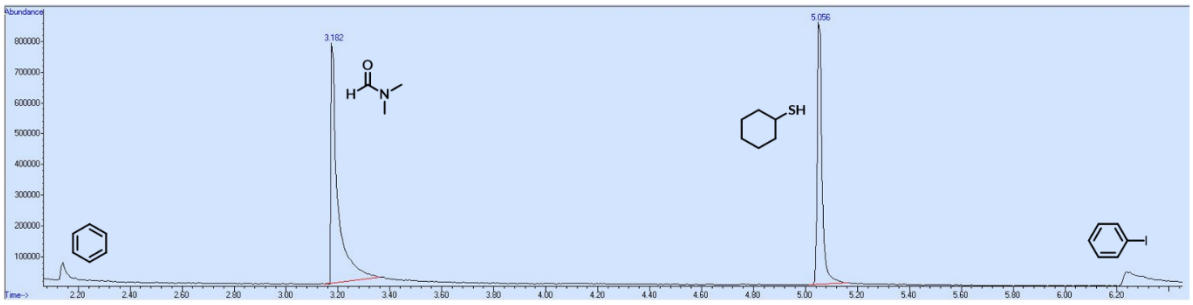

Figure 3.29. Gas chromatograph trace of crude radical trapping experiment. Benzene and iodobenzene are detected by subsequent mass spectrometry analysis (see Figure 3.30).

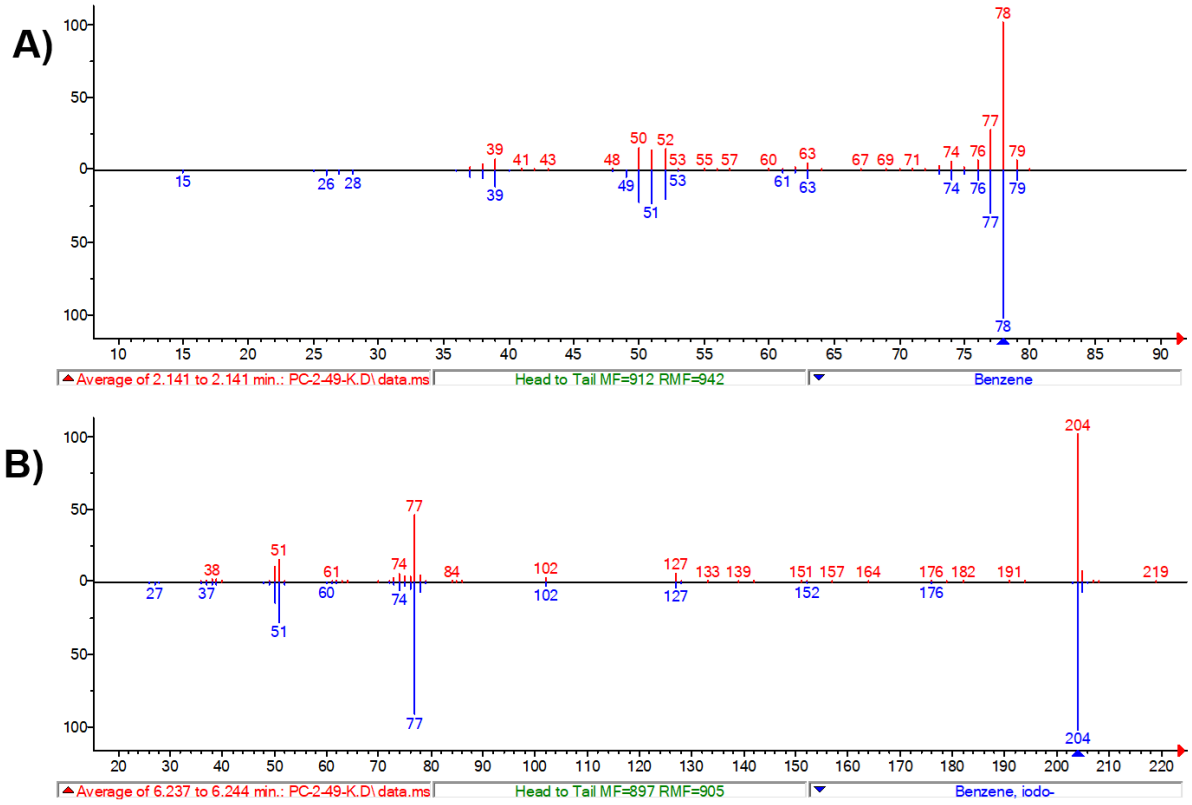

Figure 3.30. Confirmation of A) benzene and B) iodobenzene by mass spectrometry. Retention times of selected regions refer to the GC trace in Figure 3.29.

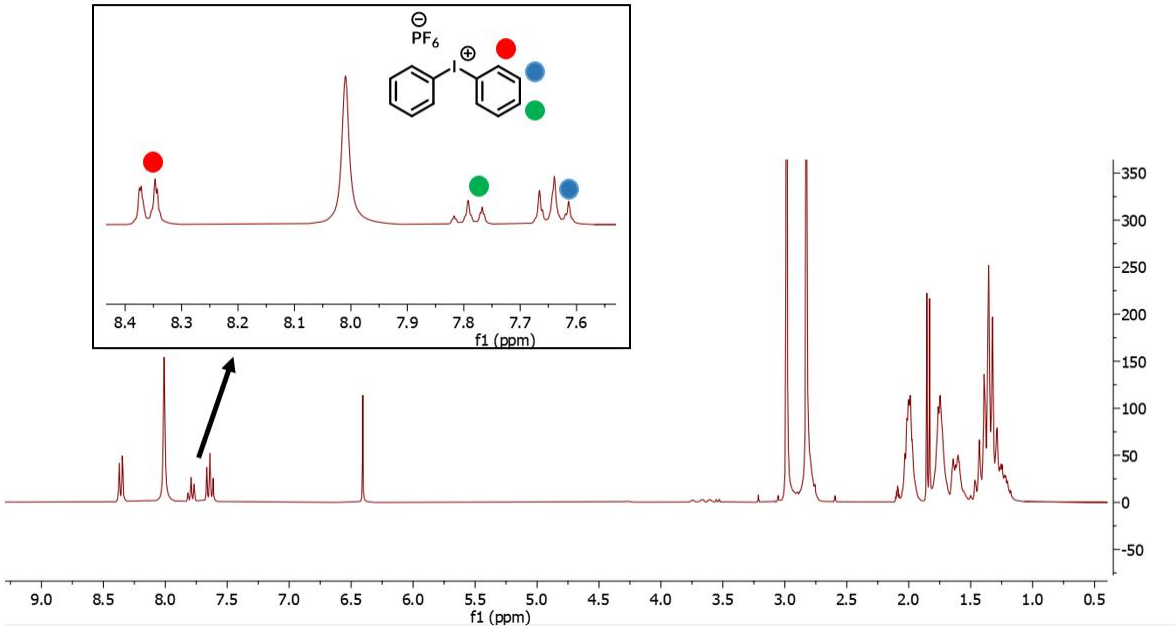

Figure 3.31. Crude ^{1}H NMR spectrum of radical trapping experiments in the absence of $BaTiO_3$.

To further probe the generation of phenyl radicals and subsequent initiation of RAFT processes, a low molar mass PBA sample synthesized in a ball mill via mechanoredox RAFT was analyzed by high resolution matrix assisted laser desorption/ionization time of flight mass spectrometry (HR-MALDI-TOF-MS). As expected, the MALDI-MS data reveal a main peak series that is spaced by the mass of BA monomer (128.17 g/mol) (Figure 3.32). The predicted mass of PBA (DP = 12) matches well with observed sodium-adduct (*m/z* = 1925.09 g/mol) and potassium-adduct (*m/z* = 1941.04) masses for a typical RAFT polymer with CTA-derived chain ends. Importantly, a minor peak series is observed that is derived from chain-chain coupling of phenyl radical initiated (i.e., from mechanoredox initiation) polymers with RAFT initiated polymers (*m/z* = 1958.04 g/mol) (Figure 3.32). Collectively, the MALDI-MS data confirm an operative RAFT mechanism that is reliant on mechnoredox phenyl radical initiation.

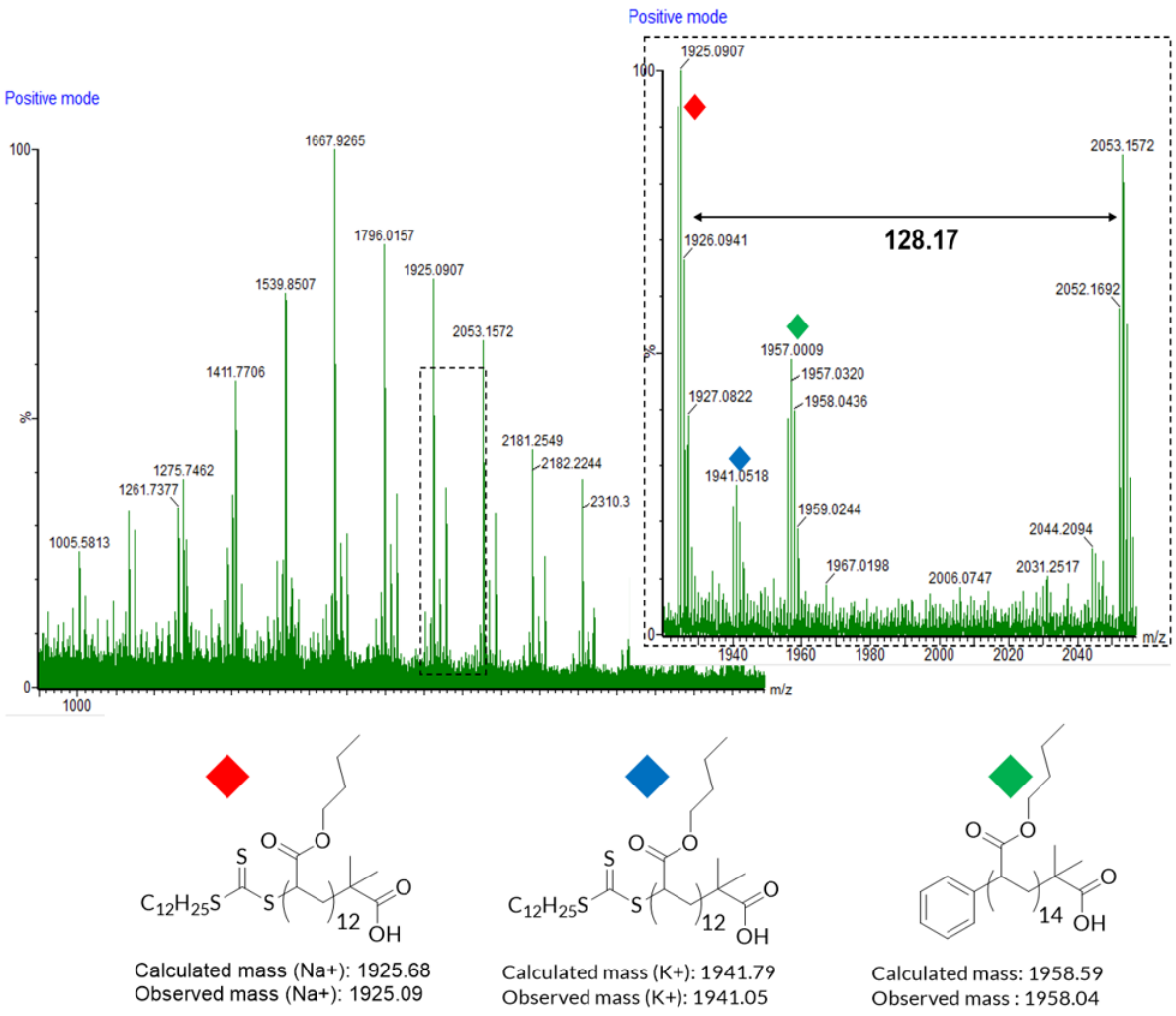

Figure 3.32. HR-MALDI-TOF-MS of PBA synthesized via mechanoredox RAFT polymerization in a ball mill.

3.6 Summary

In summary, an energy-efficient RAFT polymerization process of (meth)acrylates based on mechanoredox catalysis with $BaTiO_3$ was developed. The versatility of this developed system was shown by the successful syntheses of semifluorinated diblock copolymers and telechelic polymers at different ratios and scales. In addition, the ability to make triblock polymers in a one pot system is also demonstrated. Mechanistic studies support that DPIHP reduction under mechanoredox

conditions initiate subsequent RAFT polymerization processes. The use of complementary mechanical stimuli, minimal reaction solvent, and a widely used RAFT agent makes this work particularly significant we continue to sustainably develop complex macromolecules with otherwise synthetically challenging chemical architectures, in addition to force-responsive soft materials and polymeric composites.

3.7 Experimental

3.7.1 Materials

All chemicals were obtained from commercial sources and used as received unless otherwise stated. *Tert*-butyl acrylate (*t*BA), butyl acrylate (BA), methyl acrylate (MA), methyl methacrylate (MMA), and di(ethylene glycol) ethyl ether acrylate (DEGEEA) were purchased from Tokyo Chemical Industry (TCI). 2,2,3,3,4,4,4-Heptafluorobutyl acrylate (HFBA) was purchased from Oakwood Chemical. All acrylate monomers were passed through basic alumina before use. Diphenyl iodonium hexafluorophosphate (DPIHP) was purchased from TCI. Cubic $BaTiO_3$ nanoparticles (<100 nm size) were purchased from US Research Nanomaterials. All ball milling (BM) experiments were carried out in a Retsch Mixer Mill (MM 400) ball mill instrument in 1.5 mL stainless steel screw-top jars (Verder Scientific #014620230) equipped with a single 5 mm stainless steel grinding ball unless otherwise noted. A SPEX 8000D mixer mill was used as noted. All ultrasound reactions were performed in 4 mL vials (ChemGlass #CG-4904-05) unless otherwise stated. A Branson Ultrasonic Cleaner (Model 1510R-MT, 70 W, 40 kHz) equipped with an immersed coil of copper tubing connected to a ThermoScientific recirculating chiller for temperature control was used for all the ultrasonic reactions. All vortexing experiments were

carried out in an IKA MS3 digital vortexer in home-made stainless-steel screw top vials (see Figure 3.33 for photographs). Energy consumption readings were measured using a Suraielec Watt Meter.

Figure 3.33. Photographs of stainless-steel screw top vial used for vortexing mechanoredox RAFT studies.

Unless otherwise noted, reaction solvents, dimethylformamide (DMF), dimethylacetamide (DMAc), dimethylsulfoxide (DMSO), toluene, and acetonitrile were sourced from commercially available sources and used without further purification.

All the acrylate monomers used in glovebox experiments (experiments set up and sealed in an inert environment) were first dried over molecular sieves and then degassed via freeze-pump-thaw. Anhydrous DMF and DMSO used in the glovebox experiments were obtained from a J.C. Meyer solvent purification system.[74]

3.7.2 Characterization

All ^{1}H nuclear magnetic resonance (^{1}H NMR) spectra were obtained on a Bruker AVANCE NMR spectrometer at 25 °C at either 300 MHz or 500 MHz. ^{19}F NMR spectra were obtained on a Bruker AVANCE spectrometer at 25 °C at 470 MHz. NMR samples were prepared in chloroform-*d* ($CDCl_3$) or acetone-d_6. ^{1}H NMR spectra are referenced to Me_4Si (TMS chemical shift, δ, at 0.00 ppm) or residual proteo-solvent. ^{19}F NMR spectra are referenced to CCl_2F_2 (CCl_2F_2 chemical shift, δ, at 0.00 ppm). All NMR spectra were processed and analyzed on Bruker TopSpin or MestreNova NMR processing software. Chemical shifts are represented in parts per million (ppm). Multiplicity is presented as s = singlet, d = doublet, t = triplet, q = quartet, m = multiplet.

To calculate monomer conversion during polymerization reactions, integration values of the protons of the side chains from monomers (and their corresponding polymers) were used as internal standards and then compared to the decreasing integration values of the olefinic (ca. 5.5 – 6.5 ppm) protons of each monomer. The integration values of the side chains of each monomer in block polymers were compared to determine the block ratios.

Gel permeation chromatography (GPC) data were obtained on an Agilent 1260 HPLC equipped with a Wyatt 8-angle DAWN NEON light-scattering detector, ViscoStar NEON viscometer, and Optilab NEON refractive index detector. GPC samples were analyzed at a flow rate of 1 mL/min in chloroform stabilized with 0.5%-1.0% ethanol through two Agilent PLgel MIXED-C columns at 35 °C. GPC samples were prepared at ca. 2 – 5 mg/mL in chloroform and were filtered through 0.2 μm PTFE filters before analysis. The following dn/dc values were used; they were measured by the 100% mass recovery method using Wyatt Astra 7.3 software (in

mg/L): P*t*BA: 0.024; PBA: 0.033; PMMA: 0.072; PDEGEEA: 0.057; P*t*BA-*b*-BA: 0.020; PDEGEEA-*b*-HFBA: –0.056; PDEGEEA-*r*-HFBA: –0.045.

Matrix assisted laser desorption/ionization time of flight (MALDI-ToF) mass spectroscopy was performed on a Waters Synapt – G2 HDX QTQ (MassLynx 4.1) mass spectrometer. All the experiments were performed in positive ion mode. The matrix (trans-2-[3-(4-tert-butylphenyl)-2-methyl-2-propenylidene] malononitrile) and analyte were dissolved in THF at a concentration of 40 mg mL^{-1} and 10 mg mL^{-1} respectively and mixed in a volume ratio of 10:1. From that solution, 0.5 µL was spotted on a steel target plate. Solvent was allowed to evaporate before analysis.

Gas chromatography/mass spectrometry data were collected on an Agilent 6890 gas chromatograph coupled to an Agilent 5973 quadrupole mass spectrometer (electron impact ionization).

Glass transition temperatures (T_g) were performed on a TA instrument Discovery DSC 2500. The data were obtained in a heat−cool−heat cycle ranging from −80 °C to 200 °C with a heating rate of 10 °C per minute. The data were plotted from the second heating cycle and the glass transition temperature was determined from the inflection point.

Small-angle X-ray scattering (SAXS) experiments were carried out in a Xenocs Xeuss 3.0 with a Cu source (1.54 Angstrom) and a Dectris Eiger2 1M detector. The measurements were taken at sample to detector distances configured at ESAXS (1750 mm), SAXS (900 mm), MAXS (300 mm), WAXS (55 mm) with acquisition time of 300 s. The samples were prepared by spreading dried polymer paste in the circular area of 5 mm diameter o-ring between two Kapton films. The sample was placed in the “Powder and Gel” sample holder. Samples without embedded $BaTiO_3$ were initially centrifuged following addition of DMF (0.2 g of sample in 5 mL of DMF)

to separate the nanoparticles. The supernatant containing polymer was precipitated in 100 mL cold methanol solution (15 v/v% in water). The collected data was reduced using the software XSACT from Xenocs.

3.7.3 Synthetic and Experimental Procedures

Synthesis of 2-(dodecylthiocarbonothioylthio)-2-methylpropionic acid (DDMAT):

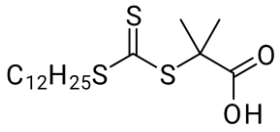

The synthesis of **ATTC** was carried out following the procedure from the literature.[1] In a 250 mL round bottom flask, a suspension of K_3PO_4 (4.2 g, 20 mmol) in acetone (60 mL) 1-dodecanthiol (4.0 g, 20 mmol) was added. The resulting mixture was stirred in an ice bath for 30 minutes. After 30 minutes, CS_2 (3.3 mL, 54 mmol) was added dropwise over 15 minutes, resulting in a yellow suspension, Then, 2-bromo-2-methylpropionic acid (3.0 g, 18 mmol) was added into the reaction mixture over the period of 20 minutes, while maintaining the internal temperature below 15 °C. After that, the reaction was left stirring overnight at room temperature. After the completion of the reaction, 50 mL dichloromethane was added and the reaction was neutralized by adding 1.0 M aq. HCl (50 mL). The resulting organic layer was washed with water (2 x 50 mL) and brine (1 x 50 mL), then dried over Na_2SO_4 and concentrated under vacuum. Finally, the crude product was recrystallized from hexane to yield yellowish solid **DDMAT** (2.5 g, 40%). The purity of the product was confirmed by ^{1}H NMR spectroscopy.

^{1}H NMR (300 MHz, $CDCl_3$): δ(ppm) 0.90 (t, 3H, J = 7.0 Hz), 1.20–1.50 (m, 18H), 1.60–1.85 (m, 8H), 3.25 (t, 2H, J = 7.0 Hz), 11.0 (s, 1H)

Synthesis of S, S′-Bis (R, R′-dimethyl-R′′-acetic acid)-trithiocarbonate (ATTC):

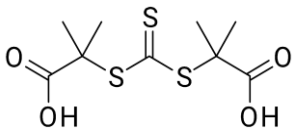

The synthesis of **ATTC** was carried out following the procedure from the literature.[2] In a 250 mL round bottom flask, acetone (5.7 g, 0.099 mol), chloroform (12 g, 0.0090 mol), and hexanes (13 mL) were mixed together and cooled in an ice bath. Into that solution, *tetra*–butyl ammonium sulfate (0.26 g, 0.00045 mmol) was added, and the resulting mixture was stirred in an ice bath for 30 minutes. After 30 minutes, carbon disulfide (3.0 g, 0.040 mol) was added dropwise over a 15 minutes time period. Then sodium hydroxide solution (22 g in 50 mL water) was added into the reaction mixture over the period of 30 minutes, while maintaining the internal temperature below 15 °C. After that, the reaction was left stirring overnight at room temperature. After the completion of the reaction, 100 mL of water was added into the mixture to dissolve the precipitate. The reaction mixture was chilled in an ice bath, and concentrated HCl was added until pH = 2 was reached. The reaction mixture was stirred for 15 minutes at a pH of 2. The reaction mixture was filtered and washed with water and dried in vacuum to yield a pale-yellow solid product. Finally, the crude product was suspended in a 4:1 mixture of toluene:acetone (40 mL:10 mL) and stirred for 30 minutes. The resulting yellow precipitate was filtered and dried under vacuum to obtain pure **ATTC** product in (3.3 g, 29%). The purity of the product was confirmed by ^{1}H NMR spectroscopy.

^{1}H NMR (300 MHz, $CDCl_3$): δ(ppm) 1.59 (s, 12H), 12.91 (s, 2H).

Synthesis of bi-functional DDMAT (biDDMAT):

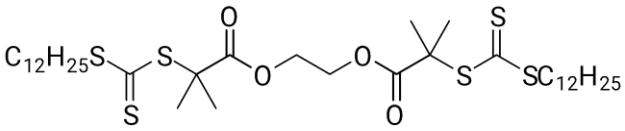

Synthesis of **biDDMAT** was carried out following the procedure from literature.[3] In a round bottom flask (solution A), ethylene glycol (0.25 g, 4.0 mmol) and dicyclohexylcarbodiimide (DCC) (2.3 g, 11 mmol) were mixed with anhydrous chloroform (20 mL). Solution B was prepared as a solution mixture of **DDMAT** (3.8 g, 10 mmol) and 4-dimethylaminopyridine (DMAP) (0.25 g, 2.0 mmol) in anhydrous chloroform (20 mL). Solution A was chilled to X temp and solution B was added dropwise under N_2 atmosphere. The reaction was stirred overnight at room temperature. After the completion of the reaction, the precipitated urea byproduct was removed by filtration and the resulting filtrate was washed with water (2 x 20 mL) and brine (2 x 20 mL). Then, the combined organic layers were dried over $MgSO_4$ and concentrated under vacuum. The crude product was purified by silica column chromatography (dichloromethane/hexane = 3:1) (2.0 g, 26%). The purity of the product was confirmed by ^{1}H NMR spectroscopy.

^{1}H NMR (300 MHz, $CDCl_3$): δ(ppm) 0.9 (t, 3H, *J* = 6.9 Hz), 1.20-1.35 (m, 18H), 1.60-1.72 (m, 8H), 3.25 (t, 2H, *J* = 7.3 Hz), 4.30 (s, 2H).

General procedure for mechanoredox RAFT in an ultrasonication bath:

In a typical experiment, DDMAT (0.014 g, 0.039 mmol, 1 equiv), DPIHP (0.017 g, 0.039 mmol, 1 equiv) and dimethylformamide (0.50 g) were loaded into a 4 mL glass vial and mixed until all **DDMAT** and DPIHP were fully dissolved in solvent. Then, *tert*-butyl acrylate (0.50 g, 3.9 mmol, 100 equiv) was added into that solution, followed by the addition of $BaTiO_3$ nanoparticles (0.072 g, 7 wt%). Finally, the reaction vial was capped with a rubber septum (Sigma

#Z167258) and sealed with electrical tape. The solution mixture was then degassed by sparging with N_2 for 40 minutes. After sparging, the vial was immersed into the ultrasonic bath (20 °C, 70 W, 40 kHz) via clamps and sonicated for 20 h. After the completion of the reaction, a small aliquot was removed with a glass pipette and diluted with an appropriate solvent ($CDCl_3$ or $CHCl_3$). The solution was then centrifuged to separate the nanoparticles, and supernatant was collected for NMR spectroscopy (ca. 5 – 10 mg/mL in $CDCl_3$) or GPC analysis (ca. 2 – 5 mg/mL in $CHCl_3$).

General procedure for mechanoredox RAFT in a ball mill:

In a 1.5 mL stainless steel milling jar equipped with a 5 mm diameter ball, **DDMAT** (0.0081 g, 0.019 mmol, 1 equiv), DPIHP 0(.0084 g, .019 mmol, 1 **eq**) and $BaTiO_3$ (0.037 g, .160 mmol) were added and transferred into the glove box. To that mixture, DMF (20 µl) and BA (0.25 g, 1.9 mmol, 100 eq) were added, and the jar was closed under an inert atmosphere. The sealed jar was placed in the ball mill and milled at 30 Hz. After 3 h, a small aliquot was removed with a glass pipette and diluted with an appropriate solvent ($CDCl_3$ or $CHCl_3$). The solution was then centrifuged to separate the nanoparticles, and supernatant was collected for NMR spectroscopy (ca. 5 – 10 mg/mL in $CDCl_3$) or GPC analysis (ca. 2 – 5 mg/mL in $CHCl_3$).

General procedure for $BaTiO_3$ recycling:

$BaTiO_3$ used in a typical mechanoredox RAFT process in ball mill was recovered by centrifuging at 2500 rpm, decanting the supernatant, and drying overnight in a vacuum oven at 50 °C. No residual organic material was detected by subsequent ^1H NMR spectroscopy (Figure 3.6B). The recovered $BaTiO_3$ was used for a second round of mechanoredox RAFT polymerization, and subsequently recovered following the above procedure and used for a third round of mechanoredox RAFT polymerization (Figure 3.6).

General procedure for one pot chain extension in a ball mill:

In a 1.5 mL stainless steel milling jar equipped with a 5 mm diameter ball, **DDMAT** (0.0081 g, 0.019 mmol, 1 equiv), DPIHP (0.0084 g, 0.019 mmol, 1 eq) and $BaTiO_3$ (0.037 g, 0.160 mmol) were added and transferred into the glove box. To that mixture, DMF (20 µl) and *t*BA (0.25 g, 1.9 mmol, 100 eq) were added, and the jar was closed in an inert atmosphere. The sealed jar was placed in the ball mill and milled at 30 Hz. After 3 h of polymerization, the ball mill jar is transferred into the glove box and samples were taken for ^{1}H NMR spectroscopy and GPC analysis. After confirming quantitative monomer conversion, into the same jar, DPIHP (.084 g, .019 mmol, 1 eq), DMF (20 µl, 180 µl/mg), BA (0.025 g, 1.9 mmol, 100 eq) and $BaTiO_3$ (0.037 g, 0.16 mmol) were added inside the glove box. The jar was closed and placed in the ball mill and milled at 30 Hz for 3 h. After the completion of the reaction, a small aliquot was removed with a glass pipette and diluted with an appropriate solvent ($CDCl_3$ or $CHCl_3$). The solution was then centrifuged to separate the nanoparticles and supernatant was collected for NMR spectroscopy (ca. 5 – 10 mg/mL in $CDCl_3$) or GPC analysis (ca. 2 – 5 mg/mL in $CHCl_3$).

General procedure for the synthesis of telechelic P*t*BA using ATTC in a ball mill:

In a 1.5 mL stainless steel milling jar equipped with a 5 mm diameter ball, **ATTC** (0.0028 g, 0.009 mmol, 1 equiv), DPIHP 0(.0042 g, 0.009 mmol, 1 equi) and $BaTiO_3$ (0.037 g, .160 mmol) were added and transferred into the glove box. To that mixture, DMF (20 µl) and BA (0.25 g, 1.9 mmol, 200 eq) were added, and the jar was closed under an inert atmosphere. The sealed jar was placed in the ball mill and milled at 30 Hz. After 3 h, a small aliquot was removed with a glass pipette and diluted with an appropriate solvent ($CDCl_3$ or $CHCl_3$). The solution was then

centrifuged to separate the nanoparticles and supernatant was collected for NMR spectroscopy (ca. 5 – 10 mg/mL in $CDCl_3$) or GPC analysis (ca. 2 – 5 mg/mL in $CHCl_3$).

General procedure for aminolysis of telechelic P*t*BA (from mechanoredox RAFT):

The aminolysis of the telechelic P*t*BA (from mechanoredox RAFT using **ATTC**) was carried out following procedure from the literature.[4] In a 10 mL round bottom flask equipped with a magnetic stirrer bar, 0.40 g of p*t*BA (M_n = 21.5 kDa) was dissolved in 1 mL of tetrahydrofuran. Into that polymer solution, isopropyl amine (0.0050 g, 0.028 mmol) was added. The reaction was then capped with a rubber septum and deoxygenated with nitrogen for 30 minutes. Then, 1 drop of tributyl phosphine was added using a 10 µL Air-tite syringe into the reaction mixture under a nitrogen atmosphere. The reaction was then left to stir at room temperature for 24 h. The resulting polymer was characterized by GPC (see Figure 3.10B).

General procedure for the synthesis of telechelic PBA using bi-DDMAT in ball mill:

In a 1.5 mL stainless steel milling jar equipped with a 5 mm diameter ball, **biDDMAT** (0.014 g, 0.019 mmol, 1 equiv), DPIHP (0.0042 g, 0.019 mmol, 1 equi) and $BaTiO_3$ (0.037 g, .160 mmol) were added and transferred into the glove box. To that mixture, DMF (20 µl) and BA (0.25 g, 1.9 mmol, 200 eq) were added, and the jar was closed under an inert atmosphere. The sealed jar was placed in the ball mill and milled at 30 Hz. After 3 h, a small aliquot was removed with a glass pipette and diluted with an appropriate solvent ($CDCl_3$ or $CHCl_3$). The solution was then centrifuged to separate the nanoparticles and supernatant was collected for NMR spectroscopy (ca. 5 – 10 mg/mL in $CDCl_3$) or GPC analysis (ca. 2 – 5 mg/mL in $CHCl_3$).

General procedure for the synthesis of semifluorinated co-polymers:

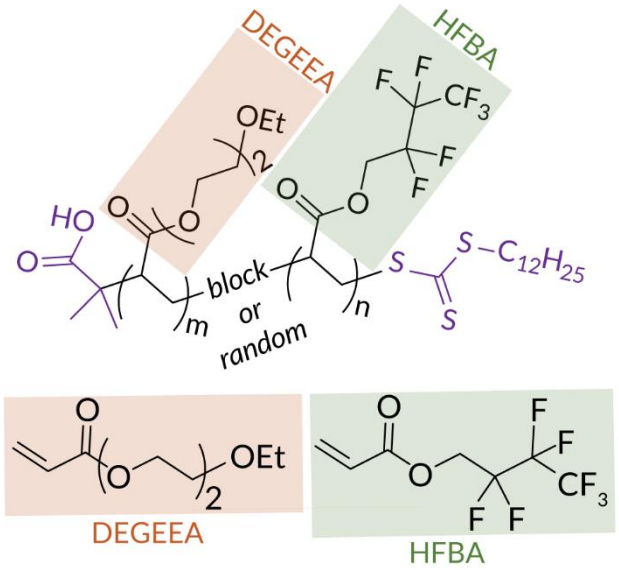

<u>PDEGEEA-*b*-PHFBA</u>

In a 1.5 mL stainless steel milling jar equipped with a 5 mm diameter ball, DDMAT (0.0077 g, .020 mmol, 1 equiv), DPIHP (0.0090 g, 0.020 mmol, 1 eq) and $BaTiO_3$ (0.037 g, 0.160 mmol) were added and transferred into the glove box. To that mixture, DMF (15 µl) and DEGEEA (0.20 g, 1.0 mmol, 50 eq) were added, and the jar was closed under an inert atmosphere. The sealed jar was placed in the ball mill and milled at 30 Hz. After 3 h of polymerization, the ball mill jar was transferred into the glove box and small samples were taken for ^1H NMR spectroscopy (> 95% monomer consumption) and GPC analyses. Into the same jar, DPIHP (0.010 g, 0.023 mol, 1 eq), DMF (15 µl), HFBA (0.30 g, 1.1 mmol) and $BaTiO_3$ (0.037 g, 0.160 mmol) were added inside the glove box. The jar was closed and placed in the ball mill and milled at 30 Hz for 3 h. After 3 h, a small aliquot was removed with a glass pipette and diluted with an appropriate solvent ($CDCl_3$ or $CHCl_3$). The solution was then centrifuged to separate the nanoparticles, and supernatant was

collected for NMR spectroscopy (ca. 5 – 10 mg/mL in $CDCl_3$) or GPC analysis (ca. 2 – 5 mg/mL in $CHCl_3$).

PDEGEEA-*r*-PHFBA

In a 1.5 mL stainless steel milling jar equipped with a 5 mm diameter ball, DDMAT (0.0028 g, 0.0078 mmol, 1 equiv), DPIHP 0(.0034 g, 0.0078 mmol, 1 eq) and $BaTiO_3$ (0.052 g, .200 mmol) were added and transferred into the glove box. To that mixture, DMF (35 µl) and HFBA (0.20 g, .78 mmol) and DEGEEA (0.15 g, .78 mmol) were added, and the jar was closed under an inert atmosphere. The sealed jar was placed in the ball mill and milled at 30 Hz. After 3 h, a small aliquot was removed with a glass pipette and diluted with an appropriate solvent ($CDCl_3$ or $CHCl_3$). The solution was then centrifuged to separate the nanoparticles, and supernatant was collected for NMR spectroscopy (ca. 5 – 10 mg/mL in $CDCl_3$) or GPC analysis (ca. 2 – 5 mg/mL in $CHCl_3$).

General procedure for larger scale diblock synthesis in a ball mill:

In a 5 mL stainless steel milling jar equipped with 3 5 mm diameter balls, **DDMAT** (0.0766 g, 0.21 mmol, 1 equiv), DPIHP (0.0903 g, 0.019 mmol, 1 eq) and $BaTiO_3$ (0.373 g, 1.60 mmol) were added and transferred into the glove box. To that mixture, DMF (151 µl) and monomer (10.5 mmol, 50 eq) were added, and the jar was closed in an inert atmosphere. The sealed jar was placed in the ball mill and milled at 30 Hz. After 3 h of polymerization, the ball mill jar is transferred into the glove box and samples were taken for ^1H NMR spectroscopy and GPC analysis. After confirming quantitative monomer conversion, into the same jar, DPIHP (0.0989 g, 0.23 mmol, 1 eq), DMF (108 µl,), and HFBA (varying equivalents) and $BaTiO_3$ (0.370 g, 1.60 mmol) were added inside the glove box. The jar was closed and placed in the ball mill and milled at 30 Hz for

3 h. After the completion of the reaction, a small aliquot was removed with a glass pipette and diluted with an appropriate solvent ($CDCl_3$ or $CHCl_3$). The solution was then centrifuged to separate the nanoparticles, and supernatant was collected for NMR spectroscopy (ca. 5 – 10 mg/mL in $CDCl_3$) or GPC analysis (ca. 2 – 5 mg/mL in $CHCl_3$).

Procedure for triblock synthesis in a ball mill:

In a 1.5 mL stainless steel milling vial (see Figure 3.33) equipped with a 5 mm diameter ball, **DDMAT** (0.0181 g, 0.042 mmol, 1 equiv.), DPIHP (0.0153 g, 0.042 mmol, 1 eq) and $BaTiO_3$ (0.0746 g, 0.32 mmol) were added and transferred into the glove box. To that mixture, DMF (15 µl) and BA (0.135 g, 1.05 mmol, 25 eq) were added, and the jar was closed in an inert atmosphere. The sealed jar was placed in the SPEX ball mill and milled for 4 h. After 4 h, the ball mill jar is transferred into the glove box and samples were taken for ^1H NMR spectroscopy and GPC analysis. After confirming quantitative monomer conversion, into the same jar, DPIHP (0.0153 g, 0.042 mmol, 1 eq), DMF (11 µl), EA (0.1051 g, 1.05 mmol, 25 eq) and $BaTiO_3$ (0.0746 g, 0.32 mmol) were added inside the glove box. The jar was closed and placed in the SPEX ball mill and milled for 4 h. After 4 h, the ball mill jar is transferred into the glove box and samples were taken for ^1H NMR spectroscopy and GPC analysis. After confirming quantitative monomer conversion, into the same jar, DPIHP (0.0153 g, 0.042 mmol, 1 eq), DMF (11 µl), MA (0.0904 g, 1.05 mmol, 25 eq) and $BaTiO_3$ (0.0746 g, 0.32 mmol) were added inside the glove box. The jar was closed and placed in the SPEX ball mill and milled for 4 h. After the completion of the reaction, a small aliquot was removed with a glass pipette and diluted with an appropriate solvent ($CDCl_3$ or $CHCl_3$). The solution was then centrifuged to separate the nanoparticles and supernatant was

collected for NMR spectroscopy (ca. 5 – 10 mg/mL in $CDCl_3$) or GPC analysis (ca. 2 – 5 mg/mL in $CHCl_3$).

General procedure for mechanoredox RAFT in vortexer:

Into a 1.5 mL stainless steel milling vial (see Figure 3.33) equipped with two 5 mm diameter stainless steel milling balls, DDMAT (0.0070 g, 0.020 mmol, 1 equiv), DPIHP (0.0080 g, 0.020 mmol, 1 equiv), and BaTiO3 (0.038 g, 10 wt.%). butyl acrylate (0.250 g, 2.0 mmol, 100 equiv) and DMF (20 µl) were added in the glovebox, and the vial was sealed under nitrogen. The vial was then placed into the vortexer and shaken at 3000 rpm for the desired amount of time. A small aliquot was removed with a glass pipette and diluted with an appropriate solvent ($CDCl_3$ or $CHCl_3$). The solution was then centrifuged to separate the nanoparticles, and supernatant was collected for NMR spectroscopy (ca. 5 – 10 mg/mL in $CDCl_3$) or GPC analysis (ca. 2 – 5 mg/mL in $CHCl_3$).

General procedure for energy consumption study:

Mechanoredox RAFT of *t*BA was carried out in triplicate in either a ball mill or vortexer for 3 h and 8 h, respectively, following the standard procedures described above.

Solution-state thermal RAFT of *t*BA was carried out in triplicate as follows: To a round bottom flask equipped with a magnetic stir bar *t*BA (4.0 g, 0.031 mol), DDMAT (0.110 g, 0.0031 mol), azobisisobutyronitrile (AIBN) (0.005 g, 3.1×10^{-5} mol), and 8 g of DMF were added. Then, the reaction mixture was capped with a rubber septum and deoxygenated for 30 minutes with N_2. The flask was placed in an oil bath on an IKA RET hotplate and left to stir for 20 h at 75 °C until >95% conversion achieved.

For each set of experiments, the stimuli source (ball mill, vortexer, or hot plate) was plugged into an a Suraielec Watt energy meter which was connected to a standard wall outlet (120 V) to record the energy consumed throughout the experiment. The readings were then averaged from three runs.

General procedure for radical trapping

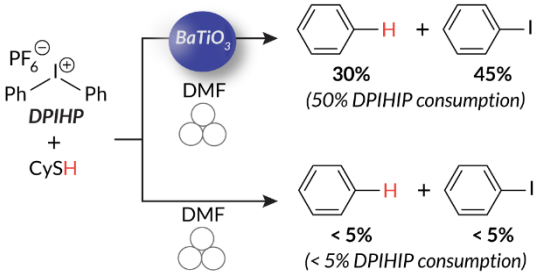

In a 1.5 mL stainless steel milling jar equipped with a 5 mm diameter ball, DPIHP (0.020 g, 0.047 mmol, 1 eq) and $BaTiO_3$ (0.025 g, 0.11 mmol) were added and the jar was transferred into the glove box. To that mixture, DMF (20 µl) and cyclohexanethiol (0.016 g, 0.014 mmol, 3 eq) were added and the jar was sealed under an inert atmosphere. The sealed jar was placed in the ball mill and milled at 30 Hz. After 3 h, maleic acid (0.0055 g, 0.041 mmol) and 0.6 mL of acetone-d_6 were added into the jar mixture. The following mixture was then centrifuged to separate out $BaTiO_3$, and the supernatant was collected for ^{1}H NMR spectroscopy and GC-MS characterization. The crude NMR yields of benzene and iodobenzene were determined by using maleic acid as an internal standard in ^{1}H NMR spectroscopy analysis (Figure 3.28). The triplets at 7.36 ppm & 7.14 ppm and the doublet at 7.74 ppm are assigned to iodobenzene. The singlet at 7.34 ppm is assigned to benzene. Additionally, both benzene and iodobenzene were detected by GC-MS (Figures 3.29-3.30).

A control experiment was carried out without $BaTiO_3$ following the same procedure. After 3 h, the crude material was characterized by ^1H NMR spectroscopy using maleic acid as an internal standard. No formation of benzene and iodobenzene was observed (Figure 3.31).

3.8 Acknowledgements and Publications

This mechanoredox RAFT methodology was conducted in collaboration with Dr. Progya Chakma who developed the sonoRAFT and ball milling RAFT methods, Waseem Shindy who conducted the energy studies, Jiatong Yu who synthesized the telechelic CTA, and Dr. Fabio Baum who worked under the direction of Prof. Lilo Pozzo to conduct SAXS studies. The milling jars for vortexing were manufactured by Kevin Soderlund and Brian Wadey. The self-assembly of semi fluorinated diblock polymers in solution was studied by Dr. Sage Scheiwiller and Karen Li under the direction of Prof. Lilo Pozzo.

This chapter was adapted from the publication below publication(s):

- P. Chakma, **S. Zeitler**, F. Baum, Y. Yu, W. Shindy, L. Pozzo, M. Golder, *Angew. Chem. Int. Ed*,. 2022, **62**, e202215733.
- S. Scheiwiller, **S. Zeitler**, K. Vaddi, K. Li, J. Mata, M. Golder, L. Pozzo, Structural Characterization of Mechanochemically Synthesized High-χ Ethylene Glycol Based Fluorinated Amphiphilic Block-Copolymers through Small Angle Neutron Scattering, *manuscript in preparation for Macromolecules.*
- **S. Zeitler,*** M. Hodges,* M. Golder, One pot synthesis to multiblock copolymers of immiscible monomers via mechanoredox RAFT, *manuscript in preparation.* *co-first author

3.9 References

1 J. Li, C. Nagamani, J. S. Moore, *Acc. Chem. Res.*, 2015, **48**, 2181-2190.

2 J.-L. Do, T. Friščić, *ACS Cent. Sci.*, 2017, **3**, 13-19.

3 T. Friščić, C. Mottillo, H. M. Titi, *Angew. Chem. Int. Ed.*, 2020, **132**, 1030-1041.

4 J. L. Howard, Q. Cao, D. L. Browne, *Chem. Sci.*, 2018, **9**, 3080-3094.

5 E. Boldyreva, *Chem. Soc. Rev.*, 2013, **42**, 7719-7738.

6 C. R. Hickenboth, J. S. Moore, S. R. White, N. R. Sottos, J. Baudry, S. R. Wilson, *Nature*, 2007, **446**, 423-427.

7 T. Friščić, *J. Mater. Chem.*, 2010, **20**, 7599-7605.

8 G. A. Bowmaker, *Chem. Commun.*, 2013, **49**, 334-348.

9 K. J. Ardila-Fierro, J. G. Hernández, *ChemSusChem*, 2021, **14**, 2145-2162.

10 H. Staudinger, W. Heuer, *Ber. Dtsch. Chem. Ges. B*, 1934, **67**, 1159-1164.

11 J. Kost, K. Leong, R. Langer, *Proc. Natl. Acad. Sci.*, 1989, **86**, 7663-7666.

12 H. Melville, A. Murray, *Trans. Faraday Soc.*, 1950, **46**, 996-1009.

13 A. Horn, E. Merrill, *Nature*, 1984, **312**, 140-141.

14 J. Ayarza, Z. Wang, J. Wang, C.-W. Huang, A. P. Esser-Kahn, *ACS Macro Lett.*, 2020, **9**, 1237-1248.

15 J. D. Rule, S. R. Wilson, J. S. Moore, *J. Am. Chem. Soc.*, 2003, **125**, 12992-12993.

16 M. B. Larsen, A. J. Boydston, *J. Am. Chem. Soc.*, 2013, **135,** 8189-8192.

17 Z. Shi, J. Wu, Q. Song, R. Göstl, A. Herrmann, *J. Am. Chem. Soc.*, 2020, **142**, 14725-14732.

18 E. Izak-Nau, D. Campagna, C. Baumann, R. Göstl, *Polym. Chem.*, 2020, **11**, 2274-2299.

19 H. Xia, Z. Wang, *Science*, 2019, **366**, 1451-1452.

20 J. A. Leitch, D. L. Browne, *Chem. Eur. J.*, 2021, **27**, 9721-9726.

21 A. Cafarelli, A. Marino, L. Vannozzi, J. Puigmartí-Luis, S. Pané, G. Ciofani, L. Ricotti, *ACS Nano*, 2021, **15**, 11066-11086.

22 A. Marino, M. Battaglini, D. De Pasquale, A. Degl'Innocenti, G. Ciofani, *Sci. Rep.*, 2018, **8**, 1-13.

23 R. Caliò, U. B. Rongala, D. Camboni, M. Milazzo, C. Stefanini, G. De Petris, C. M. Oddo, *Sensors*, 2014, **14**, 4755-4790.

24 K.-S. Hong, H. Xu, H. Konishi, X. Li, *J. Phys. Chem. Lett.*, 2010, **1**, 997-1002.

25 Y. Pang, J. W. Lee, K. Kubota, H. Ito, *Angew. Chem. Int. Ed.*, 2020, **59**, 22570-22576.

26 K. Kubota, Y. Pang, A. Miura, H. Ito, *Science*, 2019, **366**, 1500-1504.

27 C. Schumacher, J. G. Hernández, C. Bolm, *Angew. Chem. Int. Ed.*, 2020, **59,** 16357-16360.

28 Z. Wang, J. Wang, J. Ayarza, T. Steeves, Z. Hu, S. Manna, A. P. Esser-Kahn, *Nat. Mater.,* 2021, **20**, 869-874.

29 Z. Wang, J. Ayarza, A. P. Esser-Kahn, *Angew. Chem. Int. Ed.,* 2019, **131**, 12151-12154.

30 Z. Wang, X. Pan, L. Li, M. Fantin, J. Yan, Z. Wang, Z. Wang, H. Xia, K. Matyjaszewski, *Macromolecules,* 2017, **50**, 7940-7948.

31 S. M. Zeitler, P. Chakma, M. R. Golder, *Chem. Sci.,* 2022, **13**, 4131-4138.

32 H. Mohapatra, J. Ayarza, E. C. Sanders, A. M. Scheuermann, P. J. Griffin, A. P. Esser-Kahn, *Angew. Chem. Int. Ed.,* 2018, **57**, 11208-11212.

33 Z. Wang, J. Wang, J. Ayarza, T. Steeves, Z. Hu, S. Manna, A. P. Esser-Kahn, *Nat. Mater.,* **2021**, *20*, 869-874.

34 C. Ding, Y. Yan, Y. Peng, D. Wu, H. Shen, J. Zhang, Z. Wang, Z. Zhang, *Macromolecules,* 2022, **10**, 4056-4063.

35 M. R. Hill, R. N. Carmean, B. S. Sumerlin, *Macromolecules,* 2015, **48**, 5459-5469.

36 A. Kerr, G. Moriceau, M. A. Przybyla, T. Smith, S. Perrier, *Macromolecules,* 2021, **54**, 6649-6661.

37 J. Chiefari, Y. K. Chong, F. Ercole, J. Krstina, J. Jeffery, T. P. T. Le, R. T. A. Mayadunne, G. F. Meijs, C. L. Moad, G. Moad, *Macromolecules,* 1998, **31**, 5559-5562.

38 A. Gregory, M. H. Stenzel, *Prog. Polym. Sci.,* 2012, **37,** 38-105.

39 G. Moad, E. Rizzardo, S. H. Thang, *Chem. Asian J.,* 2013, **8**, 1634-1644.

40 S. Perrier, *Macromolecules,* 2017, **50**, 7433-7447.

41 R. Whitfield, K. Parkatzidis, N. P. Truong, T. Junkers, A. Anastasaki, *Chem,* 2020, **6**, 1340-1352.

42 C. A. Figg, B. S. Sumerlin, in *Reversible Deactivation Radical Polymerization: Materials and Applications*, ACS Publications, 2018, 43-56.

43 J. Collins, T. G. McKenzie, M. D. Nothling, S. Allison-Logan, M. Ashokkumar, G. G. Qiao, *Macromolecules,* 2018, ***52***, 185-195.

44 F. Lorandi, M. Fantin, K. Matyjaszewski, in *RAFT Polymerization: Methods, Synthesis and Applications,* Wiley Publications, 2021, **2**, 647-677.

45 J. Phommalysack-Lovan, Y. Chu, C. Boyer, J. Xu, *Chem. Commun.,* 2018, **54**, 6591-6606.

46 M. L. Allegrezza, D. Konkolewicz, *ACS Macro Lett.,* 2021, **10**, 433-446.

47 I. N. Egorov, S. Santra, D. S. Kopchuk, I. S. Kovalev, G. V. Zyryanov, A. Majee, B. C. Ranu, V. L. Rusinov, O. N. Chupakhin, *Green Chem.* 2020, **22**, 302-315.

48 Z.-J. Jiang, Z.-H. Li, J.-B. Yu, W.-K. Su, *J. Org. Chem.*, 2016, **81**, 10049-10055.

49 G. I. Peterson, W. Ko, Y.-J. Hwang, T.-L. Choi, *Macromolecules*, 2020, **53**, 7795-7802.

50 H. Zhou, J. A. Johnson, *Angew. Chem. Int. Ed.*, 2013, **125**, 2291-2294.

51 M. A. Tasdelen, M. U. Kahveci, Y. Yagci, *Prog. Polym. Sci.*, 2011, **36**, 455-567.

52 Y. Mai, A. Eisenberg, *Chem. Soc. Rev.*, 2012, **41**, 5969-5985.

53 G. Riess, *Prog. Polym. Sci.*, 2003, **28**, 1107-1170.

54 R. P. Quirk, D. J. Kinning, L. J. Fetters, *Comp. Polym. Sci. Supp.*, 1989, **7**, 1-26.

55 H. Dau, G. R. Jones, E. Tsogtgerel, D. Nguyen, A. Keyes, Y. Liu, H. Rauf, E. Ordonez, V. Puchelle, H. B. Alhan, C. Zhao, E. Harth, *Chem Rev*, 2022, **122**, 14471-14553.

56 M. H. Acar, K. Matyjaszewski, *Macromol. Chem. Phys.*, 1999, **200**, 1094-1100.

57 D. J. Keddie, *Chem. Soc. Rev.*, 2014, **43**, 496-505.

58 S. Qu, R. Liu, W. Duan, W. Zhang, *Macromolecules.*, 2019, **52**, 5168-5176.

59 C. L. Mccormick, A. B. Lowe, *Acc. Chem. Res.*, 2004, **37**, 312-325.

60 G. S. Lee, H. W. Lee, H. S. Lee, T. Do, J.-L. Do, J. Lim, G. I. Peterson, T. Friščić, J. G. Kim, *Chem. Sci.*, 2022, **13**, 11496-11505.

61 H. Gong, Y. Zhao, X. Shen, J. Lin, M. Chen, *Angew. Chem. Int. Ed.*, 2018, **57**, 333-337.

62 H. Gong, Y. Gu, M. Chen, *Synlett*, 2018, **29**, 1543-1551.

63 E. H. Discekici, A. Anastasaki, R. Kaminker, J. Willenbacher, N. P. Truong, C. Fleischmann, B. Oschmann, D. J. Lunn, J. Read de Alaniz, T. P. Davis, M. C. Bates, J. C. Hawker, *J. Am. Chem. Soc.*, 2017, **139**, 5939-5945.

64 N. G. Taylor, S. H. Chung, A. L. Kwansa, R. R. Johnson III, A. J. Teator, N. J. Milliken, K. M. Koshlap, Y. G. Yingling, Y. Z. Lee, F. A. Leibfarth, *Chem. Eur. J.*, 2020, **26**, 9982-9990.

65 Q. Quan, H. Wen, S. Han, Z. Wang, Z. Shao, M. Chen, *ACS Appl. Mater. Interfaces*, 2020, **12**, 24319-24327.

66 Y. Zhao, M. Ma, X. Lin, M. Chen, *Angew. Chem. Int. Ed.*, 2020, **59**, 21470-21474.

67 Q. Quan, H. Gong, M. Chen, *Polym. Chem.*, 2018, **9**, 4161-4171.

68 H. Gong, Y. Gu, Y. Zhao, Q. Quan, S. Han, M. Chen, *Angew. Chem. Int. Ed.*, 2020, **59**, 919-927.

69 A. Ryan, I. Hamley, W. Bras, F. S. Bates, *Macromolecules*, 1995, **28**, 3860-3868.

70 J. J. Haven, J. De Neve, A. C. Villavicencio, T. Junkers, *Polym. Chem.*, 2019, **10**, 6540-6544.

71 B. P. Koiry, M. Moukwa, N. K. Singha, *J. Fluor. Chem.*, 2013, **153**, 137-142.

72 S. P. Yelgaonkar, D. C. Swenson, L. R. MacGillivray, *Chem. Sci.*, 2020, **11**, 3569-3573.

73 Y. Y. Loh, K. Nagao, A. J. Hoover, D. Hesk, N. R. Rivera, S. L. Colletti, I. W. Davies, D. W. MacMillan, *Science*, 2017, **358**, 1182-1187.

74 A. B. Pangborn, M. A. Giardello, R. H. Grubbs, R. K. Rosen and F. J. Timmers, *Organometallics*, 1996, **15**, 1518–1520.